

Replica Keldysh field theory of quantum-jump processes: General formalism and application to imbalanced and inefficient fermion counting

Felix Kloiber-Tollinger[✉] and Lukas M. Sieberer^{✉*}

Institute for Theoretical Physics, University of Innsbruck, 6020 Innsbruck, Austria

Measurement-induced phase transitions have largely been explored for projective or continuous measurements of Hermitian observables, assuming perfect detection without information loss. Yet such transitions also arise in more general settings, including quantum-jump processes with non-Hermitian jump operators, and under inefficient detection. A theoretical framework for treating these broader scenarios has been missing. Here we develop a comprehensive replica Keldysh field theory for general quantum-jump processes in both bosonic and fermionic systems. Our formalism provides a unified description of pure-state quantum trajectories under efficient detection and mixed-state dynamics emerging from inefficient monitoring, with deterministic Lindbladian evolution appearing as a limiting case. It thus establishes a direct connection between phase transitions in nonequilibrium steady states of driven open quantum matter and in measurement-induced dynamics. As an application, we study imbalanced and inefficient fermion counting in a one-dimensional lattice system: monitored gain and loss of fermions occurring at different rates, with a fraction of gain and loss jumps undetected. For imbalanced but efficient counting, we recover the qualitative picture of the balanced case: entanglement obeys an area law for any nonzero jump rate, with an extended quantum-critical regime emerging between two parametrically separated length scales. Inefficient detection introduces a finite correlation length beyond which entanglement, as quantified by the fermionic logarithmic negativity, obeys an area law, while the subsystem entropy shows volume-law scaling. Numerical simulations support our analytical findings. Our results offer a general and versatile theoretical foundation for studying measurement-induced phenomena across a wide class of monitored and open quantum systems.

I. INTRODUCTION

In recent years, measurement-induced phase transitions have emerged as a central theme in the study of nonequilibrium quantum matter. Originally identified in spin systems evolving under hybrid quantum circuits that combine random unitary gates with projective measurements [1–4], it is now clear that such transitions arise in far broader settings. They occur not only in spin but also bosonic and fermionic systems; not only in discrete circuit models but also in continuous-time Hamiltonian evolution; and not only under projective measurements of Hermitian observables but also under continuous monitoring described by quantum state diffusion or quantum-jump processes, including jump processes with non-Hermitian jump operators [5–34]. At the same time, the stability of measurement-induced critical phenomena under imperfect detection has become an active topic of research [35–40].

While these investigations are often numerical in nature, substantial progress has also been achieved in the development of analytical methods for understanding measurement-induced phase transitions. These methods typically rely on the replica trick, familiar from the theory of spin glasses [41] and disordered electronic systems [42]. In spin systems evolving under circuit dynamics, the replica trick enables mappings to classical statistical-mechanics models [43, 44]; in fermionic systems, analytical progress has predominantly come from replica field-theoretic approaches [13, 17, 19–21, 23, 24, 26, 28–31, 34, 35]. Replica Keldysh field theory [45–49], in particular, has enabled major progress in understanding measurement-induced phenomena in both free

and interacting fermions. However, this framework has so far been limited to quantum state diffusion and to random projective or generalized measurements [50], assuming perfect detection. A general theoretical framework for quantum-jump processes, including the ability to incorporate imperfect measurements [51–54], has remained unavailable.

We close this gap by developing a replica Keldysh field theory for *general* quantum-jump processes. Our formalism applies to bosonic and fermionic many-body systems, including interacting ones, evolving under continuous monitoring with arbitrary jump operators. A central technical challenge is performing the average over quantum trajectories within the replica field-theory framework. This requires averaging over both jump times and jump types. Prior work resolved this issue only in settings with externally imposed measurement rates, such as random projective [19] or generalized measurements [30]. In contrast, the physically relevant jump rates in quantum-jump trajectories are state-dependent and thus fluctuate in time, necessitating a new approach, which we provide.

As a key example of measurement imperfections, we incorporate inefficient detection, where only a fraction of quantum jumps is registered, into our formalism [51–54]. The detection efficiency $\eta \in [0, 1]$ interpolates between fully efficient monitoring at $\eta = 1$, which yields pure-state trajectories, and fully inefficient monitoring at $\eta = 0$, where the dynamics reduce to deterministic Lindbladian evolution. In this limit, Hermitian jump operators, as realized by random projective and generalized measurements, typically drive the system to an infinite-temperature steady state, thereby erasing all signatures of the measurement-induced phenomena present at $\eta = 1$. By contrast, non-Hermitian jump operators can stabilize nontrivial stationary states even at $\eta = 0$, which represents the natural setting of driven open quantum matter. The Keldysh formalism provides a well-established framework for analyzing the

* lukas.sieberer@uibk.ac.at

resulting nonequilibrium steady states in this regime [46–49].

Incorporating inefficient detection into our framework therefore serves a dual purpose. First, it enables analytical progress in understanding the impact of imperfect monitoring on measurement-induced phenomena. Second, it establishes a conceptual and technical bridge between measurement-induced dynamics and the nonequilibrium steady states of driven open quantum systems. Providing this link is a first step toward a unified perspective on phases and phase transitions in continuously monitored and driven open quantum matter, as well as on broader questions such as topology and symmetry classifications [55–60].

As an illustration of the formalism, we analyze imbalanced and inefficient fermion counting in a one-dimensional (1D) lattice system. We use the term “fermion counting” in analogy with photon counting in quantum optics [51–54] to denote continuously monitored fermion gain and loss. Technically, fermion counting is described by a quantum-jump process with quantum jumps generated by fermionic annihilation and creation operators. Reference [30] studied the *balanced and efficient* case, where gain and loss occur at equal rates, $\gamma_+ = \gamma_-$, and each quantum jump is detected. For balanced rates, fermion counting can be formulated as a random generalized measurement. This formulation formed the basis for the analytical approach of Ref. [30]. Building on the formalism developed in the present paper, we extend this analysis in two important directions:

(i) We consider *imbalanced* fermion counting with $\gamma_+ \neq \gamma_-$, a setting more natural for potential experimental implementations where fermion gain and loss would be induced by coupling to two distinct reservoirs acting as particle drain and source, respectively. In this scenario, balanced coupling represents a fine-tuned limit. We show analytically and numerically that the qualitative behavior identified in Ref. [30] persists without fine tuning: the model exhibits no measurement-induced phase transition. For any nonzero gain and loss rates, $\gamma_\pm > 0$, the entanglement entropy obeys an area law. However, area-law scaling appears only beyond a length scale exponentially large in the inverse mean rate $\gamma = (\gamma_+ + \gamma_-)/2$. On intermediate scales, between $l_0 \sim \gamma^{-1}$ and $l_c \sim \gamma^{-2}$, the system displays signatures of quantum criticality and emergent conformal invariance. For scales larger than l_c , the system undergoes a slow crossover to the area-law regime. This behavior is captured by a long-wavelength nonlinear sigma model (NLSM) describing Goldstone-mode fluctuations associated with breaking an $SU(R)$ replica symmetry. In the presence of particle-hole symmetry, as in the nearest-neighbor hopping model with real amplitudes studied here, the NLSM target manifold changes from $SU(R)$ to $SU(2R)/Sp(R)$, but the qualitative physics remains the same [16, 26, 29].

(ii) We examine *inefficient* fermion counting, where only a fraction η of gain and loss jumps is detected. Undetected jumps generate additional time-continuous incoherent gain and loss. Interestingly, these processes explicitly break the $SU(R)$ symmetry and introduce a mass term in the NLSM Lagrangian proportional to the detection inefficiency $\delta\eta = 1 - \eta$. This mass induces a correlation length $\xi \sim \delta\eta^{-1/2}$, beyond which correlations decay exponentially. The von Neumann

entropy exhibits volume-law scaling, reflecting the mixed character of the trajectories, while genuine entanglement as quantified by the fermionic logarithmic negativity [61, 62] retains area-law behavior on scales larger than ξ . Numerical simulations are made feasible by the fact that incoherent gain and loss preserve Gaussianity of the mixed states, allowing us to access system sizes up to $L = 1000$. This contrasts with inefficient monitoring of occupation numbers, where Gaussianity is lost and the simulation cost increases dramatically [35].

The paper is organized as follows. In Sec. II, we introduce the Kraus-operator formulation of quantum-jump processes. Section III briefly reviews the replica formalism used to compute trajectory averages of observables that are nonlinear in the quantum state such as the von Neumann entropy. Building on this foundation, Sec. IV presents the derivation of the replica Keldysh field theory for quantum-jump processes. The resulting theory applies to pure-state trajectories under efficient detection; Sec. V explains how to extend it to the case of inefficient detection. A minimal physical model that leads to discrete-time dynamics in terms of Kraus operators is discussed in Appendix A. This completes the general formal developments of the paper. In Sec. VI, we apply the general formalism to imbalanced and inefficient fermion counting. We benchmark the analytical results obtained from replica Keldysh field theory against direct numerical simulations of quantum-jump trajectories. Technical details are given in Appendices B and C. Conclusions are presented in Sec. VII.

II. QUANTUM-JUMP PROCESSES

We begin by introducing the description of discrete-time quantum-jump processes in terms of Kraus operators. In the main text, we focus on formal aspects; we review the physical realization of quantum-jump processes in Appendix A.

A. Kraus operators

We consider the dynamics of a fermionic or bosonic quantum system subjected to continuous measurements. At time t_0 the system is initialized in the pure state $|\psi_0\rangle$. The time interval from t_0 to $t = t_0 + T$ is partitioned into N time steps of duration $\Delta t = T/N$. Evolution during a single time step is described by a set of Kraus operators \hat{K}_α with $\alpha \in \mathcal{A}_0 = \{0, \dots, A\}$. The operator \hat{K}_0 corresponds to no quantum jump occurring during the time step and is defined by [54]

$$\hat{K}_0 = 1 - i \left(\hat{H} \Delta t - \frac{i}{2} \sum_{a=1}^A \hat{K}_a^\dagger \hat{K}_a \right) = 1 - i \hat{H}_{\text{eff}} \Delta t, \quad (1)$$

where \hat{H} is the Hamiltonian. No-jump evolution described by \hat{K}_0 is continuous in the sense that $\hat{K}_0 \rightarrow 1$ for $\Delta t \rightarrow 0$. In contrast, quantum jumps, which are described by the remaining Kraus operators \hat{K}_a with $a \in \mathcal{A} = \{1, \dots, A\}$, induce discontinuous evolution with

$$\hat{K}_a = \sqrt{\gamma_a \Delta t} \hat{c}_a. \quad (2)$$

We do not impose any restrictions on the jump operators \hat{c}_a : they can be arbitrary fermionic or bosonic operators. In terms of the jump operators, the effective non-Hermitian Hamiltonian introduced in Eq. (1) is given by

$$\hat{H}_{\text{eff}} = \hat{H} - \frac{i}{2} \sum_{a=1}^A \gamma_a \hat{c}_a^\dagger \hat{c}_a. \quad (3)$$

Throughout, Greek indices label the full set of Kraus operators, while Latin indices label only those corresponding to quantum jumps:

$$\alpha \in \mathbb{A}_0 = \{0, \dots, A\}, \quad a \in \mathbb{A} = \{1, \dots, A\}. \quad (4)$$

The Kraus operators satisfy the completeness relation

$$\sum_{a=0}^A \hat{K}_a^\dagger \hat{K}_a = 1, \quad (5)$$

up to corrections that vanish in the continuous-time limit $N \rightarrow \infty$ such that $\Delta t \rightarrow 0$. Consequently, the set of Kraus operators defines a quantum channel describing the deterministic evolution of the density matrix over a single time step,

$$\hat{\rho} \mapsto \sum_{a=0}^A \hat{K}_a \hat{\rho} \hat{K}_a^\dagger = (1 + \mathcal{L}\Delta t) \hat{\rho}, \quad (6)$$

starting from the initial pure state $\hat{\rho}_0 = |\psi_0\rangle\langle\psi_0|$. The Liouville superoperator or Lindbladian is

$$\mathcal{L}\hat{\rho} = -i[\hat{H}, \hat{\rho}] + \sum_{a=1}^A \gamma_a \left(\hat{c}_a \hat{\rho} \hat{c}_a^\dagger - \frac{1}{2} \{ \hat{c}_a^\dagger \hat{c}_a, \hat{\rho} \} \right). \quad (7)$$

In the continuous-time limit, Eq. (6) can be recast as a Markovian quantum master equation in Lindblad form.

B. Quantum trajectories

Formally, a quantum-jump process is a stochastic unraveling of the quantum channel (6). As a computational tool, such unravelings find widespread application in the numerical simulation of open-system dynamics [63, 64]. We begin by considering the unraveling into pure-state quantum trajectories corresponding to perfectly efficient detection of quantum jumps; modifications arising from finite detection efficiency will be introduced further below in Sec. V.

In such a stochastic unraveling, one Kraus operator \hat{K}_α is drawn at random and applied to the state during each time step. For a system in the state $|\psi\rangle$, the operator \hat{K}_α is chosen with probability

$$P_\alpha = \|\hat{K}_\alpha|\psi\rangle\|^2 = \langle\psi|\hat{K}_\alpha^\dagger \hat{K}_\alpha|\psi\rangle. \quad (8)$$

If $\alpha = 0$ meaning that no jump occurs during the time step, the system evolves continuously according to

$$|\psi\rangle \mapsto \frac{\hat{K}_0|\psi\rangle}{\sqrt{P_0}} = \left[1 - i \left(\hat{H}_{\text{eff}} - i \sum_{a=1}^A \gamma_a \langle\psi|\hat{c}_a^\dagger \hat{c}_a|\psi\rangle \right) \Delta t \right] |\psi\rangle, \quad (9)$$

Otherwise, for $\alpha = a \in \{1, \dots, A\}$, the system undergoes a discontinuous quantum jump described by

$$|\psi\rangle \mapsto \frac{\hat{K}_a|\psi\rangle}{\sqrt{P_a}} = \frac{\hat{c}_a|\psi\rangle}{\|\hat{c}_a|\psi\rangle\|}. \quad (10)$$

While we introduce quantum-jump processes here from a formal perspective, a microscopic derivation is presented in Appendix A. There, we consider a minimal setup in which the system is coupled to independent bosonic or fermionic baths, one for each jump channel. Bath occupations are monitored continuously: Detection of no excitation in any bath occurs with probability P_0 and yields no-jump evolution, whereas detection of an excitation in bath a , with probability P_a , induces the corresponding jump [51–54]. Continuously measuring bath occupations thus produces precisely the stochastic unraveling of Eq. (6) described above. For this reason, we refer to the index α specifying the evolution during a given time step as a measurement outcome.

A quantum trajectory over N time steps is specified by a sequence of measurement outcomes α_n with $n \in \mathbb{N} = \{1, \dots, N\}$, collected into the vector $\alpha = (\alpha_1, \dots, \alpha_N) \in \mathbb{A}_0^N$. The probability for this sequence is

$$P_\alpha = \|\hat{K}_{\alpha_N} \cdots \hat{K}_{\alpha_1}|\psi_0\rangle\|^2, \quad (11)$$

and the corresponding normalized state is

$$|\psi_\alpha\rangle = \hat{K}_{\alpha_N} \cdots \hat{K}_{\alpha_1}|\psi_0\rangle / \sqrt{P_\alpha}. \quad (12)$$

This expression describes the evolution of the quantum state *conditioned* on a specific sequence of measurement outcomes. By contrast, Eq. (6) captures the *unconditional* dynamics, in which one averages over all possible outcomes.

Observables of interest are functions f_α of the normalized state or, more generally, of the measurement record itself. The average of f_α over the ensemble of trajectories is

$$\overline{f_\alpha} = \sum_{\alpha \in \mathbb{A}_0^N} P_\alpha f_\alpha. \quad (13)$$

For observables linear in the state, such as the expectation value $f_\alpha = \langle\psi_\alpha|\hat{O}|\psi_\alpha\rangle$, this reduces to

$$\overline{\langle\psi_\alpha|\hat{O}|\psi_\alpha\rangle} = \text{tr}(\hat{O}\hat{\rho}), \quad \hat{\rho} = \sum_{\alpha \in \mathbb{A}_0^N} P_\alpha |\psi_\alpha\rangle\langle\psi_\alpha|. \quad (14)$$

That is, the expectation value may be expressed in terms of the ensemble-averaged density matrix. Nonlinear observables, such as the von Neumann entropy of a subsystem, do not admit such a simplification.

This framework encompasses random projective [19] or generalized measurements [30], performed at a fixed rate γ , as a special case. In this setting, the rates γ_a in Eq. (2) are identical and equal to the measurement rate, $\gamma_a = \gamma$, and the jump operators are measurement operators and thus obey the completeness relation

$$\sum_{a=1}^A \hat{c}_a^\dagger \hat{c}_a = 1, \quad (15)$$

in addition to the Kraus-operator completeness relation (5). The completeness relation (15) leads to the total probability of a jump occurring in a single time step being state-independent,

$$P_{\text{jump}} = \sum_{a \in \mathcal{A}} P_a = \gamma \Delta t. \quad (16)$$

Therefore, jumps may indeed be identified with measurements performed at a fixed rate γ . For projective measurements, the measurement operators additionally satisfy $\hat{c}_a = \hat{c}_a^\dagger = \hat{c}_a^2$ and project onto eigenspaces of the measured observable. Then, the Liouvillian (7) takes the form

$$\mathcal{L}\hat{\rho} = -i[\hat{H}, \hat{\rho}] + \gamma \left(\sum_{a=1}^A \hat{c}_a \hat{\rho} \hat{c}_a - \hat{\rho} \right). \quad (17)$$

The completely mixed state $\hat{\rho} = 1/D$, with D the Hilbert-space dimension, is stationary under evolution generated by this Liouvillian and, for spatially extended systems with local measurements, is generically the unique steady state— independent of all system parameters, including the measurement rate γ . Consequently, random projective measurements yield nontrivial effects only in nonlinear trajectory-dependent observables. By contrast, for general non-Hermitian jump operators, the steady state of Eq. (7) is typically nontrivial, implying that both linear and nonlinear observables depend sensitively on system parameters.

C. Rescaled Kraus operators and continuous-time limit

We have introduced quantum-jump processes in discrete time, which provides a convenient starting point for the construction of a functional-integral representation of the trajectory average (13) presented in Sec. IV. However, in this construction, we ultimately want to take the continuous-time limit. Therefore, we now discuss how Eq. (13) can be rewritten in a form that is suitable for taking this limit.

As we will see, taking the continuous-time limit is facilitated by introducing rescaled Kraus operators,

$$\hat{J}_a = \hat{K}_a / \sqrt{q_a}, \quad q_0 = 1 - \Gamma_0 \Delta t, \quad q_a = \Gamma_a \Delta t, \quad (18)$$

which take the explicit form

$$\hat{J}_0 = 1 - i \left(\hat{H}_{\text{eff}} + \frac{i \Gamma_0}{2} \right) \Delta t, \quad \hat{J}_a = \sqrt{\frac{\gamma_a}{\Gamma_a}} \hat{c}_a. \quad (19)$$

The rates Γ_a may be chosen freely. We will consider two natural choices: a *uniform rescaling* with identical rates $\Gamma_a = \Gamma_1$, and a *detailed rescaling* with arbitrary Γ_a . Although these choices lead to slightly different intermediate representations of the replica Keldysh field theory, the differences disappear in the replica limit. Detailed rescaling includes the uniform case as a special instance, yet we discuss both separately because they lend themselves to different intermediate interpretations.

In terms of the rescaled Kraus operators, the trajectory probability P_α in Eq. (11) factorizes as $P_\alpha = Q_\alpha O_\alpha$, with

$$Q_\alpha = \prod_{n=1}^N q_{\alpha_n}, \quad O_\alpha = \left\| \hat{J}_{\alpha_N} \cdots \hat{J}_{\alpha_1} |\psi_0\rangle \right\|^2. \quad (20)$$

The average of f_α can then be written as

$$\overline{f_\alpha} = \sum_{\alpha \in \mathcal{A}_0^N} Q_\alpha O_\alpha f_\alpha. \quad (21)$$

This expression naturally suggests interpreting the average as being taken with respect to the distribution Q_α , which is defined in Eq. (20) as a product of the probabilities q_0 and q_a , Eq. (18), for no jump and a jump of type a to occur in a given time step. Under this interpretation, the quantity being averaged is the product $O_\alpha f_\alpha$. It is important to stress, however, that Q_α is *not* the physical probability of the trajectory α ; the physical probability remains P_α .

We next rewrite Eq. (21) in a form suitable for taking the continuous-time limit, first considering the case of uniform rescaling and subsequently turning to the more general case of detailed rescaling.

1. Uniform rescaling

For uniform rescaling, the probabilities q_a all take the same value $q_1 = \Gamma_1 \Delta t$. Then, the probability Q_α in Eq. (20) depends only on the total number of jumps M_α , that is, the number of measurement outcomes $\alpha_n \neq 0$ in the sequence α ,

$$Q_\alpha = Q_{M_\alpha} = q_0^{N-M_\alpha} q_1^{M_\alpha}. \quad (22)$$

To perform the average over trajectories in Eq. (21), we choose a different parameterization of trajectories: instead of specifying the values of α_n in each time step, we fully determine a trajectory by specifying the total number of jumps M , the time steps n_m with $m \in \{1, \dots, M\}$ or corresponding times $t_m = t_0 + n_m \Delta t$ at which the jumps occur, and the types of jumps $a_m \in \mathcal{A}$. We collect the time-step and jump indices in vectors $\mathbf{n} = (n_1, \dots, n_M)$ with $n_1 < \dots < n_M$ and $\mathbf{a} = (a_1, \dots, a_M)$. These vectors uniquely determine a vector $\alpha_{\mathbf{n}, \mathbf{a}}$ of length N : all elements with index n not contained in \mathbf{n} vanish $(\alpha_{\mathbf{n}, \mathbf{a}})_n = 0$, corresponding to no-jump evolution, whereas $(\alpha_{\mathbf{n}, \mathbf{a}})_{n_m} = a_m$. We can thus write the average (21) as

$$\overline{f_\alpha} = \sum_{M=0}^N Q_M \sum_{\mathbf{a} \in \mathcal{A}^M} \sum_{\mathbf{n} \in \mathcal{O}_{M,N}} O_{\alpha_{\mathbf{n}, \mathbf{a}}} f_{\alpha_{\mathbf{n}, \mathbf{a}}}, \quad (23)$$

where the third sum is over all ordered M -tuples with each element in $\mathbf{N} = \{1, \dots, N\}$,

$$\mathcal{O}_{M,N} = \left\{ \mathbf{N}^M : n_1 < \dots < n_M \right\}. \quad (24)$$

As stated above, we want to bring this in a form that enables taking the continuous-time limit. For the quantities $O_{\alpha_{\mathbf{n}, \mathbf{a}}}$ and $f_{\alpha_{\mathbf{n}, \mathbf{a}}}$, this is achieved by noting that they are functions of the jump times, $\mathbf{t} = (t_1, \dots, t_M)$, with $t_m = t_0 + n \Delta t \in [t_0, t]$, and the jump indices,

$$O_{\alpha_{\mathbf{n}, \mathbf{a}}} = O_{\mathbf{a}}(\mathbf{t}), \quad f_{\alpha_{\mathbf{n}, \mathbf{a}}} = f_{\mathbf{a}}(\mathbf{t}). \quad (25)$$

Furthermore, in the sums in Eq. (23), we first remove the restriction of the elements of \mathbf{n} being ordered and extend the

summation over all $\mathbf{n} \in \mathbb{N}^M$. When we do this, we have to include a factor $d_{\mathbf{n}}$ that ensures that all elements n_m are different, that is, $d_{\mathbf{n}} = 0$ if $n_m = n_{m'}$ for at least one pair of elements, and $d_{\mathbf{n}} = 1$ otherwise. Further, for any given ordered sequence \mathbf{n} , the unrestricted sum contains all possible $M!$ permutations of the elements n_m . Therefore, we have to include a factor $1/M!$ to compensate the resultant overcounting,

$$\overline{f_{\alpha}} = \sum_{M=0}^N \frac{1}{M!} Q_M \sum_{\mathbf{a} \in \mathbb{A}^M} \sum_{\mathbf{n} \in \mathbb{N}^M} d_{\mathbf{n}} O_{\mathbf{a}}(\mathbf{t}) f_{\mathbf{a}}(\mathbf{t}). \quad (26)$$

In the continuous-time limit, the sums over the components of \mathbf{n} become integrals. The factor $d_{\mathbf{n}}$ has support on a set of measure zero in the domain of integration $[t_0, t]^M$, and may thus be dropped,

$$\sum_{\mathbf{n} \in \mathbb{N}^M} d_{\mathbf{n}} = \frac{1}{\Delta t^M} \sum_{n_1=1}^N \Delta t \cdots \sum_{n_M=1}^N \Delta t d_{\mathbf{n}} \sim N^M \prod_{m=1}^M \int_{t_0}^t \frac{dt_m}{T}. \quad (27)$$

Combining the prefactor N^M with $Q_M/M!$ in Eq. (26), we obtain in the limit $N \rightarrow \infty$ a Poisson distribution for the number of jumps during the evolution time $T = t - t_0$,

$$\frac{N^M}{M!} Q_M = \frac{(\Gamma_1 T)^M}{M!} \left(1 - \frac{\Gamma_0 T}{N}\right)^{N-M} \rightarrow \left(\frac{\Gamma_1}{\Gamma_0}\right)^M P_M(T), \quad (28)$$

where

$$P_M(T) = \frac{(\Gamma_0 T)^M}{M!} e^{-\Gamma_0 T}, \quad (29)$$

and we have used

$$\left(1 - \frac{\Gamma_0 T}{N}\right)^N \rightarrow e^{-\Gamma_0 T}, \quad \left(1 - \frac{\Gamma_0 T}{N}\right)^{-M} \rightarrow 1. \quad (30)$$

Therefore, in the continuous-time limit, Eq. (26) becomes

$$\overline{f_{\alpha}} \sim \sum_{M=0}^{\infty} \left(\frac{\Gamma_1}{\Gamma_0}\right)^M P_M(T) \left(\prod_{m=1}^M \int_{t_0}^t \frac{dt_m}{T} \sum_{a_m=1}^A \right) O_{\mathbf{a}}(\mathbf{t}) f_{\mathbf{a}}(\mathbf{t}). \quad (31)$$

This expression is directly analogous to the average over random projective or generalized measurements performed at a rate γ [19, 30]. To make the analogy explicit, consider for concreteness a 1D fermionic lattice of size L with local measurements. Quantum jumps correspond to applying measurement operators, and the jump-type index a becomes a double index, where n labels the measurement outcome and l labels the lattice site. We focus here on projective measurements of local occupation numbers with outcomes $n \in \{0, 1\}$. For the choice $\Gamma_1 = \gamma$ and $\Gamma_0 = L\Gamma_1$, Eq. (31) takes the form

$$\overline{f_{\alpha}} \sim \sum_{M=0}^{\infty} P_M(T) \left(\prod_{m=1}^M \int_{t_0}^t \frac{dt_m}{LT} \sum_{l_m=1}^L \sum_{n_m=0}^1 \right) O_{\mathbf{a}}(\mathbf{t}) f_{\mathbf{a}}(\mathbf{t}). \quad (32)$$

This representation has a clear interpretation: when measurements occur at rate γ , the number of measurements in a time

interval T is Poisson distributed (29) with mean γT . Conditional on M measurements, the measurement times are uniformly distributed in $t_m \in [t_0, t]$, and one further averages over the measurement locations and outcomes. This reproduces precisely the ensemble average employed in Refs. [19, 30].

More generally, an analogous interpretation applies to Eq. (31) even for non-Hermitian jump operators, provided one chooses $\Gamma_0 = A\Gamma_1$. In this view, the expression resembles an average over the number of jumps, their times, and their types. It is important to stress, however, that this should be regarded only as an interpretation suggested by the algebraic structure of Eq. (31). Physically, jumps do not occur at the externally chosen rate Γ_0 . The true probability of a trajectory with a given jump sequence is determined by Eq. (11), which is manifestly independent of the artificial rates Γ_0 and Γ_1 introduced through the rescaling in Eq. (18). In the replica Keldysh functional integral developed in Sec. IV, we will see explicitly that these rates indeed drop out.

Finally, we consider the special case that we average over an observable that factorizes over jumps:

$$O_{\mathbf{a}}(\mathbf{t}) f_{\mathbf{a}}(\mathbf{t}) = \prod_{m=1}^M g_{a_m}(t_m). \quad (33)$$

Then, using

$$\prod_{m=1}^M \int_{t_0}^t \frac{dt_m}{T} \sum_{a_m=1}^A g_{a_m}(t_m) = \left[\int_{t_0}^t \frac{dt'}{T} \sum_{a=1}^A g_a(t') \right]^M, \quad (34)$$

Eq. (31) can be rewritten as

$$\overline{f_{\alpha}} \sim \exp \left\{ \int_{t_0}^t dt' \left[\Gamma_1 \sum_{a=1}^A g_a(t') - \Gamma_0 \right] \right\}. \quad (35)$$

2. Detailed rescaling

For detailed rescaling with $\Gamma_a = \gamma_a$, the probability Q_{α} in Eq. (20) depends on the number of jumps $M_{\alpha,a}$ for each individual type of jump $a \in \mathbb{A}$,

$$Q_{\alpha} = Q_{\mathbf{M}_{\alpha}} = q_0^{N-M_{\alpha}} \prod_{a=1}^A q_a^{M_{\alpha,a}}, \quad (36)$$

where $\mathbf{M}_{\alpha} = (M_{\alpha,1}, \dots, M_{\alpha,A})$, and again $M_{\alpha} = \sum_{a=1}^A M_{\alpha,a}$ is the total number of jumps. We now choose a different parameterization of trajectories: for each type of jump a , we specify the total number of jumps M_a , as well as the time steps $\mathbf{n}_a = (n_{a,1}, \dots, n_{a,M_a})$ with $n_{a,1} < \dots < n_{a,M_a}$ or equivalently the times $t_{a,n_a} = t_0 + n_{a,n_a} \Delta t$ at which the jumps occur. Each sequence \mathbf{n}_a is ordered, and we again include a factor $d_{\mathbf{n}_a}$ that is unity when all n_{a,n_a} with $a \in \mathbb{A}$ and $m_a \in \{1, \dots, M_a\}$ are different, and zero otherwise. By $\mathbf{n}_{\alpha} = (\mathbf{n}_1, \dots, \mathbf{n}_A)$ we denote the collection of all vectors \mathbf{n}_a . This collection uniquely determines a vector $\alpha_{\mathbf{n}_{\alpha}}$ of length N : we set $(\alpha_{\mathbf{n}_{\alpha}})_n = a$ for

all n that are contained in \mathbf{n}_a . Using this parameterization of trajectories, we can express the average (21) as

$$\overline{f_\alpha} = \sum_{M_1=0}^N \sum_{M_2=0}^{N-M_1} \cdots \sum_{M_A=0}^{N-\sum_{a=2}^A M_a} Q_{\mathbf{M}} \times \sum_{\mathbf{n}_1 \in \mathcal{O}_{M_1, N}} \cdots \sum_{\mathbf{n}_A \in \mathcal{O}_{M_A, N}} d_{\mathbf{n}_a} O_{\alpha_{\mathbf{n}_a}} f_{\alpha_{\mathbf{n}_a}}. \quad (37)$$

In analogy to Eq. (25), we regard $O_{\alpha_{\mathbf{n}_a}}$ and $f_{\alpha_{\mathbf{n}_a}}$ as functions of $\mathbf{t}_a = (t_1, \dots, t_A)$, where for each type of jump a , the vector $\mathbf{t}_a = (t_{a,1}, \dots, t_{a,M_a})$ collects the times at which jumps occurs:

$$O_{\alpha_{\mathbf{n}_a}} = O(\mathbf{t}_a), \quad f_{\alpha_{\mathbf{n}_a}} = f(\mathbf{t}_a). \quad (38)$$

Furthermore, as we did before for uniform rescaling, we can remove the restrictions on the sums over \mathbf{n}_a if we compensate the resultant overcounting by introducing factors of $1/M_a!$,

$$\overline{f_\alpha} = \sum_{M_1=0}^N \sum_{M_2=0}^{N-M_1} \cdots \sum_{M_A=0}^{N-\sum_{a=2}^A M_a} Q_{\mathbf{M}} \left(\prod_{a=1}^A \frac{1}{M_a!} \right) \times \sum_{\mathbf{n}_1 \in \mathbb{N}^{M_1}} \cdots \sum_{\mathbf{n}_A \in \mathbb{N}^{M_A}} d_{\mathbf{n}_a} O(\mathbf{t}_a) f(\mathbf{t}_a). \quad (39)$$

In the continuous-time limit $N \rightarrow \infty$, the sums over the components of the vectors \mathbf{n}_a are converted to integrals,

$$\sum_{\mathbf{n}_a \in \mathbb{N}^{M_a}} \sim N^{M_a} \prod_{m_a=1}^{M_a} \int_{t_0}^t \frac{dt_m}{T}. \quad (40)$$

The factors N^{M_a} can again be combined with other factors appearing in Eq. (39) to yield a product of Poisson distributions:

$$\left(\prod_{a=1}^A \frac{N^{M_a}}{M_a!} \right) Q_{\mathbf{M}} = \prod_{a=1}^A \frac{(\Gamma_a T)^{M_a}}{M_a!} \left(1 - \frac{\Gamma_0 T}{N} \right)^{N-M_a} \rightarrow e^{-(\Gamma_0 - \sum_{a=1}^A \Gamma_a)T} \prod_{a=1}^A P_{a,M_a}(T), \quad (41)$$

where

$$P_{a,M_a}(T) = \frac{(\Gamma_a T)^{M_a}}{M_a!} e^{-\Gamma_a T}. \quad (42)$$

For the same reason as above, the factor $d_{\mathbf{n}_a}$ can be dropped in the continuous-time limit $N \rightarrow \infty$. Thus, Eq. (39) becomes

$$\overline{f_\alpha} \sim e^{-(\Gamma_0 - \sum_{a=1}^A \Gamma_a)T} \times \left[\prod_{a=1}^A \sum_{M_a=0}^{\infty} P_{a,M_a}(T) \prod_{m_a=1}^{M_a} \int_{t_0}^t \frac{dt_{a,m_a}}{T} \right] O(\mathbf{t}_a) f(\mathbf{t}_a). \quad (43)$$

The exponential in the first line vanishes for the choice $\Gamma_0 = \sum_{a=1}^A \Gamma_a$. Under this condition, Eq. (43) admits the following interpretation: jumps of type a may be viewed as occurring with rate Γ_a . For each jump type, one then averages over the number of jumps in the interval T , which obeys the Poisson

distribution (42) with mean $\Gamma_a T$, and over the associated jump times, uniformly distributed in $t_{a,m_a} \in [t_0, t]$. As in the case of uniform rescaling, this interpretation is merely suggested by the structure of Eq. (43). The actual distribution of jump types and times is fixed by Eq. (11), which is insensitive to the auxiliary rates Γ_a introduced by the rescaling prescription.

Analogous to the discussion for uniform rescaling, let us examine the special case in which the observable factorizes over quantum jumps:

$$O(\mathbf{t}_a) f(\mathbf{t}_a) = \prod_{a=1}^A \prod_{m_a=1}^{M_a} g_a(t_{a,m_a}). \quad (44)$$

Substituting this expression into Eq. (43) and using

$$\prod_{m_a=1}^{M_a} \int_{t_0}^t \frac{dt_{a,m_a}}{T} g_a(t_{a,m_a}) = \left[\int_{t_0}^t \frac{dt'}{T} g_a(t') \right]^{M_a}, \quad (45)$$

we arrive at

$$\overline{f_\alpha} \sim \exp \left\{ \int_{t_0}^t dt' \left[\sum_{a=1}^A \Gamma_a g_a(t') - \Gamma_0 \right] \right\}. \quad (46)$$

III. REPLICA FORMALISM

Having shown, for both uniform and detailed rescaling, how the trajectory average in Eq. (21) can be rewritten in a form amenable to the continuous-time limit, we now specify the quantities whose averages we aim to compute.

In the dynamics of quantum many-body systems under continuous measurements, particular interest lies in observables that depend nonlinearly on the quantum state (12). Prominent examples include subsystem entropies and connected correlation functions. Such observables are built from trajectory averages of products of quantum expectation values. The latter can be expressed as expectation values with respect to the k -replica density matrix defined as [65]

$$\hat{\mu}_k(t) = \overline{\bigotimes_{r=1}^k \hat{\rho}_r(t)}, \quad (47)$$

where the overbar again denotes the trajectory average, and the index r labels identical copies or replicas of the original system. For instance, for two operators \hat{A} and \hat{B} ,

$$\begin{aligned} \overline{\langle \hat{A}(t) \rangle \langle \hat{B}(t) \rangle} &= \overline{\text{tr}[\hat{A}\hat{\rho}(t)] \text{tr}[\hat{B}\hat{\rho}(t)]} \\ &= \text{tr}[(\hat{A}_1 \otimes \hat{B}_2) [\hat{\rho}_1(t) \otimes \hat{\rho}_2(t)]] \\ &= \text{tr}[(\hat{A}_1 \otimes \hat{B}_2) \hat{\mu}_2]. \end{aligned} \quad (48)$$

To evaluate the k -replica density matrix $\hat{\mu}_k(t)$, we first express a single-replica density matrix as

$$\hat{\rho}_r(t) = \hat{D}_r(t) / \text{tr}[\hat{D}_r(t)], \quad (49)$$

with the unnormalized density matrix

$$\hat{D}_r(t) = \hat{J}_{r,\alpha_N} \cdots \hat{J}_{r,\alpha_1} |\psi_{r,0}\rangle\langle\psi_{r,0}| \hat{J}_{r,\alpha_1}^\dagger \cdots \hat{J}_{r,\alpha_N}^\dagger, \quad (50)$$

where $\hat{J}_{r,\alpha}$ are the Kraus operators (19) acting on replica r , and $|\psi_{r,0}\rangle$ is the initial state in the corresponding Hilbert space. Note that since each replica is an identical copy, we have

$$\text{tr}[\hat{D}_1(t)] = \cdots = \text{tr}[\hat{D}_R(t)] = \text{tr}[\hat{D}(t)]. \quad (51)$$

The product of Kraus operators in Eq. (50) describes the evolution from t_0 to $t = t_N = t_0 + N\Delta t$, which justifies denoting this expression by $\hat{D}_r(t)$. For brevity, the explicit dependence of $\hat{D}_r(t)$ on α is suppressed.

We then insert Eq. (49) into Eq. (47) and employ Eq. (21) to write the trajectory average. Noting that the denominator in Eq. (49) is simply the quantity O_α defined in Eq. (20), namely $O_\alpha = \text{tr}[\hat{D}(t)]$, we thus obtain

$$\begin{aligned} \hat{\mu}_k(t) &= \sum_{\alpha \in \mathcal{A}_0^N} Q_\alpha \frac{\otimes_{r=1}^k \hat{D}_r(t)}{\text{tr}[\hat{D}(t)]^{k-1}} \\ &= \lim_{R \rightarrow 1} \sum_{\alpha \in \mathcal{A}_0^N} Q_\alpha \text{tr}_{r=k+1, \dots, R} \left[\bigotimes_{r=1}^R \hat{D}_r(t) \right], \end{aligned} \quad (52)$$

where the second equality implements the standard replica trick. Before this step, the rates Γ_α defined in Eq. (18) cancelled term by term in the sum over α . This cancellation is lost once we exchange the order of summing over trajectories with the limit $R \rightarrow 1$. For any $R > 1$, individual terms retain explicit dependence on Γ_α , so different choices of Γ_α become equivalent only after the replica limit is taken.

Averages such as Eq. (48) can then be obtained by introducing source fields into the Hamiltonian \hat{H} in Eq. (1) and differentiating the corresponding R -replica Keldysh partition function with respect to these sources,

$$Z_R(t) = \sum_{\alpha \in \mathcal{A}_0^N} Q_\alpha \text{tr} \left[\bigotimes_{r=1}^R \hat{D}_r(t) \right] = \sum_{\alpha \in \mathcal{A}_0^N} Q_\alpha \prod_{r=1}^R Z_r(t), \quad (53)$$

where $Z_r(t) = \text{tr}[\hat{D}_r(t)]$. After taking the derivatives that generate the desired observables, the source fields have to be set to zero. The replica limit $R \rightarrow 1$ has to be taken only at the end of the computation.

IV. REPLICA KELDYSH PARTITION FUNCTION

Building on the groundwork laid in Secs. II and III, we now derive a functional-integral representation of the partition function (53) using the Keldysh technique [45–49]. To begin, we consider a single factor $Z_r(t)$ in the product over replicas in Eq. (53). Using Eq. (50), $Z_r(t)$ takes the form

$$Z_r(t) = \text{tr} \left(\hat{J}_{r,\alpha_N} \cdots \hat{J}_{r,\alpha_1} |\psi_{r,0}\rangle\langle\psi_{r,0}| \hat{J}_{r,\alpha_1}^\dagger \cdots \hat{J}_{r,\alpha_N}^\dagger \right). \quad (54)$$

Within the Keldysh formalism, the products of Kraus operators acting on the ket and bra components of $|\psi_{r,0}\rangle\langle\psi_{r,0}|$

are interpreted as describing evolution along the forward and backward branches of the closed time contour. A functional-integral representation follows from inserting coherent-state resolutions of the identity between successive Kraus operators. This construction yields fields $\psi_{\sigma,r}(t)$ and $\psi_{\sigma,r}^*(t)$, defined on both Keldysh branches $\sigma = \pm$ and for each replica $r \in \{1, \dots, R\}$. Additional indices, such as those labeling lattice sites, are left implicit. For bosonic systems the two fields are complex conjugates, while for fermionic systems they are independent Grassmann variables. We thus obtain

$$Z_r(t) = \int D[\psi_r^*, \psi_r] e^{i(S_{r,L}[\psi_r^*, \psi_r] + S_{r,D}[\psi_r^*, \psi_r])} Z_{r,J}[\psi_r^*, \psi_r]. \quad (55)$$

The exponential factor describes continuous evolution and consists of two contributions: first, a Liouvillian term $S_{r,L}[\psi_r^*, \psi_r]$, which accounts for unitary evolution generated by the Hamiltonian \hat{H} and, as discussed in Sec. V, acquires additional dissipative contributions in the case of inefficient detection; second, a decay term $S_{r,D}[\psi_r^*, \psi_r]$ associated with the anti-Hermitian part of the effective Hamiltonian (3). The remaining factor, $Z_{r,J}[\psi_r^*, \psi_r]$, encodes the effect of quantum jumps. Collecting the contributions from all replicas, the full replica partition function (53) can be written as

$$Z_R(t) = \int D[\psi^*, \psi] e^{i(S_L[\psi^*, \psi] + S_D[\psi^*, \psi] + S_J[\psi^*, \psi])}, \quad (56)$$

where

$$S_L[\psi^*, \psi] = \sum_{r=1}^R S_{r,L}[\psi_r^*, \psi_r], \quad S_D[\psi^*, \psi] = \sum_{r=1}^R S_{r,D}[\psi_r^*, \psi_r], \quad (57)$$

and the jump contribution is defined by

$$e^{iS_J[\psi^*, \psi]} = \sum_{\alpha \in \mathcal{A}_0^N} Q_\alpha \prod_{r=1}^R Z_{r,J}[\psi_r^*, \psi_r]. \quad (58)$$

In the following, we derive explicit expressions for $S_L[\psi^*, \psi]$, $S_D[\psi^*, \psi]$, and $S_J[\psi^*, \psi]$.

A. Hamiltonian and dissipative Keldysh action

For continuous evolution, the Hamiltonian part of $\hat{J}_{r,0}$ in Eq. (19) produces, upon exponentiation, the standard Hamiltonian contribution to the Keldysh action, while the remaining terms in $\hat{J}_{r,0}$ give rise to a decay contribution. Accordingly, the Liouvillian and decay components of the Keldysh action are

$$\begin{aligned} S_L[\psi^*, \psi] &= \sum_{\sigma=\pm} \sigma \int_{t_0}^t dt' \sum_{r=1}^R \left[\psi_{\sigma,r}^*(t') i\partial_t \psi_{\sigma,r}(t') - H_{\sigma,r}(t') \right], \\ iS_D[\psi^*, \psi] &= -\frac{1}{2} \sum_{\sigma=\pm} \int_{t_0}^t dt' \sum_{r=1}^R \left[\sum_{a=1}^A \gamma_a D_{\sigma,r,a}(t') - \Gamma_0 \right]. \end{aligned} \quad (59)$$

In these expressions, $H_{\sigma,r}(t)$ and $D_{\sigma,r,a}(t)$ denote matrix elements in coherent states,

$$H_{\sigma,r}(t) = \frac{\langle \zeta_\sigma \psi_\sigma(t) | \hat{H}_r | \zeta_\sigma \psi_\sigma(t) \rangle}{\langle \zeta_\sigma \psi_\sigma(t) | \zeta_\sigma \psi_\sigma(t) \rangle}, \quad (60)$$

$$D_{\sigma,r,a}(t) = \frac{\langle \zeta_\sigma \psi_\sigma(t) | \hat{c}_{r,a}^\dagger \hat{c}_{r,a} | \zeta_\sigma \psi_\sigma(t) \rangle}{\langle \zeta_\sigma \psi_\sigma(t) | \zeta_\sigma \psi_\sigma(t) \rangle}, \quad (61)$$

where $\zeta_\sigma = +1$ for bosons and $\zeta_\sigma = \sigma$ for fermions; that is, as standard in the Keldysh formalism, the sign of fermionic fields on the backward branch is flipped [47].

According to Eq. (2), the probability of a quantum jump in a single time step is $O(\Delta t)$. As a result, a typical trajectory consists of extended periods of continuous evolution, described by $\hat{J}_{0,r}$ in Eq. (19), interrupted by isolated jumps represented by $\hat{J}_{a,r}$. In the continuous-time limit, the jump times form a set of measure zero within the evolution interval $[t_0, t]$, so that the integrals in Eq. (59) extend over the entire evolution.

B. Jump Keldysh action

Having discussed the Liouvillian and decay contributions to the Keldysh action, which encode the continuous evolution, we next turn to the contribution due to quantum jumps (58). Here we distinguish between uniform and detailed rescaling.

1. Jump Keldysh action for uniform rescaling

As discussed in Sec. II C 1, for uniform rescaling, each trajectory is specified by the jump times t_m and the jump types a_m . In this case, $Z_{r,J}$ is given by the product of coherent-state matrix elements of the rescaled jump operators (19),

$$Z_{r,J} = \prod_{m=1}^M \frac{\gamma_{a_m}}{\Gamma_1} V_{r,a_m}(t_m), \quad (62)$$

with the vertex

$$V_{r,a}(t) = c_{+,r,a}(t) c_{-,r,a}^\dagger(t), \quad (63)$$

where $c_{+,r,a}(t)$ and $c_{-,r,a}^\dagger(t)$ are defined analogously to Eqs. (60) and (61):

$$c_{\sigma,r,a}(t) = \frac{\langle \zeta_\sigma \psi_\sigma(t) | \hat{c}_{r,a} | \zeta_\sigma \psi_\sigma(t) \rangle}{\langle \zeta_\sigma \psi_\sigma(t) | \zeta_\sigma \psi_\sigma(t) \rangle}, \quad (64)$$

$$c_{\sigma,r,a}^\dagger(t) = \frac{\langle \zeta_\sigma \psi_\sigma(t) | \hat{c}_{r,a}^\dagger | \zeta_\sigma \psi_\sigma(t) \rangle}{\langle \zeta_\sigma \psi_\sigma(t) | \zeta_\sigma \psi_\sigma(t) \rangle}.$$

Since Eq. (62) factorizes over jumps, we can use Eq. (35) to perform the average over trajectories and thus derive the jump action (58), resulting in

$$iS_J[\psi^*, \psi] = \int_{t_0}^t dt' \left[\Gamma_1 \sum_{a=1}^A \prod_{r=1}^R \frac{\gamma_a}{\Gamma_1} V_{r,a}(t') - \Gamma_0 \right]. \quad (65)$$

It is straightforward to verify that terms containing Γ_0 and Γ_1 cancel in the replica limit $R \rightarrow 1$ when summing the decay and jump actions in Eq. (56).

2. Jump Keldysh action for detailed rescaling

The parameterization of trajectories for detailed rescaling is given at the beginning of Sec. II C 2: for each type of jump a , we specify the number of jumps M_a and the times t_{a,m_a} at which jumps occur. We thus obtain

$$Z_{r,J} = \prod_{a=1}^A \prod_{m_a=1}^{M_a} \frac{\gamma_a}{\Gamma_a} V_{r,a}(t_{a,m_a}). \quad (66)$$

Inserting this in Eq. (58) and using Eq. (46) to take the average over trajectories, we find

$$iS_J[\psi^*, \psi] = \int_{t_0}^t dt' \left[\sum_{a=1}^A \Gamma_a \prod_{r=1}^R \frac{\gamma_a}{\Gamma_a} V_{r,a}(t') - \Gamma_0 \right]. \quad (67)$$

This expression reduces to Eq. (65) for $\Gamma_1 = \dots = \Gamma_A$. Therefore, in the following, we continue to work with Eq. (67).

V. INEFFICIENT DETECTION

In studies of measurement-induced phase transitions, measurements are usually assumed to be perfect, meaning that they extract complete information about the measured observable. Under such idealized conditions, the dynamics preserve the purity of the quantum state. In any experimental realization, however, imperfections are unavoidable [35–40]: states decohere due to imperfect measurements, classical noise, and unwanted coupling to the environment, leading to mixed-state dynamics. A particularly relevant example is inefficient detection, where only a fraction of the quantum jumps is registered [51–54]. The fraction of detected jumps is quantified by the detection efficiency $\eta \in [0, 1]$, interpolating between the limit of fully efficient detection with $\eta = 1$, which yields pure-state trajectories, and that of fully inefficient detection with $\eta = 0$, where the dynamics become deterministic and are governed by the Liouvillian (7).

The fate of measurement-induced phase transitions at finite η depends sensitively on the structure of the jump operators. As discussed in Sec. II B, when jump operators represent random projective measurements, the stationary state of the deterministic Lindbladian dynamics is typically a featureless infinite-temperature state, regardless of the measurement rate. Consequently, signatures of measurement-induced phase transitions vanish entirely in the limit $\eta \rightarrow 0$. By contrast, for non-Hermitian jump operators, the steady state is generically nontrivial even at $\eta = 0$. The parameter η therefore provides a natural interpolation between measurement-induced phase transitions of continuously monitored systems and phase transitions in the nonequilibrium steady states of driven open quantum matter.

We model a detector of finite efficiency $\eta \in [0, 1]$ by splitting each time step Δt into two substeps of duration $\eta \Delta t$ and $(1 - \eta) \Delta t$, respectively [54]. The Kraus operators in Eqs. (1) and (2) are then modified as follows: For the first time substep,

$$\hat{K}_{1,0} = 1 - i\eta \hat{H}_{\text{eff}} \Delta t, \quad \hat{K}_{1,a} = \sqrt{\eta \gamma_a \Delta t} \hat{c}_a, \quad (68)$$

and for the second substep,

$$\hat{K}_{2,0} = 1 - i(1-\eta)\hat{H}_{\text{eff}}\Delta t, \quad \hat{K}_{2,a} = \sqrt{(1-\eta)\gamma_a\Delta t}\hat{c}_a. \quad (69)$$

Inefficient detection is implemented by stochastically unravelling the evolution during the first substep, while in the second substep we apply deterministic averaged evolution. The discussion of trajectories in Sec. II B generalizes accordingly: For a system in a mixed state $\hat{\rho}$, the probability for an evolution of type α to occur in a single time step is

$$P_\alpha = \text{tr}(\mathcal{K}_2\mathcal{K}_{1,\alpha}\hat{\rho}) = \text{tr}(\mathcal{K}_{1,\alpha}\hat{\rho}), \quad (70)$$

where

$$\mathcal{K}_{1,\alpha}\hat{\rho} = \hat{K}_{1,\alpha}\hat{\rho}\hat{K}_{1,\alpha}^\dagger, \quad (71)$$

and

$$\mathcal{K}_2\hat{\rho} = \sum_{a=1}^A \hat{K}_{2,a}\hat{\rho}\hat{K}_{2,a}^\dagger = [1 + (1-\eta)\mathcal{L}\Delta t]\hat{\rho}, \quad (72)$$

with the Liouvillian superoperator (7). Note that evolution with \mathcal{K}_2 conserves the trace; this is why \mathcal{K}_2 may be omitted after the second equality in Eq. (70).

A trajectory over N time steps is specified by a sequence of outcomes α of the measurements performed in each first time substep; the probability for this sequence is

$$P_\alpha = \text{tr}(\mathcal{K}_2\mathcal{K}_{1,\alpha_N}\cdots\mathcal{K}_2\mathcal{K}_{1,\alpha_1}\hat{\rho}_0), \quad (73)$$

and the normalized state after N time steps is

$$\hat{\rho}_\alpha = \mathcal{K}_2\mathcal{K}_{1,\alpha_N}\cdots\mathcal{K}_2\mathcal{K}_{1,\alpha_1}\hat{\rho}_0 / \sqrt{P_\alpha}. \quad (74)$$

Having specified the discrete-time quantum jump process for inefficient detection, we now discuss how the associated Keldysh field theory is modified as compared to the one for efficient detection. As a preliminary step, it will prove convenient to modify the factors q_α appearing in the definition (18) of rescaled Kraus operators for the first substep by replacing $\Gamma_\alpha \rightarrow \eta\Gamma_\alpha$. In the second substep, where the evolution is averaged, no rescaling is required.

We begin by examining how inefficient detection modifies the Liouvillian contribution to the Keldysh action (59). Most importantly, the factors \mathcal{K}_2 appearing in Eq. (74) generate additional terms in the action: evolution implemented by \mathcal{K}_2 in Eq. (72) is governed by the Liouvillian superoperator (7), which contains both coherent and dissipative terms. The latter yield a contribution that can be obtained as described in Refs. [46–49]. We find

$$\begin{aligned} S_L[\psi^*, \psi] = & \int_{t_0}^t dt' \sum_{r=1}^R \left\{ \sum_{\sigma=\pm} \sigma \left[\psi_{\sigma,r}^*(t') i\partial_t \psi_{\sigma,r}(t') - H_{\sigma,r}(t') \right] \right. \\ & \left. - i(1-\eta) \sum_{a=1}^A \gamma_a \left[V_{r,a}(t') - \frac{1}{2} \sum_{\sigma=\pm} D_{\sigma,r,a}(t') \right] \right\}. \quad (75) \end{aligned}$$

Note that the Hamiltonian \hat{H} appears in the Kraus operators in both time substeps in Eqs. (68) and (69) with prefactors

η and $1 - \eta$, respectively. Thus, η cancels in the sum of the respective contributions to the Keldysh action. In contrast, the dissipative part stemming from the Liouvillian (7) appears only in the second time substep (72). Therefore, in Eq. (75) this contribution appears with a prefactor $1 - \eta$.

A second element of the Keldysh action associated with continuous evolution is the decay term in Eq. (59). Under inefficient detection, this term originates solely from the non-Hermitian part of the effective Hamiltonian in the first time substep, Eq. (68). Although an analogous term also appears in the second substep (69), its effect is already encoded in Eq. (75). Consequently, the decay part of the Keldysh action is simply multiplied by a factor of η :

$$iS_D[\psi^*, \psi] = -\frac{\eta}{2} \sum_{\sigma=\pm} \int_{t_0}^t dt' \sum_{r=1}^R \left[\sum_{a=1}^A \gamma_a D_{\sigma,r,a}(t') - \Gamma_0 \right]. \quad (76)$$

We now turn to the jump action. The discussion in Sec. II C of how to perform the trajectory average in the continuous-time limit for uniform and detailed rescaling relies on different ways of parameterizing quantum trajectories, which remain valid for inefficient detection. The only modification is that due to the rescaling $\Gamma_\alpha \rightarrow \eta\Gamma_\alpha$, the exponents in Eqs. (35) and (46) acquire a prefactor η . However, η drops out of the rescaled Kraus operators corresponding to quantum jumps. The action that describes jumps is thus

$$iS_J[\psi^*, \psi] = \eta \int_{t_0}^t dt' \left[\sum_{a=1}^A \Gamma_a \prod_{r=1}^R \frac{\gamma_a}{\Gamma_a} V_{r,a}(t') - \Gamma_0 \right]. \quad (77)$$

The Keldysh field theory for quantum-jump processes with inefficient detection is therefore defined by the functional integral in Eq. (56), together with the three contributions to the Keldysh action given in Eqs. (75), (76), and (77). This forms one of the central results of our work. For $R > 1$, the framework allows one to evaluate trajectory averages of observables that are nonlinear in the quantum state, such as the product of expectation values in Eq. (48). Such quantities generally exhibit a nontrivial dependence on the detection efficiency η ; we will present concrete examples in Sec. VI. In contrast, in the limit $R \rightarrow 1$, the construction reduces by design to the standard Lindblad-Keldysh field theory of Refs. [46–49], which captures the dynamics averaged over all measurement outcomes. In particular, in the sum of Eqs. (75), (76), and (77), both η and the auxiliary rates Γ_α cancel out.

VI. IMBALANCED AND INEFFICIENT FERMION COUNTING

We now apply the above formalism to the problem of imbalanced and inefficient fermion counting. Specifically, we consider a 1D fermionic lattice system subject to monitored fermion gain and loss, where the two occur at different rates and only a fraction of the corresponding jumps is detected. Our analysis extends the results of Ref. [30], which focused on the balanced and perfectly efficient case. When gain and loss rates coincide, fermion counting can be cast as a sequence

of generalized measurements performed at random times with a fixed rate, and the associated field theory was derived in Ref. [30] by adapting the framework introduced in Ref. [19] for random projective measurements. In contrast, handling imbalanced rates lies beyond that construction and requires the more general approach developed in this work.

A. Model

We consider free fermions on a 1D lattice of size L , with annihilation and creation operators $\hat{\psi}_l$ and $\hat{\psi}_l^\dagger$, respectively. The Hamiltonian is

$$\hat{H} = \sum_{l,l'=1}^L \hat{\psi}_l^\dagger H_{l,l'} \hat{\psi}_{l'}. \quad (78)$$

Our final results focus on nearest-neighbor hopping between sites l and $l \pm 1$, described by

$$H_{l,l'} = -J(\delta_{l+1,l'} + \delta_{l,l'+1}), \quad (79)$$

where Kronecker deltas are understood modulo L to impose periodic boundary conditions. In intermediate steps, however, we keep the discussion general and leave the Hermitian matrix H unspecified.

Fermion counting involves two types of jump operators on each lattice site describing fermion gain and loss,

$$\hat{c}_{+,l} = \hat{\psi}_l^\dagger, \quad \hat{c}_{-,l} = \hat{\psi}_l, \quad (80)$$

with spatially uniform jump rates γ_\pm . Thus, in the notation of the previous sections, the jump-type index a is replaced by the pair of indices $\alpha = \pm$ and l .

For balanced rates, $\gamma_+ = \gamma_-$, the stationary state of the unconditional dynamics is a featureless infinite-temperature state, independent of the jump rate [30]. Sites are uncorrelated, and each site is empty or occupied with equal probability, corresponding to a mean fermion density of $n = 1/2$. When $\gamma_+ \neq \gamma_-$, the steady state remains factorized over sites,

$$\hat{\rho}_{ss} = \prod_{l=1}^L \frac{1}{\gamma_+ + \gamma_-} [\gamma_+ \hat{n}_l + \gamma_- (1 - \hat{n}_l)], \quad (81)$$

where $\hat{n}_l = \hat{\psi}_l^\dagger \hat{\psi}_l$. However, the fermion density in the steady state is now generally different from $n = 1/2$ and given by

$$n = \frac{\gamma_+}{\gamma_+ + \gamma_-}. \quad (82)$$

Our model therefore provides a minimal example in which the stationary state of the unconditional dynamics depends non-trivially on the jump rates.

In what follows, instead of specifying the rates γ_\pm , it is often convenient to use the steady-state density n as a free parameter of the model, together with the average jump rate

$$\gamma = (\gamma_+ + \gamma_-)/2. \quad (83)$$

B. Replica Keldysh field theory

Having defined the model, we now apply the results of Sec. V to derive the replica Keldysh field theory for imbalanced and inefficient fermion counting.

1. Fermionic replica Keldysh action

The field-theoretic description of imbalanced and inefficient fermion counting is encoded in the functional-integral representation of the partition function (56), with the action consisting of the Liouvillian (75), decay (76), and jump terms (77), where we set $\Gamma_\pm = \gamma_\pm$ and $\Gamma_0 = L\gamma$. To obtain the explicit form of the action, we evaluate the coherent-state matrix elements in Eqs. (60), (61), and (64), with the last of these determining the vertex in Eq. (63). The calculation relies on fermionic anticommutation relations to normal-order operators, and on the fact that coherent bra and ket states are left and right eigenstates of creation and annihilation operators, respectively. This yields

$$H_{\sigma,r}(t) = \sum_{l,l'=1}^L \psi_{\sigma,r,l}^*(t) H_{l,l'} \psi_{\sigma,r,l'}(t). \quad (84)$$

The matrix elements (61) entering the Liouvillian and decay parts of the action take the form

$$\begin{aligned} D_{\sigma,r,+l}(t) &= 1 - \psi_{\sigma,r,l}^*(t) \psi_{\sigma,r,l}(t), \\ D_{\sigma,r,-l}(t) &= \psi_{\sigma,r,l}^*(t) \psi_{\sigma,r,l}(t), \end{aligned} \quad (85)$$

and the vertices (63) associated with fermion gain and loss are

$$\begin{aligned} V_{r,+l}(t) &= -\psi_{+,r,l}^*(t) \psi_{-,r,l}(t), \\ V_{r,-l}(t) &= -\psi_{+,r,l}(t) \psi_{-,r,l}^*(t). \end{aligned} \quad (86)$$

The fermionic replica Keldysh action is the starting point for constructing a long-wavelength effective field theory, formulated in terms of slow modes built from bilinears of fermionic fields [19, 30]. These bilinears are introduced as auxiliary bosonic degrees of freedom via a generalized Hubbard-Stratonovich transformation. Following Refs. [19, 30], below we define the bilinears in the symmetrized limit in which both fermionic fields are evaluated at the same time t . To prepare for the Hubbard-Stratonovich decoupling, we therefore rewrite the action in a strictly time-local form using the “principal-value” regularization scheme [19, 30].

We begin with the matrix elements in Eqs. (60) and (61). Although their form appears time-local in the continuous-time limit, this is not strictly the case: before taking the limit, these expressions involve matrix elements of $\hat{\psi}_{r,l}^\dagger \hat{\psi}_{r,l'}$ evaluated between coherent states separated by a single discrete time step. As a first step, we follow the procedure of Ref. [66] to render these matrix elements strictly time-local, which introduces an additive shift; as a second step, we apply the principal-value regularization, which induces an additional shift. Any such shift in Eq. (84) cancels when summing over the Keldysh

branch index in Eq. (75). The situation is different for the matrix elements in Eq. (85), which take the form

$$D_{\sigma,r,\pm,l}(t) = \frac{1}{2} \mp \psi_{\sigma,r,l}^*(t) \psi_{\sigma,r,l}(t). \quad (87)$$

Since the jump operators (80) are linear in the fermionic fields, the procedure of Ref. [66] introduces no additive shift in the matrix elements (64). Moreover, because the vertices (86) involve products of fields residing on different Keldysh branches, they are unaffected by the principal-value regularization; see Ref. [30] for details.

In what follows, it is convenient to work in the basis [29]

$$\psi = \begin{pmatrix} \psi_+ \\ \psi_- \end{pmatrix}, \quad \psi^\dagger = \begin{pmatrix} \psi_+^\dagger & -\psi_-^\dagger \end{pmatrix}, \quad (88)$$

where ψ_\pm and ψ_\pm^\dagger are column- and row-vectors in replica space. This choice of basis is motivated by the following observations: The usual Larkin-Ovchinnikov transformation of fermionic fields combines the bosonic Keldysh rotation with a sign change of ψ_-^* [45, 49]. This sign change, allowed only for fermionic fields because ψ_- and ψ_-^* are independent Grassmann variables, greatly simplifies the quadratic Hamiltonian part of the Keldysh action by reducing it to the identity in Keldysh space. Here, we implement only the sign change, which already provides a useful simplification, while omitting the bosonic rotation. This choice proves convenient for constructing the NLSM target manifold, whose structure is more transparent in this representation.

In the basis (88), the vertices (86) take the compact form

$$V_{r,\pm,l}(t) = -\psi_{r,l}^\dagger(t) \sigma_\pm \psi_{r,l}(t), \quad (89)$$

where $\sigma_\pm = (\sigma_x \pm i\sigma_y)/2$. Moreover, only the sum over branch indices of the coherent-state matrix elements in Eq. (87) enters the action in Eqs. (75) and (76). This sum can be written as

$$\sum_{\sigma=\pm} D_{\sigma,r,\pm,l}(t) = 1 \mp \psi_{r,l}^\dagger(t) \sigma_z \psi_{r,l}(t). \quad (90)$$

We now rewrite the full action in Eq. (56) using these compact expressions. First, we decompose the action as

$$S = S_L + S_D + S_J = S_H + S_M, \quad (91)$$

where S_H is the Hamiltonian part, the first line of Eq. (75), while S_M contains the remaining terms due to measurements: the second line of Eq. (75) together with Eqs. (76) and (77).

The Hamiltonian action reads

$$S_H[\psi^*, \psi] = \sum_{l,l'=1}^L \int_{t_0}^t dt' \psi_l^\dagger(t') G_{0,l,l'}^{-1} \psi_{l'}(t'), \quad (92)$$

with

$$G_0^{-1} = i\partial_t - H, \quad (93)$$

where H is the Hamiltonian matrix in Eq. (78).

The measurement action takes the form

$$S_M[\psi^*, \psi] = \sum_{l=1}^L \int_{t_0}^t dt' \mathcal{L}_M[\psi_l^*(t'), \psi_l(t')], \quad (94)$$

with measurement Lagrangian

$$\begin{aligned} i\mathcal{L}_M[\psi^*, \psi] = & -(1-\eta) \psi^\dagger \Lambda \psi + \frac{\eta \Delta \gamma}{2} \psi^\dagger \sigma_z \psi \\ & + \eta \sum_{\alpha=\pm} \gamma_\alpha \prod_{r=1}^R (-\psi_r^\dagger \sigma_\alpha \psi_r) - \gamma [R + \eta(1-R)], \end{aligned} \quad (95)$$

where the net gain rate is

$$\Delta \gamma = \gamma_+ - \gamma_-. \quad (96)$$

In Eq. (95), the matrices σ_\pm , σ_z , and

$$\Lambda = \begin{pmatrix} 1-2n & 2n \\ 2(1-n) & -1+2n \end{pmatrix}, \quad (97)$$

with density given in Eq. (82), act nontrivially in Keldysh space; the identity in replica space is left implicit. To obtain the form of Eq. (95), we used

$$\sum_{\alpha=\pm} \gamma_\alpha \left(\sigma_\alpha - \frac{\alpha}{2} \sigma_z \right) = \gamma \Lambda. \quad (98)$$

The matrix Λ encodes the symmetrized equal-time limit of the exact Green's functions for a given mean fermion density [30]. It will play an important role in our analysis of the saddle-point structure of the Keldysh action.

2. Generalized Hubbard-Stratonovich transformation

The generalized Hubbard-Stratonovich transformation is implemented by inserting the following identity into the functional integral (56) [19]:

$$1 = \int D[\mathcal{G}, \Sigma] e^{-i \text{Tr}[(\mathcal{G} + i\psi\psi^\dagger)\Sigma]}, \quad (99)$$

where \mathcal{G} and Σ are Hermitian $2R \times 2R$ matrix fields. We use Tr to denote a trace that acts in Keldysh, replica, lattice, and time spaces. The integration over Σ yields a delta functional that enforces the identity $\mathcal{G} = -i\psi\psi^\dagger$. Together with the principal-value regularization, this ensures that the expectation value $\langle \mathcal{G}(t) \rangle$ coincides with the fermionic Green's function in the symmetrized equal-time limit,

$$\langle \mathcal{G}_l(t) \rangle = -\frac{i}{2} (\langle \psi_l(t) \psi_l^*(t+0^+) \rangle + \langle \psi_l(t) \psi_l^*(t-0^+) \rangle). \quad (100)$$

The identity $\mathcal{G} = -i\psi\psi^\dagger$ further allows us to recast the measurement Lagrangian (95) entirely in terms of \mathcal{G} . For the first two terms in (95), we use

$$\psi^\dagger \Lambda \psi = -\text{tr}(\Lambda \psi \psi^\dagger) = -i \text{tr}(\Lambda \mathcal{G}), \quad \psi^\dagger \sigma_z \psi = -i \text{tr}(\sigma_z \mathcal{G}). \quad (101)$$

Following [19], we decouple the product over replicas in the third term of Eq. (95) simultaneously in all slow channels by summing over Wick contractions, which yields

$$i\mathcal{L}_M[\mathcal{G}] = i(1-\eta)\gamma \text{tr}(\Lambda\mathcal{G}) - \frac{i\eta\Delta\gamma}{2} \text{tr}(\sigma_z\mathcal{G}) + i^R\eta \sum_{\alpha=\pm} \gamma_\alpha \det_R[\text{tr}_K(\sigma_\alpha\mathcal{G})] - \gamma[R + \eta(1-R)], \quad (102)$$

where tr_K denotes a partial trace in Keldysh space, and \det_R is the determinant in the remaining replica space. The measurement Lagrangian given in Ref. [30] for balanced and efficient fermion counting is recovered by setting $\gamma_+ = \gamma_-$ and $\eta = 1$. In the limit $R \rightarrow 1$, Eq. (102) reduces to

$$i\mathcal{L}_M[\mathcal{G}] = \gamma[i \text{tr}_K(\Lambda\mathcal{G}) - 1]. \quad (103)$$

With the measurement Lagrangian rewritten in terms of \mathcal{G} , the fermionic integral (56) becomes Gaussian and can be evaluated explicitly. This yields the partition function in the form

$$Z_R(t) = \int D[\mathcal{G}, \Sigma] e^{iS[\mathcal{G}, \Sigma]}, \quad (104)$$

where the action is

$$S[\mathcal{G}, \Sigma] = S_0[\mathcal{G}, \Sigma] + \sum_{l=1}^L \int_{t_0}^t dt' \mathcal{L}_M[\mathcal{G}_l(t')], \quad (105)$$

with the measurement Lagrangian (102) and

$$iS_0[\mathcal{G}, \Sigma] = \text{Tr}[\ln(i\partial_t - H + i\Sigma) - i\mathcal{G}\Sigma]. \quad (106)$$

3. Continuous symmetries of the replica Keldysh action

A prerequisite for understanding the long-wavelength behavior of our model is a characterization of the global continuous symmetries of the replica Keldysh action. This analysis will inform both the discussion of the Gaussian theory in Sec. VI C and the construction of the NLSM in Sec. VI D. Of particular importance are unitary field transformations, $\psi \mapsto \mathcal{R}\psi$ with $\mathcal{R} \in U(2R)$, since breaking such symmetries leads to the appearance of massless Goldstone modes.

Due to the identity $\mathcal{G} = -i\psi\psi^\dagger$, the matrix field \mathcal{G} transforms as $\mathcal{G} \mapsto \mathcal{R}\mathcal{G}\mathcal{R}^{-1}$. When does such a transformation constitute a symmetry? The action in Eq. (106) is invariant under arbitrary transformations of \mathcal{G} provided Σ is transformed simultaneously as $\Sigma \mapsto \mathcal{R}\Sigma\mathcal{R}^{-1}$. Nontrivial constraints on the symmetry group $G \leq U(2R)$ therefore arise from the measurement Lagrangian (102) by requiring $\mathcal{L}_M[\mathcal{G}] = \mathcal{L}_M[\mathcal{R}\mathcal{G}\mathcal{R}^{-1}]$. To specify these constraints, we analyze the measurement Lagrangian term by term.

We first consider efficient detection with $\eta = 1$, in which case the first term in Eq. (102) vanishes. The second term, proportional to $\text{tr}(\sigma_z\mathcal{G})$, is invariant if

$$\mathcal{R}\sigma_z\mathcal{R}^{-1} = \sigma_z. \quad (107)$$

This holds when \mathcal{R} is block-diagonal in Keldysh space,

$$\mathcal{R} = \begin{pmatrix} \mathcal{V}_+ & 0 \\ 0 & \mathcal{V}_- \end{pmatrix}, \quad (108)$$

with $\mathcal{V}_\pm \in U(R)$, so that $\mathcal{R} \in U(R) \times U(R)$.

The matrices \mathcal{V}_\pm are further constrained by the third term in the measurement Lagrangian (102). Consider first the contribution with $\alpha = -$. Inserting the transformed \mathcal{G} , the determinant in replica space factorizes as

$$\det_R[\text{tr}_K(\sigma_- \mathcal{R}\mathcal{G}\mathcal{R}^{-1})] = \frac{\det_R(\mathcal{V}_+)}{\det_R(\mathcal{V}_-)} \det_R[\text{tr}_K(\sigma_- \mathcal{G})]. \quad (109)$$

The final factor appears also in the original expression in Eq. (102). Hence, \mathcal{R} is a symmetry if the prefactor reduces to unity, which is the case if $\det_R(\mathcal{V}_+) = \det_R(\mathcal{V}_-)$. The same condition follows from the term with $\alpha = +$.

To determine the symmetry group G , note that the unitary group factorizes as $U(R) = U(1) \rtimes SU(R)$, separating the global phase from the special-unitary part. Because \mathcal{V}_+ and \mathcal{V}_- must have equal determinants, only a single global $U(1)$ factor remains. Thus the symmetry group is

$$G \cong U(1) \rtimes [SU(R) \times SU(R)]. \quad (110)$$

The block-diagonal constraint (108) arises from the second term in Eq. (102), which vanishes for balanced fermion counting with $\Delta\gamma = 0$. We did not find a way to exclude the possibility that, for $\Delta\gamma = 0$, the remaining third term might admit non-block-diagonal symmetries. However, in particle-number-conserving models, \mathcal{R} can indeed be shown to be block-diagonal [29, 30]. Since fermion counting breaks particle-number conservation, the symmetry group of the action is expected to be more restricted in this case. Therefore, transformations \mathcal{R} should remain block-diagonal.

We now turn to inefficient detection with $\eta < 1$. The first term in Eq. (102) introduces the additional constraint

$$\mathcal{R}\Lambda\mathcal{R}^{-1} = \Lambda, \quad (111)$$

which forces $\mathcal{V}_+ = \mathcal{V}_-$. The symmetry group (110) is therefore reduced to

$$G \cong U(R). \quad (112)$$

4. Continuous symmetries in the operator formalism

We briefly digress to connect the symmetries of the Keldysh action to weak and strong symmetries of the time-evolution superoperator [67, 68]. A constructive approach to identifying operator symmetries is presented in Ref. [30]; instead, here we derive them from the field-theoretic formulation.

The identity $\mathcal{G} = -i\psi\psi^\dagger$, together with the definition of the field vectors in Eq. (88) and the block-diagonal form of \mathcal{R} in Eq. (108), implies that the two blocks \mathcal{V}_\pm act separately on the field components ψ_\pm on the forward and backward branches of the closed time contour. In general, field transformations that act independently on the two branches

correspond to strong symmetries of the time-evolution superoperator, whereas transformations acting identically on both branches correspond to weak symmetries [47].

For $\eta = 1$, we found that $\mathcal{V}_\pm \in \text{U}(R)$ with the constraint $\det_R(\mathcal{V}_+) = \det_R(\mathcal{V}_-)$. The common determinant defines a weak $\text{U}(1)$ symmetry. Aside from sharing this determinant, the matrices \mathcal{V}_\pm remain independent, giving rise to a strong $\text{SU}(R)$ symmetry. As we will see in Sec. VID, it is precisely this strong $\text{SU}(R)$ symmetry that underlies the NLSM.

For $\eta < 1$, we obtained the additional constraint $\mathcal{V}_+ = \mathcal{V}_-$, reducing the symmetry group from Eq. (110) to Eq. (112) and thus leaving only a weak $\text{U}(R)$ symmetry. That inefficient detection breaks the symmetry required for the NLSM description was already anticipated for balanced fermion counting in Ref. [30]. Furthermore, Ref. [30] also shows that two conditions are necessary for the strong $\text{SU}(R)$ symmetry underlying the NLSM to emerge in free fermionic systems: (i) conservation of the total particle number of the system and reservoirs, and (ii) conservation of the purity of the state of the system. The latter requires keeping a complete record of measurement outcomes, which is fulfilled only when $\eta = 1$.

C. Gaussian theory

Following Refs. [19, 30], we first analyze the theory within the Gaussian approximation. Specifically, we determine the replica-symmetric saddle point of the Keldysh action and restrict the functional integral (104) to quadratic fluctuations around this saddle point. This approximation is valid for small γ and on short to intermediate length scales.

1. Saddle point and fluctuations

The saddle-point equations $\delta S/\delta\mathcal{G} = 0$ and $\delta S/\delta\Sigma = 0$ admit a unique replica-diagonal solution. Replica-asymmetric or replicon saddle points, which form a finite-dimensional manifold, will be discussed in Sec. VID. Setting $R = 1$ in numerical prefactors, the replica-symmetric saddle point is

$$\mathcal{G} = -iQ/2, \quad \Sigma = \gamma Q, \quad Q = \Lambda, \quad (113)$$

independent of η , and with Λ defined in Eq. (97). Gaussian fluctuations around this saddle point can be parameterized as

$$\mathcal{G} = -i(\Lambda + \delta\mathcal{Q}_\mathcal{G})/2, \quad \Sigma = \gamma(\Lambda + \delta\mathcal{Q}_\Sigma)/2, \quad (114)$$

where $\delta\mathcal{Q}_\mathcal{G}$ and $\delta\mathcal{Q}_\Sigma$ are $2R \times 2R$ matrices. The Gaussian theory is obtained by expanding the Keldysh action (105) to second order in $\delta\mathcal{Q}_\mathcal{G}$ and $\delta\mathcal{Q}_\Sigma$ as detailed in Refs. [19, 30].

A key feature of fluctuations around the saddle point can be anticipated from the discussion of symmetries in Sec. VIB 3: since the saddle point (113) partially breaks these symmetries, certain types of fluctuations become massless Goldstone modes. The manifold of these modes is the quotient G/H , where G is the symmetry group of the Keldysh action, given by Eqs. (110) and (112) for $\eta = 1$ and $\eta < 1$, respectively,

and H is the subgroup of G that leaves the saddle point invariant, as expressed by Eq. (111). In Sec. VIB 3, we already identified $H \cong \text{U}(R)$ for inefficient detection.

It follows that for $\eta = 1$, the Goldstone manifold $G/H \cong \text{SU}(R)$ is nontrivial, whereas for $\eta < 1$, $G = H$ and the quotient G/H is trivial. Hence, massless modes arise for $\eta = 1$ due to the strong $\text{SU}(R)$ symmetry discussed in Sec. VIB 4, and they acquire a mass when this strong symmetry is broken for $\eta < 1$.

The physics of fluctuations of these Goldstone modes on the nonlinear manifold is discussed in Sec. VID. But first, we focus on linearized fluctuations. As we show, within this approximation, the massless modes for $\eta = 1$ generate algebraic correlations and logarithmic growth of entanglement, whereas the mass term for $\eta < 1$ introduces a finite correlation length.

2. Connected density correlation function

As discussed in Sec. III, the nontrivial effects of measurements become apparent in nonlinear observables. We focus here on the equal-time connected density correlation function, defined in the operator formalism and in terms of field expectation values as [19]

$$\begin{aligned} C_{l,l'}(t) &= \frac{1}{2} \langle \{\hat{n}_l(t), \hat{n}_{l'}(t)\} \rangle - \langle \hat{n}_l(t) \rangle \langle \hat{n}_{l'}(t) \rangle \\ &= C_{r,r',l,l'}(t,t) - C_{r,r',l,l'}(t,t), \end{aligned} \quad (115)$$

where the correlation function of density fluctuations is

$$C_{r,r',l,l'}(t,t') = \langle \delta\rho_{r,l}(t) \delta\rho_{r',l'}(t') \rangle. \quad (116)$$

Permutation symmetry among replicas renders the specific choice of r and r' in Eq. (115) irrelevant, provided that $r \neq r'$. The density fluctuations in Eq. (116) are related to the $\delta\mathcal{Q}_\mathcal{G}$ in Eq. (114) via [19]

$$\delta\rho_{r,l}(t) = -\frac{1}{4} \text{tr}_K[\sigma_x \delta\mathcal{Q}_{\mathcal{G},r,r,l}(t)]. \quad (117)$$

The correlation function (115) can be calculated explicitly in the Gaussian approximation. In the steady state, $C_{l,l'}(t)$ becomes time-independent and translationally invariant, allowing us to write $C_{l,l'}(t) = C_{l-l'}$. When calculating C_l , boundary effects due to stopping the measurement process at finite time t must be taken into account [19]. This leads to an expression for the correlation function in momentum space, C_q , in terms of the solution of an integral equation that depends on the two parameters $u = 2l_0 \sin(q/2)$ and η , where

$$l_0 = \frac{J}{\sqrt{2}\gamma}. \quad (118)$$

However, the leading asymptotic behavior of C_q for small momenta and small detection inefficiency $\delta\eta = 1 - \eta$ is correctly reproduced in the bulk approximation [19], in which the boundary condition in time is neglected and we rescale $u \rightarrow 2u$ and $\delta\eta \rightarrow 4\delta\eta$, leading to the following expression for the correlation function:

$$C_q \approx n(1-n)\tilde{c}(ql_0), \quad (119)$$

with

$$\tilde{c}(u) = \frac{2}{\pi} \int_0^\infty dv \left\{ \text{Re}[b(2u, v)] - (1 - 4\delta\eta) |b(2u, v)|^2 \right\} \\ \times \left(1 - (1 - 4\delta\eta)^2 |b(2u, v)|^2 - 4(1 - 4\delta\eta) n(1 - n) \right. \\ \left. \times \left\{ \text{Re}[b(2u, v)] - (1 - 4\delta\eta) |b(2u, v)|^2 \right\} \right)^{-1}, \quad (120)$$

where

$$b(u, v) = \left[(1 - iv)^2 + 2u^2 \right]^{-1/2}. \quad (121)$$

For low momenta $q \rightarrow 0$, C_q behaves as

$$C_q \sim \begin{cases} g_0 q - 4n(1-n)(ql_0)^2, & \delta\eta = 0, \\ \frac{g_0}{l_0} \sqrt{(ql_0)^2 + \delta\eta}, & \delta\eta \rightarrow 0, \end{cases} \quad (122)$$

with

$$g_0 = \frac{\sqrt{2}n(1-n)l_0}{\sqrt{1-2n(1-n)}}. \quad (123)$$

Transforming to real space yields

$$C_l \sim \begin{cases} -\frac{g_0}{\pi l^2}, & \delta\eta = 0, \\ -\frac{g_0}{\sqrt{\pi l_0}} \frac{\delta\eta^{1/4}}{l^{3/2}} e^{-l/\xi}, & \delta\eta \rightarrow 0, \end{cases} \quad (124)$$

where

$$\xi = \frac{l_0}{\sqrt{\delta\eta}}. \quad (125)$$

For $\delta\eta = 0$, this reproduces the result of Ref. [30]: Algebraic correlations arise as a manifestation of a massless Goldstone mode, even though particle-number conservation is broken. For $\delta\eta > 0$, correlations are cut off at the scale ξ (125).

3. Subsystem entropy

The second key nonlinear observable we consider is the subsystem entropy. For a system in the state $\hat{\rho}$, the reduced density matrix of a contiguous block of ℓ sites is obtained by tracing out the remaining $L - \ell$ sites, $\hat{\rho}_\ell = \text{tr}_{L-\ell}(\hat{\rho})$. The corresponding von Neumann subsystem entropy is then

$$S_\ell = -\overline{\text{tr}[\hat{\rho}_\ell \ln(\hat{\rho}_\ell)]}. \quad (126)$$

Efficient detection with $\eta = 1$ yields pure-state quantum trajectories, $\hat{\rho} = |\psi\rangle\langle\psi|$, making S_ℓ a genuine measure of entanglement. However, for inefficient detection with $\eta < 1$, the conditional state $\hat{\rho}$ becomes mixed. Then, entanglement can be quantified by the fermionic logarithmic negativity [61, 62], which we discuss further in Sec. VIF4.

The subsystem entropy can be computed using another property of quantum trajectories: evolution under the quadratic Hamiltonian (78) and linear jump operators (80) preserves Gaussianity of the state. For a Gaussian state, S_ℓ is obtained from fluctuations of the subsystem particle number,

$\hat{N}_\ell = \sum_{l=1}^\ell \hat{n}_l$, through a cumulant expansion with coefficients given by the Riemann zeta function $\zeta(k)$ [69]:

$$S_\ell = 2 \sum_{k=1}^\infty \zeta(2k) C_\ell^{(2k)} = \frac{\pi^2}{3} C_\ell^{(2)} + \frac{\pi^4}{45} C_\ell^{(4)} + \dots. \quad (127)$$

We restrict ourselves to the leading term of the expansion, which involves the second cumulant,

$$C_\ell^{(2)} = \overline{\langle (\hat{N}_\ell - \langle \hat{N}_\ell \rangle)^2 \rangle}. \quad (128)$$

Inserting here the explicit expression for \hat{N}_ℓ and using the definition of the conditional density correlation function (115), we obtain

$$S_\ell = \frac{\pi^2}{3} \sum_{l,l'=1}^\ell C_{l-l'} = \frac{2\pi}{3} \int_0^\infty \frac{dq}{q^2} C_q [1 - \cos(q\ell)]. \quad (129)$$

The behavior of the subsystem entropy for large subsystem sizes, $\ell \gg l_0$, follows by inserting the asymptotic form (122) of the density correlation function. For efficient detection, $\delta\eta = 0$, we find

$$S_\ell \sim \frac{2\pi g_0}{3} \ln(\ell/l_0), \quad \delta\eta = 0. \quad (130)$$

That is, for efficient detection, the Gaussian theory predicts logarithmic growth of entanglement on large scales, as in a 1D conformal field theory (CFT) [70].

On short scales $\ell \lesssim l_0$, the system is expected to behave like a Fermi gas at infinite temperature [19], leading to volume-law behavior of the entropy:

$$S_\ell \sim -[n \ln(n) + (1-n) \ln(1-n)] \ell. \quad (131)$$

The prefactor is not fully reproduced by Eq. (129) since higher cumulants in Eq. (127) become significant in this case [19]. We expect volume-law behavior $S_\ell \sim \ell$ to persist for inefficient detection, $\eta < 1$, also at large scales $\ell \gg l_0$. In particular, in the limit $\eta \rightarrow 0$, Eq. (131) describes the exact subsystem entropy of the fully mixed steady state (81).

Deviations from the CFT behavior (130) for $\eta = 1$ arising at short scales and, as discussed below, also at large scales due to nonlinear fluctuations, can be characterized by the scale-dependent effective central charge [30]:

$$c_\ell = 3 \frac{\partial S_\ell}{\partial \ln(\ell)}. \quad (132)$$

Using the Gaussian prediction (130), one finds

$$c_\ell \sim 2\pi g_0, \quad \ell \rightarrow \infty, \quad (133)$$

with g_0 defined in Eq. (123). Nonlinear fluctuations of Goldstone modes drive a renormalization-group (RG) flow of g_0 toward zero on large scales, causing the effective central charge to vanish and the entanglement entropy to cross over from logarithmic to area-law scaling. Next, we discuss how this RG flow can be obtained from an NLSM description.

D. Nonlinear sigma model

As anticipated in Sec. VIC 1, the replica-symmetric saddle point (113) breaks global continuous symmetries of the Keldysh action, thereby giving rise to Goldstone modes. For $\eta = 1$, these modes span a nonlinear manifold, with fluctuations within this manifold described by an NLSM, which we derive in the present section.

In our discussion of the Goldstone-mode manifold, and hence of the target manifold of the NLSM, we have thus far focused exclusively on continuous symmetries of the Keldysh action. We have neglected an important discrete symmetry, to which we now turn: particle-hole symmetry (PHS) [16, 26, 29, 30, 34].

1. Particle-hole symmetry

The quadratic hopping Hamiltonian (78) exhibits PHS if there exists a unitary matrix U with $UU^* = \pm 1$ such that the Hamiltonian matrix H satisfies $UH^*U^\dagger = -H$ [71]. Owing to the Hermiticity of H , this condition is equivalently written as $UH^\top U^\dagger = -H$. Here we focus on the case $UU^* = +1$, which, together with unitarity of U , implies that U is symmetric, $U = U^\top$. By the Autonne-Takagi factorization, such a matrix can be expressed as $U = R^\dagger R^*$, where R is unitary and we have used that all singular values of U are equal to one. For the transformed Hamiltonian $H' = RHR^\dagger$, we obtain

$$H'^\top = R^* H^\top R^\top = -R^* U^\dagger H U R^\top = -H'. \quad (134)$$

Thus, PHS of H implies that H' is skew-symmetric.

In what follows, we leave the explicit form of H unspecified in intermediate expressions. However, for any H possessing PHS, we assume that we work in a basis in which PHS reduces to skew symmetry. Our final results apply to the Hamiltonian matrix (79) describing nearest-neighbor hopping with real hopping amplitudes. For this case, the necessary basis transformation corresponds to a gauge transformation of the field operators, $\hat{\psi}_l \mapsto i\hat{\psi}_l$. This renders the hopping matrix (79) purely imaginary,

$$H_{l,l'} \mapsto -iJ(\delta_{l+1,l'} - \delta_{l,l'+1}). \quad (135)$$

PHS alters the target manifold of the NLSM [16, 26, 29, 30, 34]. To determine this modification, we first explicitly symmetrize the action with respect to PHS and then carry out the generalized Hubbard-Stratonovich transformation on the symmetrized action.

We begin by considering the Hamiltonian contribution to the action (92). Working in the basis of Eq. (88) and leaving the summation over σ , r , and l implicit as matrix multiplication, the Hamiltonian term takes the form

$$\begin{aligned} \psi^\dagger(t)H\psi(t) &= \frac{1}{2}\psi^\dagger(t)(H - H^\top)\psi(t) \\ &= \frac{1}{2}\left(\psi^\dagger(t)H\psi(t) + \psi^\top(t)H\psi^*(t)\right) = \bar{\Psi}(t)H\Psi(t), \end{aligned} \quad (136)$$

where we have introduced the doubled field vectors

$$\Psi = \frac{1}{\sqrt{2}}\begin{pmatrix} \psi \\ -i\sigma_y\psi^* \end{pmatrix}, \quad \bar{\Psi} = \frac{1}{\sqrt{2}}\left(\psi^\dagger, \psi^\top i\sigma_y\right) = \Psi^\top C. \quad (137)$$

To avoid ambiguity, we clarify the notation:

$$\psi^* = \left(\psi^\dagger\right)^\top = \begin{pmatrix} \psi_+^* \\ -\psi_-^* \end{pmatrix}, \quad \psi^\top = (\psi_+, \psi_-). \quad (138)$$

The charge-conjugation matrix C is defined as

$$C = -\sigma_y \otimes \tau_y = C^\top = C^* = C^{-1}, \quad (139)$$

where σ_y and τ_y are Pauli matrices acting in Keldysh and charge-conjugation space, respectively; the identity in replica space is implicit. Note that the doubled field vectors defined in Eq. (137) coincide with those in Ref. [30]. The difference here is that we work in the basis of Eq. (88), which is related to the basis used in Ref. [30] by a bosonic Keldysh rotation.

In terms of the doubled field vectors, the Hamiltonian contribution to the action (92) can thus be written as

$$S_H[\Psi] = \sum_{l,l'=1}^L \int_{t_0}^t dt' \bar{\Psi}_l(t') G_{0,l,l'}^{-1} \Psi_{l'}(t'). \quad (140)$$

The matrices $\pm i\sigma_y$ in Eq. (137) are not strictly required to symmetrize the Hamiltonian part of the action. Their choice is not unique, and an alternative is used in Ref. [29] for projective measurements. However, with the present definition of Ψ and $\bar{\Psi}$, the measurement Lagrangian (95) acquires a form devoid of structure in charge-conjugation space and is therefore manifestly particle-hole symmetric: Using

$$\sigma_y \Lambda^\top \sigma_y = -\Lambda, \quad \sigma_y \sigma_z \sigma_y = -\sigma_z, \quad \sigma_y \sigma_\pm^\top \sigma_y = -\sigma_\pm, \quad (141)$$

we obtain

$$\begin{aligned} i\mathcal{L}_M[\Psi] &= -(1-\eta)\bar{\Psi}\Lambda\Psi + \frac{\eta\Delta\gamma}{2}\bar{\Psi}\sigma_z\Psi \\ &\quad + \eta \sum_{\alpha=\pm} \gamma_\alpha \prod_{r=1}^R \left(-\bar{\Psi}_r \sigma_\alpha \Psi_r\right) - \gamma [R + \eta(1-R)]. \end{aligned} \quad (142)$$

This is formally equivalent to Eq. (95) with the replacements $\psi \rightarrow \Psi$ and $\psi^\dagger \rightarrow \bar{\Psi}$.

The presence or absence as well as the precise form of PHS depends on the details of the model. In contrast, a chiral symmetry is always present, as it is intrinsic to the Keldysh formalism [28, 29]. Consequently, if the Hamiltonian matrix H exhibits PHS, the model belongs to the chiral orthogonal symmetry class BDI; if PHS is broken, it instead falls into the chiral unitary class AIII.

2. Generalized Hubbard-Stratonovich transformation with PHS

We proceed with a generalized Hubbard-Stratonovich transformation of the particle-hole symmetrized action. For systems with PHS, Eq. (99) must be modified to

$$1 = \int D[G, \Sigma] e^{-i\text{Tr}[(G+i\Psi\Psi^\top)\Sigma]}, \quad (143)$$

where \mathcal{G} and Σ are now Hermitian $4R \times 4R$ matrix fields. As before, integrating over Σ produces a delta functional enforcing the identity $\mathcal{G} = -i\Psi\bar{\Psi}$. Using the relation $\bar{\Psi} = \Psi^\top C$ from Eq. (137), this identity implies

$$\bar{\mathcal{G}} = C\mathcal{G}^\top C = -\mathcal{G}. \quad (144)$$

By Eq. (143), the same condition holds for Σ .

The identity $\mathcal{G} = -i\Psi\bar{\Psi}$ allows us to rewrite the measurement Lagrangian (142) in terms of \mathcal{G} . Details of this derivation are given in Appendix B. We find

$$i\mathcal{L}_M[\mathcal{G}] = i(1-\eta)\gamma \text{tr}(\Lambda\mathcal{G}) - \frac{i\eta\Delta\gamma}{2} \text{tr}(\sigma_z\mathcal{G}) + i^R\eta \sum_{\alpha=\pm} \gamma_\alpha e^{\beta \text{tr}_{CR} \ln \text{tr}_K(\frac{1}{\beta}\sigma_\alpha\mathcal{G})} - \gamma[R + \eta(1-R)], \quad (145)$$

where $\beta = 1/2$ for class BDI with PHS, and tr_{CR} denotes a partial trace in charge-conjugation and replica spaces. This result, in a different basis and for the special case of balanced and efficient fermion counting with $\gamma_+ = \gamma_-$ and $\eta = 1$, was stated without proof in Ref. [30]. Formally, it reduces to Eq. (102) when $\beta = 1$, corresponding to class AIII with broken PHS.

With the measurement Lagrangian expressed in terms of \mathcal{G} , performing the remaining integral over Ψ yields the Keldysh partition function in the same form as in Eqs. (104) and (105), where now

$$iS_0[\mathcal{G}, \Sigma] = \text{Tr}[\beta \ln(i\partial_t - H + i\Sigma) - i\mathcal{G}\Sigma], \quad (146)$$

which again formally reduces to Eq. (106) for $\beta = 1$.

3. NLSM target manifold for efficient detection, $\eta = 1$

In Sec. VIB, we derived the Gaussian theory by expanding the action to quadratic order in fluctuations around the saddle point (113). For simplicity, we chose the replica-symmetric saddle point as the reference for this expansion. Applying symmetry transformations to the replica-symmetric saddle point generates other saddle points. The NLSM describes long-wavelength fluctuations of the Goldstone modes within the manifold formed by these saddle points. Therefore, to derive the NLSM, we first need to determine the structure of its target manifold, meaning the manifold of saddle points, and obtain an explicit parameterization. We anticipate that the symmetry underlying the NLSM description is broken for inefficient detection with $\eta < 1$, and hence we first focus on the case of efficient detection with $\eta = 1$.

As a preliminary step, we determine the replica-symmetric saddle point of the particle-hole symmetrized action. Due to the factor β in Eq. (146), the replica-symmetric solution to the saddle-point equations is now

$$\mathcal{G} = -i\beta Q/2, \quad \Sigma = \gamma Q, \quad Q = \Lambda, \quad (147)$$

where, as before, $\beta = 1/2$ for class BDI. For class AIII, we formally recover Eq. (113) by setting $\beta = 1$. Note that the matrix Λ defined in Eq. (97) satisfies condition (144), as follows from Eq. (141):

$$\bar{\Lambda} = C\Lambda^\top C = \sigma_y\Lambda^\top\sigma_y = -\Lambda. \quad (148)$$

We obtain the NLSM target manifold by applying continuous unitary transformations to the replica-symmetric saddle point (147). Specifically, we replace $Q = \Lambda$ by

$$Q = \mathcal{R}\Lambda\mathcal{R}^{-1}, \quad (149)$$

where $\mathcal{R} \in \text{U}(2R)$ for symmetry class AIII and $\mathcal{R} \in \text{U}(4R)$ for class BDI. In the latter case, the transformations must additionally preserve the condition (148), so that $Q = -CQ^\top C$. This requirement is satisfied if $\mathcal{R}^{-1} = \bar{\mathcal{R}}$, which, together with unitarity $\mathcal{R}^{-1} = \mathcal{R}^\dagger$, implies

$$\mathcal{R} = C\mathcal{R}^*C. \quad (150)$$

Equation (147), with Q given by Eq. (149), parameterizes the NLSM manifold if the transformations \mathcal{R} satisfy two conditions: (i) They must be symmetries of the Keldysh action. This ensures that if $Q = \Lambda$ is a saddle point, then $Q = \mathcal{R}\Lambda\mathcal{R}^{-1}$ is also a saddle point. The set of such transformations forms a group G . (ii) They must act nontrivially on the saddle point Λ . Transformations that leave Λ invariant satisfy Eq. (111) and form a subgroup H . To isolate the transformations that satisfy condition (ii), one must factor out the subgroup H . The resulting target manifold of the NLSM is then G/H .

We first determine the restrictions on \mathcal{R} imposed by requirement (i). Note that symmetries for class AIII have already been discussed in Sec. VIB 3. Here, we repeat the key points and indicate the modifications required for class BDI.

The action (146) is symmetric under arbitrary transformations. Therefore, nontrivial symmetry constraints on the group G arise solely from the measurement Lagrangian (145), where $\beta = 1$ for class AIII and $\beta = 1/2$ for class BDI. The explicit form for class AIII is given in Eq. (102). Symmetry transformations must satisfy $\mathcal{L}_M[\mathcal{G}] = \mathcal{L}_M[\mathcal{R}\mathcal{G}\mathcal{R}^{-1}]$.

As in Sec. VIB 3, we check this condition term by term. Considering efficient counting with $\eta = 1$, the first term of the measurement Lagrangian (145) vanishes. The second term is invariant if \mathcal{R} is block-diagonal in Keldysh space, as given in Eq. (108). For class AIII, the blocks are arbitrary unitary matrices, $\mathcal{V}_\pm \in \text{U}(R)$; for class BDI, Eq. (150) imposes the constraint $\mathcal{V}_\pm = \tau_y \mathcal{V}_\mp^* \tau_y$, so that \mathcal{R} can be parameterized in terms of a single matrix $\mathcal{V} \in \text{U}(2R)$ as

$$\mathcal{R} = \begin{pmatrix} \mathcal{V} & 0 \\ 0 & \tau_y \mathcal{V}^* \tau_y \end{pmatrix}. \quad (151)$$

Next, we consider the third term of the measurement Lagrangian, starting with class AIII. As discussed in Sec. VIB 3, this term is invariant if $\det_R(\mathcal{V}_+) = \det_R(\mathcal{V}_-)$. This yields $\mathcal{R} \in G \cong \text{U}(1) \rtimes [\text{SU}(R) \times \text{SU}(R)]$.

Turning to class BDI, we examine the contribution to the third term of the measurement Lagrangian (145) with $\alpha = -$. Inserting here the transformed matrix \mathcal{G} , the exponential factor becomes

$$e^{\beta \text{tr}_{CR} \ln \text{tr}_K(\frac{1}{\beta}\sigma_- \mathcal{R}\mathcal{G}\mathcal{R}^{-1})} = e^{\beta \text{tr}_{CR} \ln(\tau_y \mathcal{V}^\top \tau_y \mathcal{V})} e^{\beta \text{tr}_{CR} \ln \text{tr}_K(\frac{1}{\beta}\sigma_- \mathcal{G})}. \quad (152)$$

The final factor on the right-hand side is already present in Eq. (145). Hence, invariance of the measurement Lagrangian

requires the first factor to reduce to unity. To rewrite this factor, we use the following general relation for skew-symmetric $2D \times 2D$ matrices A and B :

$$\text{pf}(A) \text{pf}(B) = e^{\beta \text{tr} \ln(A^\top B)} = (-1)^D e^{\beta \text{tr}(AB)}, \quad (153)$$

where pf denotes the Pfaffian. Here, we apply this to the $2R \times 2R$ matrices $A = \tau_y$, with 1_R left implicit, and $B = \mathcal{V}^\top \tau_y \mathcal{V}$. Invariance of the measurement Lagrangian thus requires

$$e^{\beta \text{tr}_{CR} \ln(\tau_y \mathcal{V}^\top \tau_y \mathcal{V})} = (-1)^R \text{pf}_{CR}(\tau_y) \text{pf}_{CR}(\mathcal{V}^\top \tau_y \mathcal{V}) = 1. \quad (154)$$

Using

$$\begin{aligned} \text{pf}_{CR}(\tau_y) &= \text{pf}_C(\tau_y)^R = (-i)^R, \\ \text{pf}_{CR}(\mathcal{V}^\top \tau_y \mathcal{V}) &= \det_{CR}(\mathcal{V}) \text{pf}_{CR}(\tau_y), \end{aligned} \quad (155)$$

this reduces to $\det_{CR}(\mathcal{V}) = 1$. The same condition arises for the contribution with $\alpha = +$. We therefore conclude that $\mathcal{V} \in \text{SU}(2R)$ and thus $\mathcal{R} \in G \cong \text{SU}(2R)$.

We now turn to condition (ii) and determine the group H of transformations \mathcal{R} that leave the saddle point Λ invariant. Consider the explicit parameterization of the NLSM target manifold, obtained using Eqs. (97) and (149), with transformations \mathcal{R} given by Eq. (108) for class AIII and by Eq. (151) for class BDI, respectively:

$$Q = \begin{pmatrix} 1 - 2n & 2nU \\ 2(1-n)U^{-1} & -1 + 2n \end{pmatrix}, \quad (156)$$

where, for AIII, $U = \mathcal{V}_+ \mathcal{V}_-^{-1}$, and for BDI, $U = \mathcal{V} \sigma_y \mathcal{V}^\top \sigma_y$. Evidently, $Q = \mathcal{R} \Lambda \mathcal{R}^{-1} = \Lambda$ is invariant for class AIII if $\mathcal{V}_+ = \mathcal{V}_-$. Transformations (108) satisfying this condition form the group $H \cong \text{U}(R) = \text{U}(1) \rtimes \text{SU}(R)$. The NLSM target manifold is therefore given by $U \in G/H = \text{SU}(R)$.

For class BDI, the saddle point Λ is invariant for matrices \mathcal{V} satisfying $\mathcal{V}^\top \sigma_y \mathcal{V} = \sigma_y$, which form the compact symplectic group, $H \cong \text{Sp}(R)$. The NLSM target manifold is thus $U \in G/H = \text{SU}(2R)/\text{Sp}(R)$.

For both symmetry classes AIII and BDI, the NLSM target manifold becomes trivial in the replica limit $R \rightarrow 1$. In other words, the replica-symmetric manifold is trivial, and only the replicon manifold is nontrivial. For $R = 1$, the theory describes the unconditional dynamics of free fermions with incoherent gain and loss, which in the steady state (81) leads to short-range correlations in space and time. Such behavior corresponds to the theory being massive even for $\eta = 1$ [30].

4. Trivial target manifold for inefficient detection, $\eta < 1$

We now turn to inefficient detection with $\eta < 1$. In this case, the first term in the measurement Lagrangian (145), which contains $\text{tr}(\Lambda \mathcal{G})$ with coefficient $1 - \eta$, is nonzero. Invariance of this term requires \mathcal{R} to satisfy condition (111). However, this is precisely the condition that determines the group H . Thus, as discussed below Eq. (156), for class AIII we have $G = H \cong \text{U}(R)$, while for class BDI we have $G = H \cong \text{Sp}(R)$. In both cases, the coset G/H is the trivial group. The fact

that inefficient detection breaks the symmetries underlying the NLSM description was anticipated for balanced fermion counting in Ref. [30].

5. Nonlinear sigma model Lagrangian

The general form of the NLSM action for $\eta = 1$ can be obtained by inserting the parameterization of the NLSM manifold from Eq. (156) into Eq. (146), taking the spatial continuum limit in which the lattice-site index l is replaced by the continuous coordinate x , and performing a gradient expansion [29]. This procedure does not, however, account for the renormalization of the coefficients in the NLSM Lagrangian that results from integrating out massive modes. To determine this renormalization, we instead begin with the most general form of the NLSM obtained from the gradient expansion of Eq. (146) but leave its coefficients unspecified. Linearizing the NLSM action and matching it to the Gaussian theory, after all massive fluctuations have been integrated out there, then fixes these coefficients. Implementing this program yields the NLSM Lagrangian for the replicon manifold:

$$i\mathcal{L}_R[U] = -\frac{\beta g}{2} \text{tr}_{CR} \left(\frac{1}{v} \partial_t U^{-1} \partial_t U + v \partial_x U^{-1} \partial_x U \right), \quad (157)$$

where the bare value g_0 of the dimensionless NLSM coupling g is given in Eq. (123), and

$$v = 2J \sqrt{1 - 2n(1-n)}. \quad (158)$$

As noted above:

$$\text{AIII:} \quad \beta = 1, \quad U \in \text{SU}(R), \quad (159)$$

$$\text{BDI:} \quad \beta = 1/2, \quad U \in \text{SU}(2R)/\text{Sp}(R). \quad (160)$$

Thus, the same NLSM arises for all values of γ_\pm . The physics discussed in Ref. [30] is therefore not restricted to balanced gain and loss with $\gamma_+ = \gamma_-$.

For $\eta < 1$, the first term in Eq. (145) yields a mass contribution proportional to the detection inefficiency $\delta\eta = 1 - \eta > 0$, which takes the form

$$i\delta\mathcal{L}_R[U] = 2n(1-n)\delta\eta\gamma \left[\beta \text{tr}_{CR}(U + U^{-1}) - 2R \right]. \quad (161)$$

This mass term suppresses long-wavelength fluctuations of U . We may thus parameterize $U = e^{i\Phi}$ with a Hermitian matrix Φ and expand the NLSM Lagrangian to second order,

$$\begin{aligned} i(\mathcal{L}_R[\Phi] + \delta\mathcal{L}_R[\Phi]) &= -\beta \text{tr}_{CR} \left[\frac{g}{2} \left(\frac{1}{v} \partial_t \Phi^{-1} \partial_t \Phi \right. \right. \\ &\quad \left. \left. + v \partial_x \Phi^{-1} \partial_x \Phi \right) + 2n(1-n)\delta\eta\gamma\Phi^2 \right]. \end{aligned} \quad (162)$$

This form of the NLSM Lagrangian is consistent with the low-momentum expansion (122) of the correlation function.

6. Renormalization-group flow of the NLSM

For $\eta = 1$, the large-scale behavior of our model is governed by the RG flow of the NLSM coupling constant g . The NLSM description and thus the RG flow is identical to that obtained for balanced counting in Ref. [30]. For completeness, we briefly recall the relevant results. We then analyze how the RG flow is modified by inefficient detection.

On scales $l \gtrsim l_0$, the NLSM coupling constant acquires a logarithmic renormalization [19, 29],

$$g = g_0 - \frac{1}{4\pi\beta} \ln(l/l_0), \quad (163)$$

where, as above, $\beta = 1$ for symmetry class AIII and $\beta = 1/2$ for class BDI. This expression is valid in the weak-coupling regime $g \gg 1$, which, according to Eq. (123), corresponds to a low rate of fermion gain and loss. The flow reaches the strong-coupling regime, where g becomes of order unity, at the characteristic scale

$$l_* = l_0 e^{4\pi\beta g_0}. \quad (164)$$

As discussed in Sec. VIC 3, the renormalization of g controls the long-distance behavior of the effective central charge. Thus, the flow of g toward small values for $l \gtrsim l_*$ implies that the logarithmic growth of the entanglement entropy (130) eventually saturates, leading to area-law scaling for subsystem sizes $\ell \gtrsim l_*$ [19]. Accordingly, our model exhibits no measurement-induced transition between critical and area-law phases; all choices of γ_\pm yield area-law entanglement beyond the scale l_* . Nevertheless, because l_* grows exponentially with $g_0 \sim J/\gamma$, the onset of area-law behavior falls far outside the window accessible to our numerical simulations when J/γ is large—even though such scales can be reached in principle [33]; see Sec. VIF for details.

For small but finite measurement inefficiency, $0 < \delta\eta = 1 - \eta \ll 1$, the mass term in Eq. (162) suppresses fluctuations of Φ at large scales and thereby cuts off the RG flow. The resulting infrared cutoff is the correlation length ξ of Eq. (125), but with the microscopic scale $l_0 \sim g_0$ renormalized. Even though this renormalization modifies prefactors, the functional dependence $\xi \sim \delta\eta^{-1/2}$ remains correct, as we confirm numerically in Sec. VIF. Beyond the scale ξ , the long-wavelength behavior is governed by the Gaussian theory, with g replaced by its renormalized value. We examine this regime in detail below.

E. RG-corrected Gaussian theory

To assess how the renormalization of g affects physical observables, we incorporate the RG correction Eq. (163) into the Gaussian correlation function (122) [19, 30]. The infrared cutoff of the RG flow is set by the larger of the two scales: $l = 1/q$, where q is the momentum at which the correlation function is evaluated, or the correlation length (125) associated with the mass generated by $\delta\eta > 0$.

For $\eta = 1$, inserting Eq. (163) into Eq. (122) yields

$$\frac{C_q}{g_0 q} \sim 1 - 4 \sqrt{\frac{1 - 2n(1-n)}{2}} q l_0 + \frac{1}{4\pi\beta g_0} \ln(ql_0). \quad (165)$$

In the limit $q \rightarrow 0$, the logarithmic renormalization dominates and suppresses $C_q/(g_0 q)$, whereas the Gaussian approximation predicts $C_q/(g_0 q) \rightarrow 1$ as $q \rightarrow 0$. The momentum scale at which the logarithmic term becomes comparable to the Gaussian contribution marks the onset of the crossover from the regime in which the Gaussian theory is valid to the fluctuation-dominated strong-coupling regime. Following Ref. [30], we associate this crossover with the maximum of the rescaled correlation function, which occurs at $q_c \sim \gamma^2$. The corresponding length scale is $l_c \sim \gamma^{-2}$. Because l_c grows only algebraically with γ , it remains accessible in numerical studies.

As shown in Ref. [30], the length scale $l_c \sim \gamma^{-2}$ serves as the upper boundary of a critical window within which the model exhibits emergent conformal invariance, as expected for a critical phase [11]. Its lower boundary is $l_0 \sim \gamma^{-1}$ (118). Within this interval, the system displays signatures of conformal behavior, including algebraic decay of density correlations, $C_l \sim l^{-2}$, and logarithmic entanglement scaling, $S_\ell \sim \ln(\ell)$. While these features also arise from the Gaussian approximations in Eqs. (124) and (130), the Gaussian central charge Eq. (133) is valid only in the combined limits $\gamma \rightarrow 0$ and $\ell \rightarrow \infty$. For any finite γ , approximately logarithmic entanglement growth appears instead on intermediate scales where c_ℓ varies slowly and reaches a maximum at $\ell = l_m \sim \gamma^{-3/2}$. The scaling of l_m ensures that this length lies within the critical regime, $l_0 < l_m < l_c$. Logarithmic entanglement growth and additional hallmarks of conformal symmetry, including the universal functional form of the mutual information, are captured by the renormalized value of the effective central charge at its maximum [30].

For $\delta\eta > 0$, the RG flow is terminated when $l \sim q^{-1} \sim \xi$. Using Eq. (122) at this scale gives

$$C_q \sim \frac{g_0}{\xi} \left[1 - \frac{1}{4\pi\beta g_0} \ln(\xi/l_0) \right] \sim \sqrt{\delta\eta}, \quad \delta\eta \rightarrow 0. \quad (166)$$

This is consistent with Eq. (165): substituting $q \sim \xi^{-1}$ into that expression and retaining only the leading terms for $\xi \gg l_0$ reproduces the same scaling.

F. Numerical simulations of quantum-jump trajectories

We validate our analytical results by comparing them with direct numerical simulations of the model. Before presenting our findings in detail, we briefly summarize the numerical methods employed, which differ from those used for balanced and efficient fermion counting [30].

1. Numerical methods

For balanced and efficient fermion counting, the rates of gain and loss jumps are state-independent and constant in

time. This enables the use of a simulation scheme that captures the continuous-time limit $\Delta t \rightarrow 0$ numerically exactly [30, 64]. In contrast, for imbalanced and inefficient fermion counting, the jump probabilities depend on the instantaneous state of the system and therefore vary in time. In principle, one can address this by directly implementing the evolution of individual trajectories as outlined in Secs. II and V for efficient and inefficient detection, respectively. As explained in Appendix A, this amounts to integrating the underlying stochastic Schrödinger equation to first order in Δt . Within this approach, the time step must be chosen such that the probability for any jump within a single step remains small [64]. However, for local jump operators in an extended lattice system, the number of such operators scales extensively with system size, implying $\Delta t \sim L^{-1}$. This scaling severely restricts simulations at large L .

To circumvent this limitation, we treat jumps at different lattice sites as approximately independent. Concretely, during each time step we sweep through the lattice and independently determine whether a jump occurs at each site. The full numerical procedure is detailed in Appendix C.

All simulations begin from the initial state

$$|\psi_0\rangle = \prod_{l=1}^{L/2} \hat{\psi}_{2l-1}^\dagger |0\rangle, \quad (167)$$

where $|0\rangle$ denotes the vacuum, yielding an initial density $n = N/L = 1/2$. Purity of the state is preserved only when $\eta = 1$. Nevertheless, the Gaussian structure of the initial state is maintained under time evolution generated by the quadratic Hamiltonian (78) and the linear jump operators (80). Consequently, at all times t the state is fully characterized by the $L \times L$ single-particle density matrix

$$D_{l,l'}(t) = \text{tr}[\hat{\psi}_{l'}^\dagger \hat{\psi}_l \hat{\rho}(t)]. \quad (168)$$

This representation allows us to simulate systems of size up to $L = 1000$. In our simulations, we treat the average jump rate γ and the fermion density n as independent parameters. These uniquely determine the gain and loss rates γ_\pm via Eqs. (82) and (83). For each set of parameters γ , n , and η , we sampled $N_{\text{traj}} = 160$ trajectories.

2. Connected density correlation function

The first observable we analyze is the connected density correlation function (115). In the steady state, this quantity becomes time-independent and translationally invariant, so that $C_{l,l'}(t) = C_{l-l'}$. Since the system remains in a Gaussian state at all times, the correlation function can be expressed through the single-particle density matrix (168) using Wick's theorem,

$$C_{l-l'} = \overline{\langle \hat{n}_l \hat{n}_{l'} \rangle} - \overline{\langle \hat{n}_l \rangle} \overline{\langle \hat{n}_{l'} \rangle} = \delta_{l,l'} \overline{D_{l,l}} - \overline{|D_{l,l'}|^2}. \quad (169)$$

In our numerical analysis, the overline denotes an average over both quantum trajectories and over lattice sites l and l' at fixed separation $l - l'$.

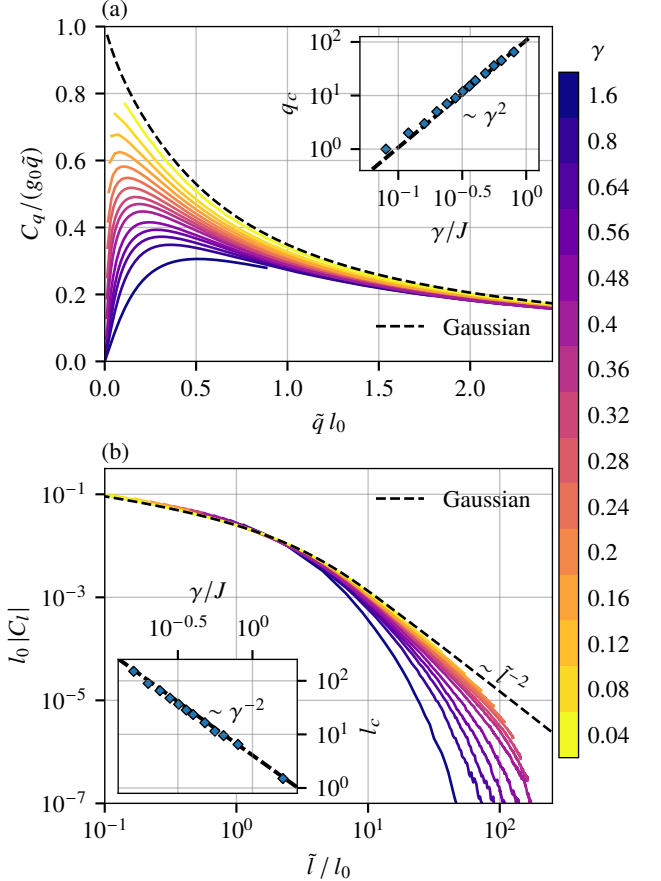


Figure 1. Rescaled density correlation function (169) in (a) momentum space and (b) real space for $n = 0.4$ and $\eta = 1$. (a) The numerical data deviate significantly from the Gaussian correlation function (119) (black dashed line) for $\tilde{q}l_0 \rightarrow 0$: while the Gaussian result approaches a finite value, $C_q/(g_0 \tilde{q}) \rightarrow 1$, the numerical data exhibit a maximum at q_c and then decrease toward zero. Inset: The position of the maximum scales as $q_c \sim \gamma^2$. (b) In real space, we observe good agreement with the Gaussian prediction on short scales, $\tilde{l} \lesssim l_0$. Significant deviations appear for $\tilde{l} \gtrsim l_c$, where the Gaussian result decays algebraically, $|C_l| \sim \tilde{l}^{-2}$, while the numerical data decay more rapidly. Inset: The crossover scale at which deviations from the Gaussian result become pronounced scales as $l_c \sim \gamma^{-2}$.

For efficient detection with $\eta = 1$, the results reported in Ref. [30] for balanced fermion counting remain qualitatively unchanged for imbalanced counting with $\gamma_+ \neq \gamma_-$ and thus $n \neq 1/2$. Figure 1(a) displays the rescaled density correlation function in momentum space, $C_q/(g_0 \tilde{q})$, as a function of $\tilde{q}l_0$ for fixed density $n = 0.4$ and various values of γ/J . Here, $\tilde{q} = 2 \sin(q/2)$ accounts for the finite lattice spacing [19].

At high momenta, the numerical data converge to the Gaussian result, shown as a black dashed line in the figure. As anticipated in Sec. VI E, however, the renormalization of the NLSM coupling constant g due to strong Goldstone-mode fluctuations leads to deviations from the Gaussian prediction for $\tilde{q}l_0 \rightarrow 0$. The expected scaling of the crossover momentum, defined as the position of the maximum of the rescaled

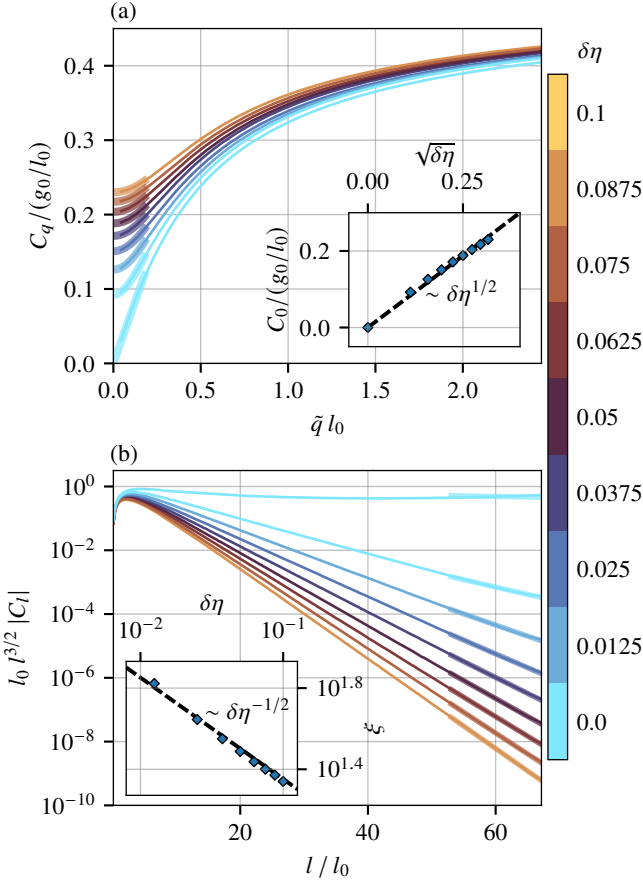


Figure 2. Rescaled density correlation function (169) in (a) momentum space and (b) real space for $n = 0.4$ and $\gamma/J = 0.1$. (a) Finite detection inefficiency leads to a nonzero axis intercept for $\tilde{q}l_0 \rightarrow 0$. Inset: The intercept follows the expected scaling $\sim \delta\eta^{1/2}$. (b) In real space, detection inefficiency induces an exponential decay of correlations on large scales. Inset: The fitted correlation length ξ agrees well with the predicted behavior $\xi \sim \delta\eta^{-1/2}$. Thick lines in (a) and (b) show fits to Eqs. (170) and (171), respectively.

correlation function, $q_c \sim \gamma^2$, is well supported by the numerical results, as illustrated in the inset.

Beyond the corresponding crossover length scale $l_c \sim q_c^{-1} \sim \gamma^{-2}$, the rescaled correlation function in real space decays faster than the algebraic form (124) predicted by the Gaussian theory. This behavior is evident in Fig. 1(b), which shows the rescaled connected density correlation function (169) as a function of the chord length $\tilde{l} = (L/\pi) \sin(\pi l/L)$ [70]. The corresponding Gaussian prediction, shown again as a black dashed line, is obtained by transforming Eq. (119) to real space. Consistent with Ref. [30], we identify l_c as the scale beyond which the deviation between the numerical data and a tangent $\sim \tilde{l}^{-2}$ exceeds 10 %. As shown in the inset, the numerical results confirm the expected scaling $l_c \sim q_c^{-1} \sim \gamma^{-2}$.

We now discuss how these results are affected by inefficient detection. As before, we set $n = 0.4$, and we choose $\gamma/J = 0.1$. For these parameters, when $\eta = 1$, the numerical data shown in Fig. 1 qualitatively follow the Gaussian be-

havior over the entire range of numerically accessible length scales. Figure 2(a) shows the density correlation function in momentum space for finite $\delta\eta = 1 - \eta$, without the rescaling by q^{-1} used in Fig. 1(a). In this representation, the RG-corrected Gaussian theory (165) predicts that the correlation function approaches zero for $\tilde{q}l_0 \rightarrow 0$ when detection is efficient with $\delta\eta = 0$. In contrast, for finite detection inefficiency $\delta\eta > 0$, the axis intercept of the correlation function for $\tilde{q}l_0 \rightarrow 0$ is expected to scale as $C_0/(g_0/l_0) \sim \delta\eta^{1/2}$, see Eq. (166).

In numerical simulations, the smallest observable momentum is limited by the inverse system size. To extract the intercept from finite-momentum data, we fit the functional form given in Eq. (122) to the data:

$$C_q/(g_0/l_0) = p_1 \sqrt{(\tilde{q}l_0)^2 + p_2}, \quad (170)$$

with fitting parameters p_1 and p_2 . These fits are shown in Fig. 2(a) as thick lines with reduced opacity. As shown in the inset, the intercept obtained in this manner is consistent with the expected scaling $\sim \delta\eta^{1/2}$.

The mass term $\sim \delta\eta$ introduces a finite correlation length $\xi \sim \delta\eta^{-1/2}$ in real space, as illustrated in Fig. 2(b). For $\delta\eta = 0$, the data exhibit approximately algebraic decay within the numerically accessible range, with faster decay expected at even larger scales. However, for $\delta\eta > 0$, correlations are cut off exponentially. To quantify this behavior, we fit the functional form of Eq. (124) to the data:

$$l_0 l^{3/2} |C_l| = p e^{-l/\xi}, \quad (171)$$

with fitting parameters p and ξ . The fitted correlation length ξ , shown in the inset, exhibits the expected scaling $\xi \sim \delta\eta^{-1/2}$.

3. Subsystem entropy and effective central charge

For the numerical evaluation of the subsystem entropy (126) in Gaussian states, we employ the formula

$$S_\ell = - \sum_{l=1}^{\ell} \overline{[\lambda_l \ln(\lambda_l) + (1 - \lambda_l) \ln(1 - \lambda_l)]}, \quad (172)$$

where λ_l are the eigenvalues of the reduced single-particle density matrix D_ℓ for a subsystem of size ℓ , obtained by restricting Eq. (168) as $D_\ell = (D_{l,l'})_{l,l'=1}^\ell$ [72]. As before, the overline indicates averaging over both spatial positions and quantum trajectories.

For efficient detection with $\eta = 1$, each trajectory remains in a pure state, so the subsystem entropy provides a direct measure of entanglement. Figure 3(a) displays the resulting entanglement entropy for subsystems of size $\ell \in \{1, \dots, L/2\}$. For small γ/J , the numerical results closely follow the Gaussian prediction obtained by integrating Eq. (129) with the Gaussian correlator (119). In particular, the data exhibit volume-law behavior (131) on short scales $\ell \lesssim l_0$ and an apparent logarithmic increase (130) on larger scales. As γ/J increases, the entropy crosses over to area-law scaling at large ℓ . Although the NLSM analysis indicates that area-law scaling eventually occurs for any nonzero γ , this regime sets in

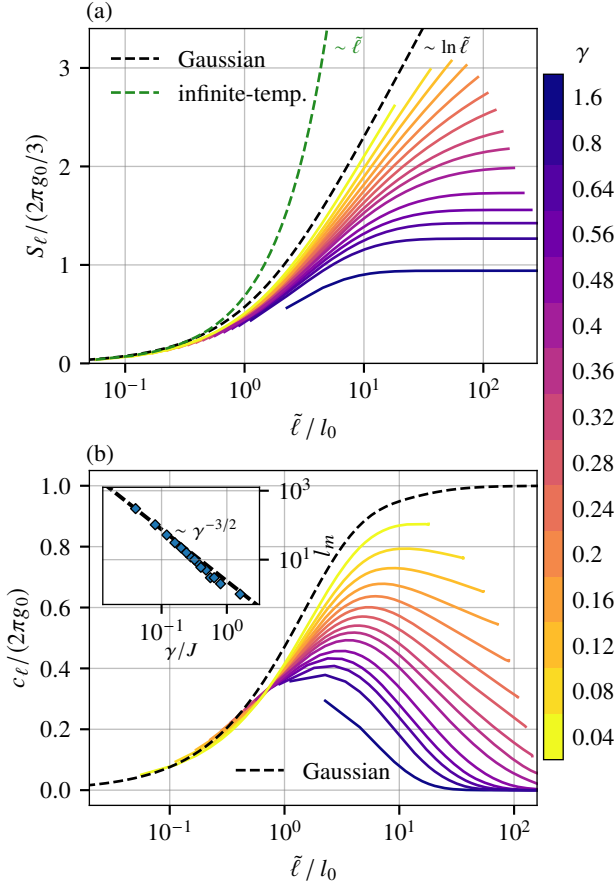


Figure 3. (a) Rescaled entanglement entropy and (b) rescaled scale-dependent effective central charge for $n = 0.4$ and $\eta = 1$. (a) For short subsystem sizes $\tilde{\ell} \lesssim l_0$, the entanglement entropy follows volume-law scaling (green dashed line), consistent with the infinite-temperature behavior in Eq. (131). At larger scales, the data show an apparent logarithmic increase for small γ/J , which transitions to area-law behavior as γ/J is increased. (b) The effective central charge rises in the volume-law regime, reaches a maximum at a characteristic scale l_m , and then decreases for $\tilde{\ell}/l_0 \gg 1$. This decay demonstrates that the logarithmic growth of entanglement observed at small γ/J does not persist asymptotically. By contrast, the Gaussian approximation (black dashed line) for c_ℓ approaches a constant value, indicating sustained logarithmic entanglement growth. Inset: The position of the numerically observed maximum of c_ℓ is consistent with the expected scaling $l_m \sim \gamma^{-3/2}$.

only beyond the exponentially large scale l_* (164). For the system size $L = 1000$ used in our simulations, this scale is accessible only for sufficiently large γ/J . Nonetheless, as discussed below, the onset of the crossover toward area-law behavior is clearly reflected in the scale-dependent effective central charge (132).

Figure 3(b) shows the effective central charge (132) extracted from the numerical data. For small γ/J , the numerical results track the Gaussian prediction on intermediate length scales. However, at large scales the Gaussian result saturates at the constant value in Eq. (133), corresponding to persistent logarithmic growth of the entanglement entropy (130). In

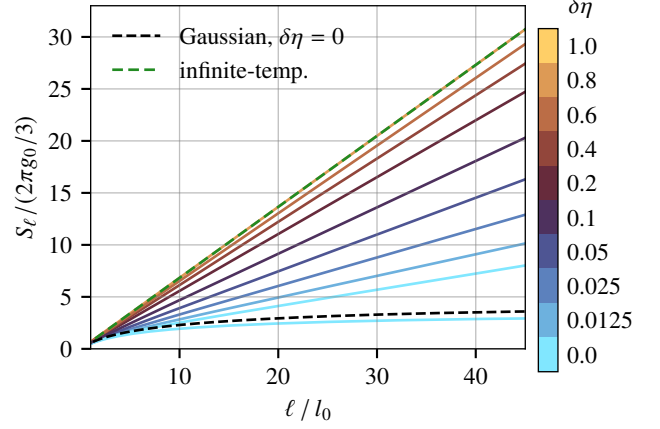


Figure 4. Rescaled subsystem entropy for $\gamma/J = 0.1$ and $n = 0.4$. For inefficient detection with $\delta\eta = 1 - \eta > 0$, the subsystem entropy exhibits volume-law scaling. In the limit $\delta\eta = 1$, the numerical data are consistent with Eq. (131), as expected for a fully mixed infinite-temperature state with fixed fermion density n .

contrast, the numerically obtained central charge remains approximately constant only near its maximum and decreases for larger ℓ . This behavior provides clear evidence of the crossover from logarithmic growth toward area-law scaling. The location l_m of the maximum of c_ℓ is shown in the inset of Fig. 3(b), and the numerical results are consistent with the expected scaling $l_m \sim \gamma^{-3/2}$ [30].

We now consider the case of inefficient detection, $\eta < 1$, for which trajectories evolve into mixed states. In this regime, the subsystem entropy (126) no longer quantifies entanglement; even for small detection inefficiency $\delta\eta = 1 - \eta$, its large-scale behavior is dominated by the statistical contribution arising from state mixedness. This trend is evident in Fig. 4. For the comparatively small value $\gamma/J = 0.1$, where efficient detection yields an apparent logarithmic entanglement growth in Fig. 3(a), the subsystem entropy in Fig. 4 instead follows a volume law for $\delta\eta > 0$. The coefficient of volume-law scaling grows as the detection inefficiency $\delta\eta$ increases and saturates to the one given in Eq. (131), characteristic of the infinite-temperature state (81) at fixed density n , in the limit $\delta\eta \rightarrow 1$.

4. Fermionic logarithmic negativity

To quantify entanglement in mixed-state dynamics for $\eta < 1$, we employ the fermionic logarithmic negativity introduced in Refs. [61, 62]. For mixed Gaussian states with vanishing anomalous correlations, $\langle \hat{\psi}_l \hat{\psi}_{l'} \rangle = 0$, the logarithmic negativity can be computed as follows [73]: We consider a bipartition into a subsystem $A = \{1, \dots, \ell\}$ of size ℓ and its complement $B = \{\ell + 1, \dots, L\}$. In terms of the single-particle density matrix (168), we define the covariance matrix G as

$$G = 2D - 1 = \begin{pmatrix} G_{AA} & G_{AB} \\ G_{BA} & G_{BB} \end{pmatrix}, \quad (173)$$

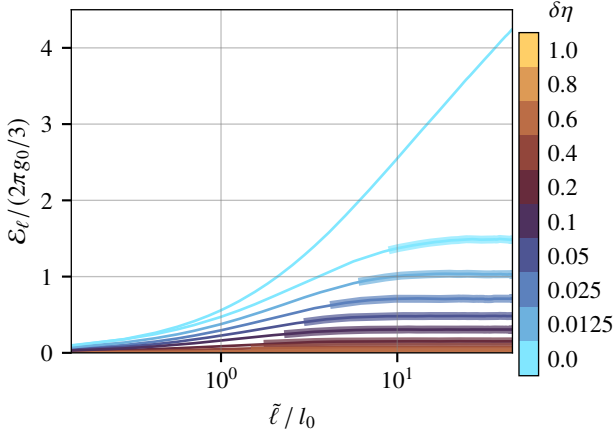


Figure 5. Rescaled logarithmic negativity for $\gamma/J = 0.1$ and $n = 0.4$ at varying measurement inefficiencies $\delta\eta = 1 - \eta$. For $\delta\eta = 0$, the data exhibit approximately logarithmic growth with subsystem size. Any finite $\delta\eta > 0$ leads to area-law scaling on scales $\tilde{\ell} \gtrsim \xi$. This region, with ξ obtained by fitting Eq. (171) to the data in Fig. 2(b), is highlighted by thicker lines. For $\delta\eta = 1$, the steady state (81) is completely disentangled, yielding $\mathcal{E}_\ell = 0$.

where each block denotes the restriction of the indices of G to the corresponding subsystems, for example $G_{AA} = (G_{l,l'})_{l,l' \in A}$. We further introduce

$$G_{\pm} = \begin{pmatrix} G_{AA} & \pm iG_{AB} \\ \pm iG_{BA} & -G_{BB} \end{pmatrix}, \quad (174)$$

and

$$G^T = \frac{1}{2} \left[1 - (1 + G_+ G_-)^{-1} (G_+ + G_-) \right]. \quad (175)$$

Let μ_l and λ_l denote the eigenvalues of G^T and D , respectively, with $l \in \{1, \dots, L\}$. The logarithmic negativity, quantifying entanglement between subsystem A and the remainder of the system, is then given by

$$\mathcal{E}_\ell = \sum_{l=1}^L \left\{ \ln(\sqrt{\mu_l} + \sqrt{1 - \mu_l}) + \frac{1}{2} \ln[\lambda_l^2 + (1 - \lambda_l)^2] \right\}. \quad (176)$$

Figure 5 displays the logarithmic negativity for the same parameters as in Fig. 4. For the pure states obtained for $\delta\eta = 0$, the logarithmic negativity reduces to the Rényi entropy of order 1/2 and shows an apparent logarithmic increase with subsystem size ℓ , consistent with the von Neumann entanglement entropy in Fig. 3(a). In contrast, even a small but finite measurement inefficiency $\delta\eta$ induces area-law scaling of the logarithmic negativity once $\ell \gtrsim \xi$. This confirms that the volume-law behavior of the subsystem entropy in Fig. 4 is entirely of statistical origin and does not indicate genuine quantum entanglement. In the limit $\eta \rightarrow 0$, the steady state (81) of the deterministic open-system dynamics is fully mixed, and the logarithmic negativity vanishes identically, $\mathcal{E}_\ell = 0$.

VII. CONCLUSIONS

In this work, we have developed a comprehensive replica Keldysh field-theory framework for general quantum-jump processes in bosonic and fermionic many-body systems. This framework encompasses, in particular, processes involving non-Hermitian jump operators with state-dependent and thus time-varying rates—going beyond the paradigmatic scenario of projective measurements performed at a fixed, externally imposed rate. Moreover, our formalism unifies the description of pure-state trajectories under efficient detection with the mixed-state dynamics arising from inefficient monitoring. It thus provides a versatile framework for exploring a broad range of measurement-induced phenomena.

Applying this framework to imbalanced and inefficient fermion counting in a 1D lattice system, we have established several key results. For imbalanced but efficient detection, we confirmed that the qualitative picture observed previously in the balanced case persists [30]: there is no measurement-induced phase transition, and entanglement obeys an area law on sufficiently large scales, while an extended quantum-critical regime emerges between parametrically separated scales $l_0 \sim \gamma^{-1}$ and $l_c \sim \gamma^{-2}$. This regime exhibits signatures of emergent conformal invariance, including algebraic correlations and approximately logarithmic entanglement growth.

We have further shown that a finite detection inefficiency $\delta\eta$, corresponding to a nonzero fraction of undetected fermion gain and loss jumps, introduces a correlation length $\xi \sim \delta\eta^{-1/2}$. On length scales larger than ξ , quantum entanglement is strongly suppressed, as evidenced by the fermionic logarithmic negativity, which obeys an area law. In contrast, the subsystem entropy exhibits volume-law scaling due to the mixedness of individual quantum trajectories.

More broadly, our results establish a direct conceptual and technical connection between measurement-induced dynamics and the steady-state physics of driven open quantum systems [46–49]. For example, imbalanced and inefficient fermion counting in the limit of inefficient detection constitutes a representative instance of driven open quadratic fermionic systems with gain-loss dissipation [74, 75]. This class of systems has been studied extensively: such models are known to host topologically nontrivial phases in their nonequilibrium steady states [76] and to exhibit signatures of non-Hermitian topology [77] in their dynamics [78], including the non-Hermitian skin effect [79]. Further paradigmatic settings include systems with impurities, both in the bulk [80] and at the boundaries [27]. The latter give rise to boundary-driven models that provide a natural platform for studying quantum transport [81]. For all of these scenarios, as well as for related phenomena beyond the class of quadratic fermionic systems, our formalism furnishes an analytical framework for exploring their unraveling into quantum trajectories. This, in turn, paves the way toward shedding further light on the question of whether universal properties exist that transcend the apparent conceptual divide between measurement-induced pure-state dynamics and the nonequilibrium steady states of driven open quantum systems.

ACKNOWLEDGMENTS

L.S. acknowledges support from the Austrian Science Fund (FWF) through the project 10.55776/COE1, and from the European Union - NextGenerationEU.

Note added

While we were completing this manuscript, a preprint appeared on the arXiv that derives a replica Keldysh field theory for quantum-jump processes using a different approach [82].

Appendix A: Minimal physical model for quantum-jump trajectories

Here we outline a minimal physical model that gives rise to the discrete-time dynamics governed by the Kraus operators in Eqs. (1) and (2). The construction follows the standard quantum-optical treatment of continuous monitoring [51–54].

We consider a generic system with Hamiltonian \hat{H} coupled to bosonic or fermionic baths. The bath annihilation and creation operators are $\hat{b}_{a,k}$ and $\hat{b}_{a,k}^\dagger$, where $a \in \mathcal{A} = \{1, \dots, A\}$ indexes the baths and k labels discrete bath modes of energies $\omega_{a,k}$. The operators satisfy

$$[\hat{b}_{a,k}, \hat{b}_{a',k'}^\dagger]_\zeta = \hat{b}_{a,k} \hat{b}_{a',k'}^\dagger - \zeta \hat{b}_{a',k'}^\dagger \hat{b}_{a,k} = \delta_{a,a'} \delta_{k,k'}, \quad (\text{A1})$$

with $\zeta = +1$ for bosons and $\zeta = -1$ for fermions. The Hamiltonian of bath a is

$$\hat{H}_a = \sum_k \omega_{a,k} \hat{b}_{a,k}^\dagger \hat{b}_{a,k}, \quad (\text{A2})$$

and the system-bath coupling is described by

$$\hat{H}_{\text{int}} = i \sum_{a=1}^A \sum_k (g_{a,k}^* \hat{c}_a \hat{b}_{a,k}^\dagger - g_{a,k} \hat{b}_{a,k} \hat{c}_a^\dagger). \quad (\text{A3})$$

Bath a inherits its bosonic or fermionic statistics from the system operator \hat{c}_a . For example, in fermionic gain and loss processes governed by jump operators (80), Eq. (A3) represents particle tunneling into and out of fermionic reservoirs [30].

All baths are assumed to start in the vacuum, $\hat{b}_{a,k}|0_a\rangle = 0$, and the joint initial state is $|\Psi(t_0)\rangle = |\psi(t_0), 0_1, \dots, 0_A\rangle$.

Following standard derivations of stochastic Schrödinger dynamics [51–54], we move to an interaction picture in which operators evolve under the bath Hamiltonians (A2), while the state evolves under

$$\hat{H}_I(t) = \hat{H} + \hat{H}_{\text{int}}(t), \quad (\text{A4})$$

with

$$\hat{H}_{\text{int}}(t) = i \sum_{a=1}^A [\hat{c}_a \hat{b}_a^\dagger(t) - \hat{b}_a(t) \hat{c}_a^\dagger], \quad (\text{A5})$$

and

$$\hat{b}_a(t) = \sum_k g_{a,k} \hat{b}_{a,k} e^{-i\omega_{a,k} t}. \quad (\text{A6})$$

The interaction-picture bath operators satisfy

$$[\hat{b}_a(t), \hat{b}_{a'}^\dagger(t')]_\zeta = \delta_{a,a'} \Gamma_a(t - t'), \quad (\text{A7})$$

where

$$\Gamma_a(t) = \sum_k |g_{a,k}|^2 e^{-i\omega_{a,k} t}. \quad (\text{A8})$$

We now invoke the Markov approximation, assuming the bath correlation times are short compared with characteristic system timescales, so that

$$\Gamma_a(t) = \gamma_a \delta(t). \quad (\text{A9})$$

In general, γ_a is complex. Its imaginary part, the Lamb shift, contributes to the unitary evolution of the system and is typically absorbed into \hat{H} . In the following, we neglect this Lamb-shift contribution.

The interaction-picture time evolution operator satisfies the integral equation

$$\hat{U}_I(t, t_0) = \mathbb{1} - i \int_{t_0}^t dt' \hat{H}_I(t') \hat{U}_I(t', t_0). \quad (\text{A10})$$

For simplicity, we set $t_0 = 0$. We integrate the integral equation in small discrete time steps, such that $t = \Delta t$.

In the weak-coupling or Born approximation, Eq. (A10) can be solved perturbatively. Iterating the integral equation to second order yields

$$|\Psi_I(\Delta t)\rangle = \hat{U}_I(\Delta t, 0)|\Psi_I(0)\rangle = |\Psi_I^{(0)}\rangle + |\Psi_I^{(1)}\rangle + |\Psi_I^{(2)}\rangle, \quad (\text{A11})$$

where $|\Psi_I^{(0)}\rangle = |\Psi_I(0)\rangle$. By using $\hat{b}_a(t)|0_a\rangle = 0$, the first-order contribution can be written as

$$\begin{aligned} |\Psi_I^{(1)}\rangle &= -i \int_0^{\Delta t} dt \hat{H}_I(t) |\Psi_I(0)\rangle \\ &= \left[-i \hat{H} \Delta t + \sum_{a=1}^A \sqrt{\gamma_a} \hat{c}_a \Delta \hat{B}_a^\dagger(0) \right] |\Psi_I(0)\rangle, \end{aligned} \quad (\text{A12})$$

where the quantum Itô increments are

$$\Delta \hat{B}_a(t) = \frac{1}{\sqrt{\gamma_a}} \int_t^{t+\Delta t} dt' \hat{b}_a(t'). \quad (\text{A13})$$

They satisfy the Markov-approximation commutation relation

$$[\Delta \hat{B}_a(t), \Delta \hat{B}_{a'}^\dagger(t')]_\zeta = \Delta t \delta_{a,a'} \delta_{t,t'}. \quad (\text{A14})$$

The second-order contribution is

$$\begin{aligned} |\Psi_I^{(2)}\rangle &= - \int_0^{\Delta t} dt' \int_0^{t'} dt'' \hat{H}_I(t') \hat{H}_I(t'') |\Psi_I(0)\rangle \\ &= -\frac{1}{2} \sum_{a=1}^A \gamma_a \hat{c}_a^\dagger \hat{c}_a \Delta t |\Psi_I(0)\rangle, \end{aligned} \quad (\text{A15})$$

where terms generating two reservoir excitations, which occurs with probability $O(\Delta t^2)$, are omitted [52].

So far, we have considered evolution from the initial time $t = 0$ to Δt . However, the evolution equation holds for arbitrary time steps from t to $t + \Delta t$. This is because the quantum Itô increments (A13) commute for different time steps according to Eq. (A14). The description in terms of the commuting operators $\Delta \hat{B}(t)$ in each time interval suggests a decomposition of each bath Hilbert space into a product of Hilbert spaces for individual time intervals [52]. This leads to an important simplification of the description of the evolution process: evolution up to time t does not affect the Hilbert spaces at later times; these remain in the vacuum state. Thus, from Eq. (A11), we obtain

$$\begin{aligned} |\Psi_I(t + \Delta t)\rangle &= \left[1 - i\hat{H}_{\text{eff}}\Delta t + \sum_{a=1}^A \sqrt{\gamma_a} \hat{c}_a \Delta \hat{B}_a^\dagger(t) \right] |\Psi_I(t)\rangle \\ &= \left(\hat{K}_0 + \sum_{a=1}^A \hat{K}_a \frac{\Delta \hat{B}_a^\dagger(t)}{\sqrt{\Delta t}} \right) |\Psi_I(t)\rangle, \end{aligned} \quad (\text{A16})$$

with \hat{H}_{eff} defined in Eq. (3). The final form makes explicit the Kraus operators in Eqs. (1) and (2).

We now incorporate continuous monitoring of the bath populations by performing, in each time step, a projective measurement of

$$\hat{N}_a(t) = \frac{\Delta \hat{B}_a^\dagger(t)}{\sqrt{\Delta t}} \frac{\Delta \hat{B}_a(t)}{\sqrt{\Delta t}}. \quad (\text{A17})$$

Since all baths begin in vacuum, the allowed outcomes are either no excitation or a single excitation in one bath. Multiple excitations occur with probability $O(\Delta t^2)$ and are neglected.

The probability of detecting no excitation is

$$P_0 = \|\hat{K}_0|\Psi_I(t)\rangle\|^2 = \|\hat{K}_0|\psi(t)\rangle\|^2, \quad (\text{A18})$$

and the system state updates as $|\psi(t)\rangle \mapsto \hat{K}_0|\psi(t)\rangle / \sqrt{P_0}$. This corresponds to continuous, no-jump evolution. The probability of detecting an excitation in bath a is

$$P_a = \frac{1}{\Delta t} \|\hat{K}_a \Delta \hat{B}_a^\dagger(t) |\Psi_I(t)\rangle\|^2 = \|\hat{K}_a |\psi(t)\rangle\|^2, \quad (\text{A19})$$

and the corresponding update is $|\psi(t)\rangle \mapsto \hat{K}_a |\psi(t)\rangle / \sqrt{P_a}$, representing a quantum jump. These probabilities and update rules reproduce precisely the quantum-trajectory description of Eqs. (8), (9), and (10).

For completeness, we note that Eq. (A16) may also be recast as a quantum stochastic Schrödinger equation for the system alone by introducing stochastic increments $\Delta N_a(t)$ that count bath excitations in each time step [51–54].

Appendix B: Generalized Hubbard-Stratonovich transformation with PHS

In this appendix, we present a detailed and self-contained derivation of the generalized Hubbard-Stratonovich transformation for systems with PHS, culminating in Eq. (145), which

expresses the measurement Lagrangian in terms of the matrix field \mathcal{G} . In Sec. B 1, we begin with an elementary evaluation of Gaussian Grassmann integrals in the presence of PHS. This serves as the foundation for the derivation of Wick's theorem in Sec. B 2, which is in turn required for establishing a useful identity that enables the simultaneous decoupling of measurement vertices in all slow channels, as discussed in Sec. B 3. The decoupled vertex is obtained by performing all possible Wick contractions, which can be viewed equivalently as evaluating a suitable Gaussian Grassmann integral. Our analysis also resolves a missing prefactor in the corresponding formula reported in Ref. [29]. Finally, exploiting the Gaussian integral representation of the decoupled measurement Lagrangian, we derive Eq. (145) in Sec. B 4.

1. Gaussian integrals with PHS

We aim to show that

$$Z = \int D[\psi^*, \psi] e^{i(\bar{\Psi}\mathcal{G}^{-1}\Psi + J^\dagger\Psi)} = \text{Pf}(-iC\mathcal{G}^{-1}) e^{\frac{1}{4}J^\dagger\mathcal{G}CJ}, \quad (\text{B1})$$

where \mathcal{G} is a matrix in Keldysh, charge-conjugation, replica, and, when applicable, position and discrete-time spaces. Thus, \mathcal{G} is a $4D \times 4D$ matrix, where 4 is the dimension of the combined Keldysh and charge-conjugation space, and $D = R$ is the dimension of replica space or $D = RLN$ when N discrete time steps are included. In the continuous-time limit, matrix multiplication in time space becomes integration, and Pf becomes a functional Pfaffian. When $D = R$, Pf reduces to the ordinary Pfaffian pf. The spinors Ψ and $\bar{\Psi}$ are defined in Eq. (137) and satisfy the constraint $\bar{\Psi} = \Psi^\dagger C$, with C given in Eq. (139). The source vector J has $4D$ Grassmann components. Finally, the integration measure is

$$\begin{aligned} D[\psi^*, \psi] &= \prod_{d=1}^D d\psi_{+,d}^* d\psi_{+,d} d\psi_{-,d}^* d\psi_{-,d} \\ &= \frac{1}{4^D} \prod_{d=1}^D \prod_{i=1}^4 d\Psi_{i,d} = \frac{1}{4^D} D[\Psi]. \end{aligned} \quad (\text{B2})$$

This ordering of fields is the natural one arising in the construction of the Keldysh functional integral [45–49].

To begin, we rewrite the quadratic form in the exponent as

$$\bar{\Psi}\mathcal{G}^{-1}\Psi = \Psi^\dagger C\mathcal{G}^{-1}\Psi = \Psi^\dagger \mathcal{P}\Psi, \quad \mathcal{P} = C\mathcal{G}^{-1}. \quad (\text{B3})$$

Without loss of generality, $\mathcal{P} = -\mathcal{P}^\dagger$ is skew-symmetric: any symmetric component of \mathcal{P} would cancel in the quadratic form $\Psi^\dagger \mathcal{P}\Psi$ due to the Grassmann nature of Ψ . Note that skew-symmetry of \mathcal{P} is equivalent to the condition (144) for \mathcal{G} . Being skew-symmetric, even-dimensional, and generally complex, \mathcal{P} can be expressed in the form

$$\mathcal{P} = U^\dagger \Sigma U, \quad U^{-1} = U^\dagger, \quad \Sigma = \bigoplus_{d=1}^{2D} \lambda_d i\sigma_y, \quad \lambda_d \geq 0. \quad (\text{B4})$$

We define

$$\Upsilon = U\Psi = V\Phi, \quad V = \bigoplus_{d=1}^{2D} v, \quad v = \frac{1}{\sqrt{2}} \begin{pmatrix} 1 & 1 \\ i & -i \end{pmatrix}. \quad (\text{B5})$$

Writing $\Phi = (\phi_1, \phi_1^*, \dots, \phi_{2D}, \phi_{2D}^*)^\top$, where ϕ_d and ϕ_d^* are independent Grassmann variables, and using $v^\top i\sigma_y v = \sigma_y$, we may further rewrite the quadratic form as

$$\begin{aligned} \Psi^\top \mathcal{P} \Psi &= \Upsilon^\top \Sigma \Upsilon = \sum_{d=1}^{2D} \lambda_d (\Upsilon_{2d-1}, \Upsilon_{2d}) i\sigma_y \begin{pmatrix} \Upsilon_{2d-1} \\ \Upsilon_{2d} \end{pmatrix} \\ &= \sum_{d=1}^{2D} \lambda_d (\phi_d, \phi_d^*) \sigma_y \begin{pmatrix} \phi_d \\ \phi_d^* \end{pmatrix} = 2i \sum_{d=1}^{2D} \lambda_d \phi_d^* \phi_d = i\phi^\dagger A \phi, \end{aligned} \quad (\text{B6})$$

where

$$\phi = (\phi_1, \dots, \phi_{2D})^\top, \quad A = 2 \operatorname{diag}(\lambda_1, \dots, \lambda_{2D}). \quad (\text{B7})$$

Next, we express the source term $J^\top \Psi$ using ϕ and ϕ^* . Define the $4D \times 2D$ matrices P_\pm as

$$P_+ = \bigoplus_{d=1}^{2D} \begin{pmatrix} 1 \\ 0 \end{pmatrix}, \quad P_- = \bigoplus_{d=1}^{2D} \begin{pmatrix} 0 \\ 1 \end{pmatrix}, \quad (\text{B8})$$

so that $\Phi = P_+ \phi + P_- \phi^*$. Then

$$J^\top \Psi = J^\top U^\dagger V \Phi = -i(\mu^\dagger \phi - \phi^\dagger \nu), \quad (\text{B9})$$

where

$$\mu^\dagger = iJ^\top U^\dagger V P_+, \quad \nu = -iP_-^\top V^\top U^* J. \quad (\text{B10})$$

We now transform the integration measure (B2) to the variables ϕ and ϕ^* . From Eq. (B5),

$$D[\psi^*, \psi] = \frac{\operatorname{Det}(U)}{4^N \operatorname{Det}(V)} D[\Phi]. \quad (\text{B11})$$

Here Det denotes a determinant over Keldysh, charge-conjugation, replica, and, when applicable, position and discrete-time spaces. In the continuous-time limit, it becomes a functional determinant; otherwise it reduces to an ordinary determinant \det . Using

$$\operatorname{Det}(V) = \prod_{d=1}^{2D} \det(v) = (-i)^{2D} = (-1)^D, \quad (\text{B12})$$

and

$$D[\Phi] = \prod_{d=1}^{2D} d\phi_d d\phi_d^* = \prod_{d=1}^{2D} d\phi_d^* d\phi_d = D[\phi^*, \phi], \quad (\text{B13})$$

we obtain

$$D[\psi^*, \psi] = \left(-\frac{1}{4}\right)^D \operatorname{Det}(U) D[\phi^*, \phi]. \quad (\text{B14})$$

Substituting Eqs. (B6), (B9), and (B14) into Eq. (B1) yields a standard Gaussian Grassmann integral [45]:

$$\begin{aligned} Z &= \left(-\frac{1}{4}\right)^D \operatorname{Det}(U) \int D[\phi^*, \phi] e^{-\phi^\dagger A \phi + \mu^\dagger \phi + \phi^\dagger \nu} \\ &= \left(-\frac{1}{4}\right)^D \operatorname{Det}(U) \operatorname{Det}(A) e^{\mu^\dagger A^{-1} \nu}. \end{aligned} \quad (\text{B15})$$

We now rewrite the prefactor in terms of the Pfaffian of \mathcal{P} . From Eqs. (B7) and (B4),

$$\operatorname{Det}(A) = \prod_{d=1}^{2D} 2\lambda_d = 4^D \operatorname{Pf}(\Sigma). \quad (\text{B16})$$

Thus,

$$\begin{aligned} \left(-\frac{1}{4}\right)^D \operatorname{Det}(U) \operatorname{Det}(A) &= (-1)^D \operatorname{Det}(U) \operatorname{Pf}(\Sigma) \\ &= (-1)^D \operatorname{Pf}(U^\top \Sigma U) = (-1)^D \operatorname{Pf}(\mathcal{P}) = \operatorname{Pf}(-i\mathcal{P}). \end{aligned} \quad (\text{B17})$$

Next, we express the exponent in Eq. (B15) in terms of the source vector J . Using Eq. (B10),

$$\mu^\dagger A^{-1} \nu = J^\top U^\dagger V P_+ A^{-1} P_-^\top V^\top U^* J. \quad (\text{B18})$$

With the explicit forms of A and P_\pm in Eqs. (B7) and (B8), respectively,

$$P_+ A^{-1} P_- = \bigoplus_{d=1}^{2D} \frac{1}{2\lambda_d} \sigma_+. \quad (\text{B19})$$

Using $\sigma_+ = (1 + i\sigma_y)/2$ together with $vv^\top = \sigma_z$ and $vi\sigma_y v^\top = \sigma_y$, we obtain

$$V P_+ A^{-1} P_- V^\top = \bigoplus_{d=1}^{2D} \frac{1}{4\lambda_d} (\sigma_z + \sigma_y) = \frac{i}{4} (E^{-1} + \Sigma^{-1}), \quad (\text{B20})$$

where Σ is defined in Eq. (B4), and

$$E = \bigoplus_{d=1}^{2D} \lambda_d i\sigma_z = E^\top. \quad (\text{B21})$$

Thus, using $U^* = (U^\top)^{-1}$, the exponent in Eq. (B15) becomes

$$\begin{aligned} \mu^\dagger A^{-1} \nu &= \frac{i}{4} J^\top U^{-1} (E^{-1} + \Sigma^{-1}) U^* J \\ &= \frac{i}{4} J^\top \left[(U^\top E U)^{-1} + \mathcal{P}^{-1} \right] J. \end{aligned} \quad (\text{B22})$$

Since J is a Grassmann vector, the term involving the symmetric matrix $(U^\top E U)^{-1}$ vanishes. Finally, using $\mathcal{P}^{-1} = \mathcal{G}C^{-1} = \mathcal{G}C$ and inserting the above into Eq. (B15), together with Eq. (B17), we recover Eq. (B1).

2. Wick's theorem

We now use Eq. (B1) to derive Wick's theorem for systems with PHS. To begin, we rewrite Eq. (B1) as

$$\langle e^{iJ^\top \Psi} \rangle = \int \frac{D[\psi^*, \psi]}{\text{Pf}(-iG^{-1})} e^{i(\Psi G^{-1} \Psi + J^\top \Psi)} = e^{\frac{i}{4} J^\top G C J}. \quad (\text{B23})$$

Expanding both sides in power series and matching terms involving the same total power of components of J , here equal to $2F$, yields

$$\frac{1}{(2F)!} \langle (iJ^\top \Psi)^{2F} \rangle = \frac{1}{F!} \left(\frac{i}{4} J^\top G C J \right)^F. \quad (\text{B24})$$

In the following we require Wick's theorem in the setting where all fields share the same position and time while differing only in their Keldysh, charge-conjugation, and replica indices. We combine these indices into a single multiindex α . Thus, we can rewrite Eq. (B24) as

$$\begin{aligned} \frac{(-1)^F}{(2F)!} \sum_{\alpha_1, \dots, \alpha_{2F}} \langle \prod_{f=1}^{2F} J_{\alpha_f} \Psi_{\alpha_f} \rangle \\ = \frac{1}{4^F F!} \sum_{\alpha_1, \dots, \alpha_{2F}} \prod_{f=1}^F J_{\alpha_{2f-1}} (iG C)_{\alpha_{2f-1}, \alpha_{2f}} J_{\alpha_{2f}}. \end{aligned} \quad (\text{B25})$$

Consider now a fixed set of indices $\alpha_1, \dots, \alpha_{2F}$. Equation (B25) must continue to hold when we restrict the sums to those terms involving only this particular set of indices. These indices must be distinct; otherwise, the product over Grassmann variables vanishes identically. Under this restriction, the sums run over all permutations of the fixed indices. Let S_{2F} denote the symmetric group of permutations of $2F$ elements. Then

$$\begin{aligned} \frac{(-1)^F}{(2F)!} \sum_{\sigma \in S_{2F}} \langle \prod_{f=1}^{2F} J_{\alpha_{\sigma_f}} \Psi_{\alpha_{\sigma_f}} \rangle \\ = \frac{1}{4^F F!} \sum_{\sigma \in S_{2F}} \prod_{f=1}^F J_{\alpha_{\sigma_{2f-1}}} (iG C)_{\alpha_{\sigma_{2f-1}}, \alpha_{\sigma_{2f}}} J_{\alpha_{\sigma_{2f}}}. \end{aligned} \quad (\text{B26})$$

We first reorder the product on the left-hand side of Eq. (B26). Because pairs of Grassmann variables commute, the labels α_{σ_f} may be replaced by α_f . The sum over permutations then yields $(2F)!$ and cancels the prefactor. Separating the J and Ψ variables gives

$$\prod_{f=1}^{2F} J_{\alpha_f} \Psi_{\alpha_f} = (-1)^F \left(\prod_{f=1}^{2F} J_{\alpha_f} \right) \left(\prod_{f=1}^{2F} \Psi_{\alpha_f} \right). \quad (\text{B27})$$

Next, we rearrange the product on the right-hand side of Eq. (B26). Separating the J factors from the factors of $iG C$ and using $\text{sgn}(\sigma)$ for the sign of σ , we obtain

$$\prod_{f=1}^F J_{\alpha_{\sigma_{2f-1}}} J_{\alpha_{\sigma_{2f}}} = \text{sgn}(\sigma) \prod_{f=1}^{2F} J_{\alpha_f}. \quad (\text{B28})$$

Having aligned both sides of Eq. (B26) with respect to the monomial $\prod_{f=1}^{2F} J_{\alpha_f}$, we compare coefficients and arrive at Wick's theorem:

$$\begin{aligned} \langle \prod_{f=1}^{2F} \Psi_{\alpha_f} \rangle &= \frac{1}{2^{2F} F!} \sum_{\sigma \in S_{2F}} \text{sgn}(\sigma) \prod_{f=1}^F (iG C)_{\alpha_{\sigma_{2f-1}}, \alpha_{\sigma_{2f}}} \\ &= \frac{1}{2^F} \text{pf} \left\{ (iG C)_{\alpha, \alpha'} \right\}_{\alpha, \alpha' \in \{\alpha_1, \dots, \alpha_{2F}\}}. \end{aligned} \quad (\text{B29})$$

3. Decoupling of measurement vertices with PHS

As shown in Ref. [19] for symmetry class AIII, when G in the generalized Hubbard-Stratonovich transformation (99) is used to describe long-wavelength fluctuations, measurement vertices must be decoupled simultaneously in all possible channels. This requirement is satisfied by summing over all Wick contractions of measurement vertices. We extend the reasoning of Ref. [19] to symmetry class BDI, which clarifies the emergence of factors $\beta = 1/2$ [29].

We denote a point in spacetime by $\mathbf{x} = (l, t)$ and the corresponding momentum by $\mathbf{q} = (q, \omega)$, with $\mathbf{q} \cdot \mathbf{x} = ql - \omega t$. For notational convenience, we work in a finite, continuous spacetime volume so that the momenta \mathbf{q} are discrete. The integration over Σ in Eq. (143) enforces

$$\mathcal{G}_{\alpha, \alpha'}(\mathbf{x}) = -i\Psi_\alpha(\mathbf{x})\bar{\Psi}_{\alpha'}(\mathbf{x}). \quad (\text{B30})$$

To explicitly implement the assumption that G represents a slow mode, we rewrite this identity in momentum space and introduce a UV cutoff Λ . Moreover, we replace $\bar{\Psi}$ by Ψ^\top by multiplying G by C :

$$(iG C)_{\alpha, \alpha'}(\mathbf{q}) = \theta(\Lambda - |\mathbf{q}|) \sum_{\mathbf{k}} \Psi_\alpha(\mathbf{k} - \mathbf{q}/2) \Psi_{\alpha'}(-\mathbf{k} - \mathbf{q}/2). \quad (\text{B31})$$

Consider now a local vertex with $2F$ fields, contributing to the action as

$$S[\Psi] = \int d^2\mathbf{x} \prod_{f=1}^{2F} \Psi_{\alpha_f}(\mathbf{x}) = \sum_{\mathbf{k}_1, \dots, \mathbf{k}_{2F}} \delta_{0, \sum_{f=1}^{2F} \mathbf{k}_f} \prod_{f=1}^{2F} \Psi_{\alpha_f}(\mathbf{k}_f). \quad (\text{B32})$$

To project this vertex onto slow modes, we retain only those contributions for which the momenta are pairwise close, $|\mathbf{k}_f - \mathbf{k}_{f'}| \lesssim \Lambda$. To enumerate all such pairings, we start from $|\mathbf{k}_{2f-1} - \mathbf{k}_{2f}| \lesssim \Lambda$ for $f \in \{1, \dots, F\}$ and apply all permutations $\sigma \in S_{2F}$. This procedure overcounts equivalent pairings: each σ can be followed by $F!$ pair permutations without changing the pair structure, and reversing the order within each pair also leaves the pairing unchanged. Correcting for this overcounting requires division by $2^F F!$:

$$\begin{aligned} S[\Psi] &= \frac{1}{2^F F!} \sum_{\sigma \in S_{2F}} \sum_{\mathbf{k}_1, \dots, \mathbf{k}_{2F}} \delta_{0, \sum_{f=1}^{2F} \mathbf{k}_f} \\ &\quad \times \left[\prod_{f=1}^F \theta(\Lambda - |\mathbf{k}_{\sigma_{2f-1}} - \mathbf{k}_{\sigma_{2f}}|) \right] \left[\prod_{f=1}^{2F} \Psi_{\alpha_f}(\mathbf{k}_f) \right]. \end{aligned} \quad (\text{B33})$$

We reorganize the product of fields:

$$\prod_{f=1}^{2F} \Psi_{\alpha_f}(\mathbf{k}_f) = \text{sgn}(\sigma) \prod_{f=1}^F \Psi_{\alpha_{\sigma_{2f-1}}}(\mathbf{k}_{\sigma_{2f-1}}) \Psi_{\alpha_{\sigma_{2f}}}(\mathbf{k}_{\sigma_{2f}}). \quad (\text{B34})$$

Define the momentum variables

$$\mathbf{K}_f = \frac{1}{2} (\mathbf{k}_{\sigma_{2f-1}} - \mathbf{k}_{\sigma_{2f}}), \quad \mathbf{q}_f = -(\mathbf{k}_{\sigma_{2f-1}} + \mathbf{k}_{\sigma_{2f}}). \quad (\text{B35})$$

This yields

$$\begin{aligned} S[\Psi] &= \frac{1}{2^F F!} \sum_{\sigma \in S_{2F}} \text{sgn}(\sigma) \sum_{\mathbf{q}_1, \dots, \mathbf{q}_F} \delta_{0, \sum_{f=1}^F \mathbf{q}_f} \\ &\times \prod_{f=1}^F \theta(\Lambda - |\mathbf{q}_f|) \sum_{\mathbf{K}_f} \Psi_{\alpha_{\sigma_{2f-1}}}(\mathbf{K}_f - \mathbf{q}_f/2) \Psi_{\alpha_{\sigma_{2f}}}(-\mathbf{K}_f - \mathbf{q}_f/2). \end{aligned} \quad (\text{B36})$$

Comparing with Eq. (B31), we identify the structure of the slow mode on the right-hand side. Transforming back to spacetime, we obtain

$$S[\Psi] = \frac{1}{2^F F!} \sum_{\sigma \in S_{2F}} \text{sgn}(\sigma) \int d^2 \mathbf{x} \prod_{f=1}^F (i\mathcal{G}C)_{\alpha_{\sigma_{2f-1}}, \alpha_{\sigma_{2f}}}(\mathbf{x}). \quad (\text{B37})$$

When we now compare Eq. (B37) with Wick's theorem (B29), we observe that the right-hand sides match up to the factor $1/2^F = \beta^F$ appearing in the latter. This factor may be absorbed by a redefinition of \mathcal{G} . Thus, the projection of the vertex onto soft modes is equivalent to averaging the original vertex as in Eq. (B23), but with \mathcal{G} replaced by \mathcal{G}/β . Writing the vertex as $S[\Psi] = \int d^2 \mathbf{x} V[\Psi(\mathbf{x})]$, we obtain

$$V[\mathcal{G}] = \int \frac{D[\psi^*, \psi]}{\text{pf}(-i\beta C \mathcal{G}^{-1})} V[\Psi] e^{i\beta \bar{\Psi} \mathcal{G}^{-1} \Psi}, \quad (\text{B38})$$

where all fields and matrices are evaluated at the same spacetime point, so the Pfaffian in the denominator is taken only over Keldysh, charge-conjugation, and replica spaces. The factor β on the right-hand side is missing in Ref. [29].

4. Generalized Hubbard-Stratonovich transformation with PHS

Building on the preceding results, we now apply the generalized Hubbard-Stratonovich transformation to the particle-hole-symmetrized action $S = S_H + S_M$ with the Hamiltonian action (140) and the measurement Lagrangian (142).

We begin by rewriting the measurement Lagrangian (142) in terms of $\mathcal{G} = -i\Psi\bar{\Psi}$. For the first two terms, we obtain

$$\bar{\Psi}\Lambda\Psi = -i \text{tr}(\Lambda\mathcal{G}), \quad \bar{\Psi}\sigma_z\Psi = -i \text{tr}(\sigma_z\mathcal{G}). \quad (\text{B39})$$

To decouple the third term, we use Eq. (B38). In preparation for performing the Grassmann integral on the right-hand side, we express the measurement vertex in exponential form,

noting that any exponential containing $\bar{\Psi}_r\sigma_{\pm}\Psi_r$ truncates after two terms. This yields

$$V_{\pm}[\Psi] = \prod_{r=1}^R (-\bar{\Psi}_r \sigma_{\pm} \Psi_r) = \lim_{\epsilon \rightarrow 0} (i\epsilon)^R e^{i\epsilon \bar{\Psi} \sigma_{\pm} \Psi}, \quad (\text{B40})$$

where the replica index r is implicitly summed in the exponent. This relation recasts Eq. (B38) as a Gaussian integral. Using Eq. (B1), we thus obtain

$$V_{\pm}[\mathcal{G}] = \lim_{\epsilon \rightarrow 0} (i\epsilon)^R \frac{\text{pf}[-i\beta C(\mathcal{G}^{-1} + \frac{1}{\beta\epsilon}\sigma_{\pm})]}{\text{pf}(-i\beta C \mathcal{G}^{-1})}. \quad (\text{B41})$$

To simplify the ratio of Pfaffians, we use that for any skew-symmetric $4R \times 4R$ matrix A , $\text{pf}(A)^{-1} = \text{pf}(A^{-1})$. We then apply Eq. (153) with $D = 2R$. After that, splitting the trace over Keldysh, charge-conjugation, and replica spaces as $\text{tr} = \text{tr}_K \text{tr}_{CR}$, and writing the prefactor as

$$\epsilon^R = e^{\beta \text{tr}_{CR}[\ln(\epsilon)]}, \quad (\text{B42})$$

we obtain

$$V_{\pm}[\mathcal{G}] = i^R \lim_{\epsilon \rightarrow 0} e^{\beta \text{tr}_{CR} \ln[\epsilon \exp \text{tr}_K \ln(1 + \frac{1}{\beta\epsilon}\sigma_{\pm}\mathcal{G})]}. \quad (\text{B43})$$

To take the limit $\epsilon \rightarrow 0$, we expand $\exp \text{tr}_K \ln$ as a power series in $1/\epsilon$. Note that since \mathcal{G} is a matrix in Keldysh, charge-conjugation, and replica spaces, tr_K is only a partial trace, and $\exp \text{tr}_K \ln$ does not reduce to a determinant in Keldysh space. The expansion of such a determinant in two dimensions would terminate at second order. While this simplification does not generally occur when tr_K is a partial trace, the appearance of σ_{\pm} causes the expansion to terminate already at first order, as we show in the following.

We obtain a formal series expansion by using the expansions of the exponential function and the logarithm:

$$\begin{aligned} e^{\text{tr}_K \ln(1 + \frac{1}{\beta\epsilon}\sigma_{\pm}\mathcal{G})} &= 1 + \sum_{K=1}^{\infty} \frac{1}{(\beta\epsilon)^K} \sum_{n=1}^{\infty} \frac{(-1)^{n+K}}{n!} \\ &\times \sum_{k_1, \dots, k_n=1}^{\infty} \delta_{K, \sum_{i=1}^n k_i} \prod_{i=1}^n \frac{1}{k_i} \text{tr}_K[(\sigma_{\pm}\mathcal{G})^{k_i}]. \end{aligned} \quad (\text{B44})$$

To simplify the final product, we note first that for any 2×2 matrices A and B , one can check by explicit calculation that

$$\text{tr}(\sigma_{\pm} A \sigma_{\pm} B) = \text{tr}(\sigma_{\pm} A) \text{tr}(\sigma_{\pm} B). \quad (\text{B45})$$

This factorization property can be seen to extend to partial traces by using the Schmidt decomposition of \mathcal{G} ,

$$\mathcal{G} = \sum_{\mu=0}^3 \sigma_{\mu} \otimes \mathcal{G}_{\mu}, \quad (\text{B46})$$

where σ_{μ} are Pauli matrices in Keldysh space \mathcal{G}_{μ} are $2R \times 2R$ matrices in charge-conjugation and replica spaces. We find

$$\text{tr}_K[(\sigma_{\pm}\mathcal{G})^k] = \text{tr}_K(\sigma_{\pm}\mathcal{G})^k. \quad (\text{B47})$$

Thus,

$$e^{\text{tr}_K \ln(1 + \frac{1}{\beta\epsilon} \sigma_{\pm} \mathcal{G})} = 1 + \sum_{K=1}^{\infty} c_K \left[\frac{1}{\beta\epsilon} \text{tr}_K (\sigma_{\pm} \mathcal{G})^K \right]^K, \quad (\text{B48})$$

where

$$c_K = \sum_{n=1}^{\infty} \frac{(-1)^{n+K}}{n!} \sum_{k_1, \dots, k_n=1}^{\infty} \delta_{K, \sum_{i=1}^n k_i} \prod_{i=1}^n \frac{1}{k_i}. \quad (\text{B49})$$

Now consider a 1×1 matrix A such that $\det(1 + A/\epsilon) = 1 + A/\epsilon$. On the other hand, we can write $\det(1 + A/\epsilon) = \exp \text{tr} \ln(1 + A/\epsilon)$ and use the exact same expansion as above—obviously, a factorization property analogous to Eq. (B45) applies also to 1×1 matrices. Then, by comparing the coefficients of equal powers of $1/\epsilon$ in $\det(1 + A/\epsilon) = 1 + A/\epsilon$ and the right-hand side of Eq. (B48), we find $c_1 = 1$ and $c_K = 0$ for $K \geq 2$. Therefore,

$$e^{\text{tr}_K \ln(1 + \frac{1}{\beta\epsilon} \sigma_{\pm} \mathcal{G})} = 1 + \frac{1}{\beta\epsilon} \text{tr}_K (\sigma_{\pm} \mathcal{G}). \quad (\text{B50})$$

Inserting this into Eq. (B43) and taking the limit $\epsilon \rightarrow 0$ yields

$$V_{\pm}[\mathcal{G}] = i^R e^{\beta \text{tr}_{CR} \ln \text{tr}_K (\frac{1}{\beta} \sigma_{\pm} \mathcal{G})}. \quad (\text{B51})$$

Finally, substituting Eqs. (B39) and (B51) into Eq. (142) yields Eq. (145).

With the measurement Lagrangian decoupled, the remaining Grassmann integral in the Keldysh partition function is quadratic and can be evaluated using Eq. (B1). Leaving the summation over lattice sites and integration over time implicit, we obtain

$$\begin{aligned} \int D[\psi^*, \psi] e^{i\bar{\Psi}G^{-1}\Psi} &= \text{Pf}(-iCG^{-1}) \\ &= (-1)^{RLN} e^{i\text{Tr}[\beta \ln(G^{-1})]}, \end{aligned} \quad (\text{B52})$$

where the Pfaffian is taken over Keldysh, charge-conjugation, replica, position, and time spaces, and where $G^{-1} = G_0^{-1} + i\mathbb{1}$ with G_0^{-1} defined in Eq. (93). In the second equality we used Eq. (153) with $A = \sigma_z C$ and $B = CG^{-1}$, and $D = 2RLN$, where LN is the dimension of position-time space, that is, lattice size times the number of time steps. The sign arises from

$$\text{Pf}(\sigma_z C) = \text{pf}_{KC}(\sigma_z C)^{RLN} = (-1)^{RLN}. \quad (\text{B53})$$

We absorb this sign into the integration measure $D[\mathcal{G}, \Sigma]$. The resulting Keldysh partition function is then given by Eqs. (104) and (105), with S_0 from Eq. (146).

Appendix C: Numerical methods

In what follows we provide a description of the numerical procedure we use to simulate quantum trajectories for imbalanced and inefficient fermion counting. Our approach builds on the formulation of quantum-jump trajectories for efficient

detection in Sec. II together with its extension to inefficient detection in Sec. V.

The dynamics proceed in discrete time steps Δt . For inefficient detection, each step is further decomposed into two substeps of duration $\eta\Delta t$ and $(1 - \eta)\Delta t$, respectively. The first substep implements measurement-conditioned evolution; its numerical treatment is presented in Sec. C1. The second substep implements unconditional evolution, corresponding to an average over measurement outcomes; the associated algorithm is detailed in Sec. C2. Additional implementation details for the no-jump evolution during the first substep are provided in Sec. C3.

For generality, we formulate the algorithm in terms of arbitrary gain and loss jump operators,

$$\hat{c}_{+,l} = \sqrt{2} \sum_{l'=1}^L B_{+,l,l'} \hat{\psi}_{l'}^{\dagger}, \quad \hat{c}_{-,l} = \sqrt{2} \sum_{l'=1}^L B_{-,l,l'} \hat{\psi}_{l'}. \quad (\text{C1})$$

Moreover, for later use, we denote the l th row and column of a matrix A by $A_{l,*}$ and $A_{*,l}$, respectively, and introduce

$$M_{+,l} = (B_{+}^{\dagger})_{*,l} B_{+,l,*}^*, \quad M_{-,l} = (B_{-}^{\dagger})_{*,l} B_{-,l,*}, \quad (\text{C2})$$

along with the Hermitian bath matrices

$$M_{+} = \sum_{l=1}^L M_{+,l} = B_{+}^{\dagger} B_{+}^*, \quad M_{-} = \sum_{l=1}^L M_{-,l} = B_{-}^{\dagger} B_{-}. \quad (\text{C3})$$

The corresponding expressions for local gain and loss as in Eq. (80) are obtained by setting

$$B_{\pm} = \sqrt{\gamma_{\pm}/2}. \quad (\text{C4})$$

1. Conditional evolution

During the first time substep, the evolution is conditioned on the measurement outcome, and the algorithm samples different outcomes stochastically. However, we do not directly implement the trajectory evolution described in Secs. II and V. Instead, exploiting the locality of the jump processes, we construct a more efficient scheme.

To begin, we outline why the first-order-in-time quantum-jump method [64] of Secs. II and V cannot be applied directly. The probability that any jump occurs during a single time step, given the system state $\hat{\rho}(t)$, is the sum of the individual jump probabilities in Eq. (70). With $\alpha = \pm$ denoting gain and loss and l the site index,

$$P_{\alpha,l} = \text{tr}[\mathcal{K}_{1,\alpha,l} \hat{\rho}(t)]. \quad (\text{C5})$$

Substituting here the jump superoperator (71) together with Eq. (68) and the general gain and loss jump operators (C1), one obtains

$$\begin{aligned} P_{+,l} &= 2\eta\Delta t \text{tr}\{M_{+,l} [1 - D(t)]\} = \eta\gamma_{+}\Delta t [1 - D_{l,l}(t)], \\ P_{-,l} &= 2\eta\Delta t \text{tr}\{M_{-,l} D(t)\} = \eta\gamma_{-}\Delta t D_{l,l}(t), \end{aligned} \quad (\text{C6})$$

where $D(t)$ is the single-particle density matrix (168), the matrices $M_{\pm,l}$ are defined in Eq. (C2), and the final equalities

apply in the case of local gain and loss. The total jump probability during the time step from t to $t + \Delta t$ becomes

$$P_{\text{jump}} = \sum_{\alpha=\pm} \sum_{l=1}^L P_{\alpha,l} = \eta \Delta t \{L\gamma_+ - \Delta\gamma \text{tr}[D(t)]\}, \quad (\text{C7})$$

where $\text{tr}[D(t)] = \langle \hat{N}(t) \rangle$ is the mean particle number. Since $\langle \hat{N}(t) \rangle$ is typically of order L , enforcing $P_{\text{jump}} \ll 1$, as required for the validity of the first-order method [64], forces $\Delta t \sim L^{-1}$, which is computationally prohibitive.

To circumvent this limitation, we treat the local measurement processes at each site independently. In each step, the lattice is traversed in a randomly chosen order. For site l , the jump probability is

$$P_{\text{jump},l} = \sum_{\alpha=\pm} P_{\alpha,l} = \eta \Delta t [\gamma_+ - \Delta\gamma D_{l,l}(t)]. \quad (\text{C8})$$

A uniformly distributed random number $r_1 \in [0, 1]$ determines whether a jump occurs: a jump is applied if $r_1 < P_{\text{jump},l}$. A second random number $r_2 \in [0, 1]$ determines whether the jump is gain or loss, with loss selected if $r_2 < \tilde{P}_{-,l}$, where

$$\tilde{P}_{\pm,l} = P_{\pm,l} / P_{\text{jump},l}. \quad (\text{C9})$$

Otherwise the jump is gain. The corresponding transformation of the state is

$$\hat{\rho}(t) \rightarrow \mathcal{K}_{1,\pm,l} \hat{\rho}(t) / \text{tr}[\mathcal{K}_{1,\pm,l} \hat{\rho}(t)], \quad (\text{C10})$$

which preserves Gaussianity. Hence the induced change in the single-particle density matrix can be computed using Wick's theorem. For a gain at site l ,

$$D(t) \rightarrow D(t) + \frac{[1 - D(t)] M_{+,l} [1 - D(t)]}{\text{tr}\{M_{+,l} [1 - D(t)]\}}. \quad (\text{C11})$$

and for a loss at site l ,

$$D(t) \rightarrow D(t) - \frac{D(t) M_{-,l} D(t)}{\text{tr}\{M_{-,l} D(t)\}}. \quad (\text{C12})$$

For local gain and loss, multiplication by $M_{\pm,l}$ merely selects specific rows and columns of $D(t)$, allowing the updates to be implemented without explicit matrix multiplications. In particular, for gain at site l , using the notation of Eq. (C2),

$$D(t) \rightarrow D(t) + \frac{[1 - D(t)]_{*,l} [1 - D(t)]_{l,*}}{1 - D_{l,l}(t)}. \quad (\text{C13})$$

and for loss at site l ,

$$D(t) \rightarrow D(t) - \frac{D_{*,l}(t) D_{l,*}(t)}{D_{l,l}(t)}. \quad (\text{C14})$$

After sweeping through the chain and applying all jumps, we carry out continuous no-jump evolution generated by $\hat{K}_{1,0}$ in Eq. (68). This evolution acts on every lattice site, including those at which jumps occurred, but the resulting error is negligible because a given site undergoes only finitely many jumps in any finite time [53]. The continuous evolution is

$$\hat{\rho}(t + \eta \Delta t) = \frac{\mathcal{K}_{1,0} \hat{\rho}(t)}{\text{tr}[\mathcal{K}_{1,0} \hat{\rho}(t)]} = \frac{\hat{K}_{1,0} \hat{\rho}(t) \hat{K}_{1,0}^\dagger}{\text{tr}[\hat{K}_{1,0} \hat{\rho}(t) \hat{K}_{1,0}^\dagger]}. \quad (\text{C15})$$

As shown in Sec. C 3, this can be recast in terms of the single-particle density matrix as

$$D(t + \eta \Delta t) = U(\eta \Delta t) \times \{D(t) + e^{-\eta \Delta \gamma \Delta t} [1 - D(t)]\}^{-1} D(t) U^\dagger(\eta \Delta t), \quad (\text{C16})$$

where $U(t) = e^{-iHt}$. This completes the first time substep.

Before discussing the unconditional evolution in the second substep, we emphasize that treating local measurements independently allows us to choose a time step that does not scale as $\Delta t \sim L^{-1}$. In practice, we select Δt such that the jump probability at a single site, estimated from Eq. (C8) with $\eta = 1$ and half filling as $P_{\text{jump},l} = \gamma \Delta t$, is 0.0125 %. We verified that the results remain unchanged upon doubling or halving Δt .

We have not attempted a rigorous analysis of the error incurred by treating local measurements independently. Instead, we performed numerical benchmarks: observables linear in the state agree quantitatively with the unconditional evolution that can be computed numerically exactly as described in Sec. C 2. Furthermore, for balanced and efficient fermion counting with $\gamma_+ = \gamma_-$ and $\eta = 1$, our results agree well with those of Ref. [30], obtained using a numerically exact method [64]. The implementation in Ref. [30] relies on the rates being balanced, $\gamma_+ = \gamma_-$, in which case fermion counting can be rephrased as a random generalized measurement. In that case, the waiting time between jumps can be sampled from an exponential distribution, and the evolution between jumps can be implemented through exact diagonalization.

2. Unconditional evolution

Unconditional evolution during the second time substep is governed by Eq. (72). This equation corresponds to the first-order expansion in Δt of the evolution over the interval $(1 - \eta) \Delta t$ generated by the Liouvillian (7). In our numerical implementation, we treat this interval exactly by evolving the state under the master equation

$$\frac{d\hat{\rho}(t)}{dt} = \mathcal{L}\hat{\rho}(t), \quad (\text{C17})$$

for a duration $(1 - \eta) \Delta t$. This master equation can be recast as a closed equation of motion for the single-particle density matrix (168), which admits an exact solution [83].

We consider the general quadratic Hamiltonian in Eq. (78) and the gain-loss jump operators in Eq. (C1). The single-particle density matrix obeys

$$\frac{dD(t)}{dt} = -i [ZD(t) - D(t)Z^\dagger] + 2M_+, \quad (\text{C18})$$

with

$$Z = H - iM, \quad M = M_- + M_+. \quad (\text{C19})$$

The solution to Eq. (C18) with initial condition D_0 at $t = 0$ is

$$D(t) = Q(t) D_0 Q(t)^\dagger + R(t), \quad (\text{C20})$$

where

$$Q(t) = e^{-iZt}. \quad (\text{C21})$$

To specify $R(t)$, write $Z = V\Lambda V^{-1}$, with $\Lambda = \text{diag}(\lambda_1, \dots, \lambda_L)$. Define the elementwise or Hadamard product $A \circ B$ via

$$(A \circ B)_{l,l'} = A_{l,l'} B_{l,l'}. \quad (\text{C22})$$

Then

$$R(t) = -2i V \left[(V^{-1} M_+ V^{-\dagger}) \circ K(t) \right] V^\dagger, \quad (\text{C23})$$

where

$$K_{l,l'}(t) = \frac{1 - e^{-i(\lambda_l - \lambda_{l'}^*)t}}{\lambda_l - \lambda_{l'}^*}. \quad (\text{C24})$$

As noted above, our numerical implementation uses Eq. (C20) to evolve the single-particle density matrix over the second substep, from the beginning time t to $t + (1 - \eta)\Delta t$.

3. No-jump evolution

It remains to derive Eq. (C16). For the jump operators in Eq. (C1), the effective Hamiltonian (3) becomes

$$\hat{H}_{\text{eff}} = \hat{H} - i \left[\hat{H}' + \text{tr}(M_+) \right]. \quad (\text{C25})$$

where

$$\hat{H}' = - \sum_{l,l'=1}^L \hat{\psi}_l^\dagger \Delta M_{l,l'} \hat{\psi}_{l'}, \quad \Delta M = M_+ - M_-. \quad (\text{C26})$$

For local gain and loss, this expression reduces to

$$\hat{H}_{\text{eff}} = \hat{H} + \frac{i}{2} (\Delta\gamma\hat{N} - L\gamma_+). \quad (\text{C27})$$

Up to first order in Δt , the no-jump Kraus operator in Eq. (68) can therefore be written as

$$\hat{K}_{1,0} = e^{-i\hat{H}_{\text{eff}}\Delta t} = e^{-i\eta\hat{H}\Delta t} e^{-\eta\hat{H}'\Delta t} e^{-\eta\text{tr}(M_+)\Delta t}. \quad (\text{C28})$$

The final exponential drops out due to the normalization in Eq. (C15) and may hence be omitted. The remaining two factors generate unitary and non-unitary evolution, respectively. We define

$$\hat{U}(t) = e^{-i\hat{H}t}, \quad \hat{V}(t) = e^{-\hat{H}'t} = e^{\Delta\gamma\hat{N}t/2} = \hat{V}^\dagger(t), \quad (\text{C29})$$

so that

$$\hat{K}_{1,0} = \hat{U}(\eta\Delta t) \hat{V}(\eta\Delta t). \quad (\text{C30})$$

The evolution in Eq. (C15) then factorizes as

$$\hat{\rho}(t + \eta\Delta t) = \hat{U}(\eta\Delta t) \frac{\hat{V}(\eta\Delta t) \hat{\rho}(t) \hat{V}(\eta\Delta t)}{\text{tr}[\hat{V}(\eta\Delta t) \hat{\rho}(t) \hat{V}(\eta\Delta t)]} \hat{U}^\dagger(\eta\Delta t). \quad (\text{C31})$$

We first analyze the evolution generated by $\hat{V}(t)$. Consider the general expression

$$\hat{\rho}(t) = \frac{\hat{V}(t) \hat{\rho}_0 \hat{V}(t)}{\text{tr}[\hat{V}(t) \hat{\rho}_0 \hat{V}(t)]}, \quad (\text{C32})$$

which reduces to the form required in Eq. (C31) when we set $t = \eta\Delta t$ and $\hat{\rho}_0 = \hat{\rho}(t)$. Differentiating with respect to t yields

$$\frac{d\hat{\rho}}{dt} = -\{\hat{H}', \hat{\rho}\} + 2 \text{tr}(\hat{H}' \hat{\rho}) \hat{\rho}. \quad (\text{C33})$$

This equation can be rewritten as an evolution equation for the single-particle density matrix (168). Since $\hat{\rho}(t)$ in Eq. (C32) is a normalized product of Gaussian operators, it remains a normalized Gaussian state. Wick's theorem therefore applies, leading to

$$\frac{dD}{dt} = \{\Delta M, D\} - 2D\Delta M D = \Delta\gamma(1 - D)D. \quad (\text{C34})$$

To solve this equation, we assume that D is invertible and introduce the matrix

$$Y = D^{-1} - 1, \quad D = (1 + Y)^{-1}. \quad (\text{C35})$$

Using

$$\frac{dD^{-1}}{dt} = -D^{-1} \frac{dD}{dt} D^{-1}, \quad (\text{C36})$$

we obtain

$$\frac{dY}{dt} = \frac{dD^{-1}}{dt} = -\{\Delta M, Y\}. \quad (\text{C37})$$

The solution of this equation reads

$$Y(t) = e^{-\Delta M t} Y_0 e^{-\Delta M t}, \quad (\text{C38})$$

which yields

$$\begin{aligned} D(t) &= \left[1 + e^{-\Delta M t} (D_0^{-1} - 1) e^{-\Delta M t} \right]^{-1} \\ &= [D_0 + e^{-\Delta\gamma t} (1 - D_0)]^{-1} D_0. \end{aligned} \quad (\text{C39})$$

In Eq. (C31), we require $t = \eta\Delta t$ and $D_0 = D(t)$. Finally, also the unitary evolution in Eq. (C31) can be reformulated in terms of the single-particle density matrix using the approach of Sec. C 2. We thus obtain Eq. (C16).

- [1] Y. Li, X. Chen, and M. P. A. Fisher, Quantum Zeno effect and the many-body entanglement transition, *Phys. Rev. B* **98**, 205136 (2018).
- [2] B. Skinner, J. Ruhman, and A. Nahum, Measurement-Induced Phase Transitions in the Dynamics of Entanglement, *Phys. Rev. X* **9**, 031009 (2019).
- [3] Y. Li, X. Chen, and M. P. A. Fisher, Measurement-driven entanglement transition in hybrid quantum circuits, *Phys. Rev. B* **100**, 134306 (2019).
- [4] M. P. Fisher, V. Khemani, A. Nahum, and S. Vijay, Random Quantum Circuits, *Annu. Rev. Condens. Matter Phys.* **14**, 335 (2023).
- [5] X. Cao, A. Tilloy, and A. De Luca, Entanglement in a fermion chain under continuous monitoring, *SciPost Phys.* **7**, 024 (2019).
- [6] Y. Fuji and Y. Ashida, Measurement-induced quantum criticality under continuous monitoring, *Phys. Rev. B* **102**, 054302 (2020).
- [7] S. Goto and I. Danshita, Measurement-induced transitions of the entanglement scaling law in ultracold gases with controllable dissipation, *Phys. Rev. A* **102**, 033316 (2020).
- [8] Q. Tang and W. Zhu, Measurement-induced phase transition: A case study in the nonintegrable model by density-matrix renormalization group calculations, *Phys. Rev. Res.* **2**, 013022 (2020).
- [9] N. Lang and H. P. Büchler, Entanglement transition in the projective transverse field Ising model, *Phys. Rev. B* **102**, 094204 (2020).
- [10] D. Rossini and E. Vicari, Measurement-induced dynamics of many-body systems at quantum criticality, *Phys. Rev. B* **102**, 035119 (2020).
- [11] O. Alberton, M. Buchhold, and S. Diehl, Entanglement Transition in a Monitored Free-Fermion Chain: From Extended Criticality to Area Law, *Phys. Rev. Lett.* **126**, 170602 (2021).
- [12] Y. Bao, S. Choi, and E. Altman, Symmetry enriched phases of quantum circuits, *Ann. Phys. (N. Y.)* **435**, 168618 (2021).
- [13] M. Buchhold, Y. Minoguchi, A. Altland, and S. Diehl, Effective Theory for the Measurement-Induced Phase Transition of Dirac Fermions, *Phys. Rev. X* **11**, 041004 (2021).
- [14] T. Botzung, S. Diehl, and M. Müller, Engineered dissipation induced entanglement transition in quantum spin chains: From logarithmic growth to area law, *Phys. Rev. B* **104**, 184422 (2021).
- [15] X. Turkeshi, A. Biella, R. Fazio, M. Dalmonte, and M. Schirò, Measurement-induced entanglement transitions in the quantum Ising chain: From infinite to zero clicks, *Phys. Rev. B* **103**, 224210 (2021).
- [16] C.-M. Jian, B. Bauer, A. Keselman, and A. W. W. Ludwig, Criticality and entanglement in nonunitary quantum circuits and tensor networks of noninteracting fermions, *Phys. Rev. B* **106**, 134206 (2022).
- [17] T. Müller, S. Diehl, and M. Buchhold, Measurement-Induced Dark State Phase Transitions in Long-Ranged Fermion Systems, *Phys. Rev. Lett.* **128**, 010605 (2022).
- [18] G. Kells, D. Meidan, and A. Romito, Topological transitions in weakly monitored free fermions, *SciPost Physics* **14**, 031 (2023).
- [19] I. Pohoiko, P. Pöpperl, I. V. Gornyi, and A. D. Mirlin, Theory of Free Fermions under Random Projective Measurements, *Phys. Rev. X* **13**, 041046 (2023).
- [20] C.-M. Jian, H. Shapourian, B. Bauer, and A. W. W. Ludwig, Measurement-induced entanglement transitions in quantum circuits of non-interacting fermions: Born-rule versus forced measurements, [arXiv:2302.09094](https://arxiv.org/abs/2302.09094) (2023).
- [21] M. Fava, L. Piroli, T. Swann, D. Bernard, and A. Nahum, Nonlinear Sigma Models for Monitored Dynamics of Free Fermions, *Phys. Rev. X* **13**, 041045 (2023).
- [22] J. Merritt and L. Fidkowski, Entanglement transitions with free fermions, *Phys. Rev. B* **107**, 064303 (2023).
- [23] K. Chahine and M. Buchhold, Entanglement phases, localization, and multifractality of monitored free fermions in two dimensions, *Phys. Rev. B* **110**, 054313 (2024).
- [24] I. Pohoiko, I. V. Gornyi, and A. D. Mirlin, Measurement-Induced Phase Transition for Free Fermions above One Dimension, *Phys. Rev. Lett.* **132**, 110403 (2024).
- [25] M. Tsitsishvili, D. Poletti, M. Dalmonte, and G. Chiriacò, Measurement induced transitions in non-Markovian free fermion ladders, *SciPost Phys. Core* **7**, 011 (2024).
- [26] M. Fava, L. Piroli, D. Bernard, and A. Nahum, Monitored fermions with conserved $U(1)$ charge, *Phys. Rev. Res.* **6**, 043246 (2024).
- [27] X. Turkeshi, L. Piroli, and M. Schirò, Density and current statistics in boundary-driven monitored fermionic chains, *Phys. Rev. B* **109**, 144306 (2024).
- [28] H. Guo, M. S. Foster, C.-M. Jian, and A. W. W. Ludwig, Field theory of monitored interacting fermion dynamics with charge conservation, *Phys. Rev. B* **112**, 064304 (2025).
- [29] I. Pohoiko, P. Pöpperl, I. V. Gornyi, and A. D. Mirlin, Measurement-induced transitions for interacting fermions, *Phys. Rev. B* **111**, 024204 (2025).
- [30] E. Starchl, M. H. Fischer, and L. M. Sieberer, Generalized Zeno Effect and Entanglement Dynamics Induced by Fermion Counting, *PRX Quantum* **6**, 030302 (2025).
- [31] T. M. Müller, M. Buchhold, and S. Diehl, Monitored interacting Dirac fermions, [arXiv:2502.02645](https://arxiv.org/abs/2502.02645) (2025).
- [32] R. D. Soares, Y. Le Gal, and M. Schirò, Entanglement transition due to particle losses in a monitored fermionic chain, *Phys. Rev. B* **111**, 064313 (2025).
- [33] B. Fan, C. Yin, and A. M. García-García, Entanglement dynamics of monitored non-interacting fermions on Graphic-Processing-Units, [arXiv:2508.18468](https://arxiv.org/abs/2508.18468) (2025).
- [34] C. Niederegger, T. Vovk, E. Starchl, and L. M. Sieberer, Absence of measurement- and unraveling-induced entanglement transitions in continuously monitored one-dimensional free fermions, [arXiv:2510.19459](https://arxiv.org/abs/2510.19459) (2025).
- [35] B. Ladewig, S. Diehl, and M. Buchhold, Monitored open fermion dynamics: Exploring the interplay of measurement, decoherence, and free Hamiltonian evolution, *Phys. Rev. Res.* **4**, 033001 (2022).
- [36] Y. Minoguchi, P. Rabl, and M. Buchhold, Continuous gaussian measurements of the free boson CFT: A model for exactly solvable and detectable measurement-induced dynamics, *SciPost Physics* **12**, 009 (2022).
- [37] G. Passarelli, X. Turkeshi, A. Russomanno, P. Lucignano, M. Schirò, and R. Fazio, Many-Body Dynamics in Monitored Atomic Gases without Postselection Barrier, *Phys. Rev. Lett.* **132**, 163401 (2024).
- [38] C. Y. Leung, D. Meidan, and A. Romito, Theory of Free Fermions Dynamics under Partial Postselected Monitoring, *Phys. Rev. X* **15**, 021020 (2025).
- [39] C. Y. Leung and A. Romito, Entanglement and operator correlation signatures of many-body quantum Zeno phases in inef-

- ficiently monitored noisy systems, *Phys. Rev. A* **111**, 022427 (2025).
- [40] A. Paviglianiti, G. D. Fresco, A. Silva, B. Spagnolo, D. Valenti, and A. Carollo, Breakdown of Measurement-Induced Phase Transitions Under Information Loss, *Quantum* **9**, 1781 (2025).
- [41] M. Mezard, G. Parisi, and M. Virasoro, *Spin Glass Theory and Beyond*, World Scientific Lecture Notes in Physics, Vol. 9 (WORLD SCIENTIFIC, Singapore, 1986).
- [42] F. Evers and A. D. Mirlin, Anderson transitions, *Rev. Mod. Phys.* **80**, 1355 (2008).
- [43] Y. Bao, S. Choi, and E. Altman, Theory of the phase transition in random unitary circuits with measurements, *Phys. Rev. B* **101**, 104301 (2020).
- [44] C.-M. Jian, Y.-Z. You, R. Vasseur, and A. W. W. Ludwig, Measurement-induced criticality in random quantum circuits, *Phys. Rev. B* **101**, 104302 (2020).
- [45] A. Altland and B. D. Simons, *Condensed Matter Field Theory*, 2nd ed. (Cambridge University Press, Cambridge, 2010).
- [46] L. M. Sieberer, M. Buchhold, and S. Diehl, Keldysh field theory for driven open quantum systems, *Reports Prog. Phys.* **79**, 096001 (2016).
- [47] L. M. Sieberer, M. Buchhold, J. Marino, and S. Diehl, Universality in driven open quantum matter, *Rev. Mod. Phys.* **97**, 025004 (2025).
- [48] F. Thompson and A. Kamenev, Field theory of many-body Lindbladian dynamics, *Ann. Phys. (N. Y.)* **455**, 169385 (2023).
- [49] A. Kamenev, *Field Theory of Non-Equilibrium Systems*, 2nd ed. (Cambridge University Press, Cambridge, 2023).
- [50] M. A. Nielsen and I. L. Chuang, *Quantum Computation and Quantum Information*, 10th ed. (Cambridge University Press, Cambridge, 2012).
- [51] C. Gardiner and P. Zoller, *The Quantum World of Ultra-Cold Atoms and Light Book I: Foundations of Quantum Optics*, Cold Atoms, Vol. 2 (Imperial College Press, London, 2014).
- [52] C. Gardiner and P. Zoller, *The Quantum World of Ultra-Cold Atoms and Light Book II: The Physics of Quantum-Optical Devices*, Cold Atoms, Vol. 4 (Imperial College Press, London, 2015).
- [53] H. M. Wiseman and G. J. Milburn, *Quantum Measurement and Control*, 1st ed. (Cambridge University Press, Cambridge, 2009).
- [54] K. Jacobs, *Quantum Measurement Theory and its Applications* (Cambridge University Press, Cambridge, 2014).
- [55] S. Lieu, M. McGinley, and N. R. Cooper, Tenfold Way for Quadratic Lindbladians, *Phys. Rev. Lett.* **124**, 040401 (2020).
- [56] A. Altland, M. Fleischhauer, and S. Diehl, Symmetry Classes of Open Fermionic Quantum Matter, *Phys. Rev. X* **11**, 021037 (2021).
- [57] L. Sá, P. Ribeiro, and T. Prosen, Symmetry Classification of Many-Body Lindbladians: Tenfold Way and Beyond, *Phys. Rev. X* **13**, 031019 (2023).
- [58] K. Kawabata, A. Kulkarni, J. Li, T. Numasawa, and S. Ryu, Symmetry of Open Quantum Systems: Classification of Dissipative Quantum Chaos, *PRX Quantum* **4**, 030328 (2023).
- [59] Z. Xiao and K. Kawabata, Topology of Monitored Quantum Dynamics, [arXiv:2412.06133](https://arxiv.org/abs/2412.06133) (2024).
- [60] A. Bhuiyan, H. Pan, and C.-M. Jian, Free Fermion Dynamics with Measurements: Topological Classification and Adaptive Preparation of Topological States, [arXiv:2507.13437](https://arxiv.org/abs/2507.13437) (2025).
- [61] H. Shapourian, K. Shiozaki, and S. Ryu, Partial time-reversal transformation and entanglement negativity in fermionic systems, *Phys. Rev. B* **95**, 165101 (2017).
- [62] H. Shapourian and S. Ryu, Entanglement negativity of fermions: Monotonicity, separability criterion, and classification of few-mode states, *Phys. Rev. A* **99**, 022310 (2019).
- [63] M. B. Plenio and P. L. Knight, The quantum-jump approach to dissipative dynamics in quantum optics, *Rev. Mod. Phys.* **70**, 101 (1998).
- [64] A. J. Daley, Quantum trajectories and open many-body quantum systems, *Adv. Phys.* **63**, 77 (2014).
- [65] For fermionic systems, the tensor product is understood within the bosonic Hilbert space obtained via a Jordan–Wigner transformation. Fermionic operators can then be implemented in the replicated Hilbert space [21, 26].
- [66] Q. Yang, Y. Zuo, and D. E. Liu, Keldysh nonlinear sigma model for a free-fermion gas under continuous measurements, *Phys. Rev. Res.* **5**, 033174 (2023).
- [67] B. Buća and T. Prosen, A note on symmetry reductions of the Lindblad equation: transport in constrained open spin chains, *New J. Phys.* **14**, 073007 (2012).
- [68] V. V. Albert and L. Jiang, Symmetries and conserved quantities in Lindblad master equations, *Phys. Rev. A* **89**, 022118 (2014).
- [69] I. Klich and L. Levitov, Quantum Noise as an Entanglement Meter, *Phys. Rev. Lett.* **102**, 100502 (2009).
- [70] P. Di Francesco, P. Mathieu, and D. Sénéchal, *Conformal Field Theory*, Graduate Texts in Contemporary Physics (Springer New York, New York, NY, 1997).
- [71] A. W. W. Ludwig, Topological phases: classification of topological insulators and superconductors of non-interacting fermions, and beyond, *Phys. Scr.* **T168**, 014001 (2016).
- [72] I. Peschel and V. Eisler, Reduced density matrices and entanglement entropy in free lattice models, *J. Phys. A Math. Theor.* **42**, 504003 (2009).
- [73] V. Alba and F. Carollo, Logarithmic negativity in out-of-equilibrium open free-fermion chains: An exactly solvable case, *SciPost Phys.* **15**, 124 (2023).
- [74] T. Prosen, Third quantization: a general method to solve master equations for quadratic open Fermi systems, *New J. Phys.* **10**, 043026 (2008); Spectral theorem for the Lindblad equation for quadratic open fermionic systems, *J. Stat. Mech. Theory Exp.* **2010**, P07020 (2010).
- [75] T. Barthel and Y. Zhang, Solving quasi-free and quadratic Lindblad master equations for open fermionic and bosonic systems, *J. Stat. Mech. Theory Exp.* **2022**, 113101 (2022).
- [76] C.-E. Bardyn, M. A. Baranov, C. V. Kraus, E. Rico, A. Imamoglu, P. Zoller, and S. Diehl, Topology by dissipation, *New J. Phys.* **15**, 085001 (2013).
- [77] E. J. Bergholtz, J. C. Budich, and F. K. Kunst, Exceptional Topology of Non-Hermitian Systems, *Rev. Mod. Phys.* **93**, 015005 (2019).
- [78] S. Sayyad, J. Yu, A. G. Grushin, and L. M. Sieberer, Entanglement spectrum crossings reveal non-Hermitian dynamical topology, *Phys. Rev. Res.* **3**, 033022 (2021).
- [79] F. Song, S. Yao, and Z. Wang, Non-Hermitian Skin Effect and Chiral Damping in Open Quantum Systems, *Phys. Rev. Lett.* **123**, 170401 (2019).
- [80] H. Fröml, A. Chiocchetta, C. Kollath, and S. Diehl, Fluctuation-Induced Quantum Zeno Effect, *Phys. Rev. Lett.* **122**, 40402 (2019).
- [81] M. Žnidarič, Exact solution for a diffusive nonequilibrium steady state of an open quantum chain, *J. Stat. Mech. Theory Exp.* **2010**, L05002 (2010).
- [82] Y. L. Gal and M. Schirò, Replica Field Theory of Quantum Jumps Monitoring: Application to the Ising Chain, [arXiv:2511.22506](https://arxiv.org/abs/2511.22506) (2025).
- [83] E. Starchl and L. M. Sieberer, Quantum quenches in driven-dissipative quadratic fermionic systems with parity-time symmetry, *Phys. Rev. Res.* **6**, 013016 (2024).